Acta Universitatis Agriculturae Sueciae

Doctoral Thesis No. 2025:77
Faculty of Forest Sciences

Expanding data availability for tree-level remote sensing-based forest inventories

Raul de Paula Pires

Expanding data availability for tree-level remote sensing-based forest inventories

Raul de Paula Pires
Faculty of Forest Sciences
Department of Forest Resource Management
Umeå

SLU
SWEDISH UNIVERSITY OF AGRICULTURAL SCIENCES

DOCTORAL THESIS
Umeå 2025

Acta Universitatis Agriculturae Sueciae
2025:77

Cover: A digital painting of a forest with tall trees and lush plants. In the center, a Terrestrial Laser Scanner and a drone are surveying the forest. (By Emanuele Papucci, 2025).

ISSN 1652-6880
ISBN (print version) 978-91-8124-061-0
ISBN (electronic version) 978-91-8124-107-5
https://doi.org/10.54612/a.7hln0kr0ta

Swedish University of Agricultural Sciences, Department of Forest Resource Management, Umeå, Sweden

Print: SLU Grafisk service, Uppsala 2025

Expanding data availability for tree-level remote sensing-based forest inventories

Abstract

Precision forestry seeks to optimize forest management by using site-specific information at fine spatial scales, often supported by remote sensing. Implementing this framework requires detailed ground-truth data of forest attributes and conditions, but the collection of such information across large areas is limited by cost and scalability. Complementary data sources can help address this demand by expanding the availability of tree-level information. This thesis explores how different data sources, namely close-range laser scanning, airborne laser scanning, harvester production reports, and synthetic point clouds, can expand data availability for precision forestry. Paper I develops and evaluates a method for deriving stem attributes such as diameter, taper, and volume from car-mounted mobile laser scanning acquired along forest roads, demonstrating its potential as an efficient source of tree-level reference data. Paper II assesses the suitability of mobile laser scanning as an alternative to conventional field plots for training airborne laser scanning-based models, showing that both sources can support tree-level modelling of diameter and volume. Paper III presents a pipeline for automatic tree species annotation by linking airborne laser scanning data with harvester production reports, demonstrating that data derived from forest operations can reduce the need for field surveys or manual labelling in species classification tasks. Finally, Paper IV introduces a semi-empirical simulation framework for generating synthetic stem defects in terrestrial laser scanning point clouds, using them to train a convolutional neural network for crook detection and discussing the implications of simulation. Taken together, the four studies show that complementary data sources have the potential to serve as ground-truth information in forest assessments, providing data of sufficient quality and quantity to support remote sensing-based forest inventories at tree-level. This thesis underlines both opportunities and limitations of these approaches, highlighting their relevance for integration into inventory frameworks.

Keywords: Precision forestry, remote sensing, forest inventory, laser scanning, mobile laser scanning, terrestrial laser scanning, harvester production reports, synthetic point clouds.

Förbättring av tillgången på data för fjärranalysbaserade skogsinventeringar på trädnivå

Sammanfattning

Skogsskötsel kan optimeras genom att använda geografisk information med hög upplösning som skapas med fjärranalys. För detta behövs detaljerade referensmätningar, men tillgången är begränsad om manuella mätmetoder används. I denna avhandling utforskas nya metoder för insamling av referensdata, såsom markbaserad och flygburen laserskanning, skördardata, och syntetiska punktmoln. I den första studien utvecklas och utvärderades en metod för att beräkna trädstammars egenskaper med laserskanning från en bil som körs på skogsbilvägar. Denna teknik vara effektiv för att samla in träningsdata till fjärranalysmetoder. I den andra studien undersöktes lämpligheten att använda mobil laserskanning för att träna metoder som tillsammans med flygburen laserskanning används för att skapa trädkartor. Utvärderingen visade liknande resultat om referensdata från mobil laserskanningen respektive manuell fältinventering användes. I den tredje artikeln presenteras en beräkningskedja för automatisk registrering av trädslag genom att länka samman data från flygburen laserskanning med georefererade skördardata. På detta sätt kunde en skördare användas för att automatisk träna en metod som i kombination med flygburen laserskanning skapar trädkartor med trädslagsinformation. I den fjärde studien introducerades en semi-empirisk simuleringsmetod för att skapa syntetiska data från markbaserad laserskanning. Syntetiska data kunde användas för att träna neurala nätverk som detekterar krokar på trädstammar med markbaserad laserskanning. Det var möjligt att dra slutsatser om hur realistiska simuleringarna behöver vara för att de ska vara användbara för att träna metoder som detekterar stamdefekter i data från en verklig laserskanning. I de fyra studierna visas att kompletterande datakällor har en potential att tjäna som referensdata i skogsinventeringar. Detta eftersom de levererar data med tillräcklig kvalitet och kvantitet för att kunna användas i olika tillämpningar, inklusive modellering och beslutsstöd i skogsbruket. Denna avhandling belyser både möjligheter och begränsningar med dessa angreppssätt och framhäver deras relevans för integration i inventeringsramverk.

Nyckelord: precisionsskogsbruk, fjärranalys, skogsinventering, laserskanning, mobil laserskanning, markbaserad laserskanning, skördardata, syntetiska punktmoln.

Dedication

To those who always see me leave yet welcome me back as if no time had passed. And to Ingrid, who has been my most reliable source of “ground-truth”

Contents

List of publications

This thesis is based on the work contained in the following papers, referred to by Roman numerals in the text:

I. Pires, R. de P., Olofsson, K., Persson, H.J., Lindberg, E. & Holmgren, J. (2022). Individual tree detection and estimation of stem attributes with mobile laser scanning along boreal forest roads. ISPRS Journal of Photogrammetry and Remote Sensing, 187, 211–224. https://doi.org/10.1016/j.isprsjprs.2022.03.004

II. Pires, R. de P., Lindberg, E., Persson, H.J., Olofsson, K. & Holmgren, J. (2024). Mobile laser scanning as reference for estimation of stem attributes from airborne laser scanning. Remote Sensing of Environment, 315, 114414. https://doi.org/10.1016/j.rse.2024.114414

III. Pires, R. de P., Axelsson, C., Lindberg, E., Persson, H.J., Olofsson, K. & Holmgren, J. (2025). Boreal tree species classification using airborne laser scanning data annotated with harvester production reports, and convolutional neural networks. International Journal of Applied Earth Observation and Geoinformation, 140, 104607. https://doi.org/10.1016/j.jag.2025.104607

IV. Pires, R. de P., Lindgren, N. & Holmgren, J. (2025). Stem crook detection in terrestrial laser scanning data using semi-empirical simulations. (manuscript)

The contribution of Raul de Paula Pires to the papers included in this thesis was as follows:

I. Methodology, Software, Validation, Formal analysis, Writing – original draft, Visualization.

II. Methodology, Conceptualization, Formal analysis, Validation, Writing – original draft, Writing – review & editing, Visualization.

III. Methodology, Conceptualization, Formal analysis, Validation, Writing – original draft, Visualization.

IV. Methodology, Software, Conceptualization, Formal analysis, Validation, Writing – original draft.

List of tables

List of figures

Abbreviations

2D	Two dimensional
3D	Three Dimensional
AGB	Above Ground Biomass
AI	Artificial Intelligence
ALS	Aerial Laser Scanning
CNN	Convolutional Neural Network
CTL	Cut-to-length
DBH	Diameter at Breast Height
FI	Forest Inventory
HPR	Harvester Production Report
IMU	Inertial Measurement Unit
IoU	Intersection over Union
LiDAR	Light Detection and Ranging
MLS	Mobile Laser Scanning
NFI	National Forest Inventory
OA	Overall Accuracy
PLS	Personal Laser Scanning
QSM	Quantitative Structure Model
RANSAC	Random Sample Consensus
RMSE	Root Mean Square Error
TLS	Terrestrial Laser Scanning

1. Introduction

In a world with increasing pressure on natural resources, forestry has become more complex, balancing multiple objectives such as biodiversity conservation, timber production, climate change mitigation, and recreational services. Meeting these different and sometimes conflicting goals requires detailed and accurate information to optimize decision-making and resource allocation. In this context, precision forestry refers to forest management conducted at high spatial and temporal resolutions, enabling optimal decisions at fine scales, such as the level of individual trees or map pixels. Rather than a single practice or technology, precision forestry represents a change in the management framework, in which decisions are based on site-specific conditions, often measured with remote sensing, with help of data analysis, modelling techniques, and automation (Venanzi et al. 2023). In a potential precision forestry management framework, remote sensing data can be used for detailed site mapping, revealing tree growth rates, soil conditions and topography (Raigosa-García et al. 2024). Later, management operations can use such information for targeted silvicultural treatments, such as fertilization, thinning and harvesting (Görgens et al. 2020; Salmivaara et al. 2020).

To support these practices, high-resolution data at multiple spatial scales is required. For example, remote sensing technologies such as Light Detection and Ranging (LiDAR) and imaging sensors mounted on different platforms can provide essential information on forest structure and composition (Valbuena et al. 2020; Ehbrecht et al. 2021). When combined with statistical tools and decision support systems (Cattaneo et al. 2024), these data sources can improve the description of forest dynamics, helping in tasks such as growth modeling (de Oliveira et al. 2021; Appiah Mensah et al. 2023; Puliti et al. 2023), species classification (Fassnacht et al. 2016; Li et al. 2024; Ma et al. 2024), and biomass estimation (Brede et al. 2022; Schäfer et al. 2024). Moreover, as forest management progresses towards a precision forestry paradigm, attributes beyond traditional stand-level averages are gaining importance. For instance, detailed descriptions of individual tree's physical characteristics - such as crown structure (Terryn et al. 2022), leaf angulation (Li et al. 2018), and wood properties (Pehkonen et al. 2025) - are important for both daily operational planning and long-term

breeding programs (Dungey et al. 2018; Jin et al. 2021), influencing forest productivity, resilience, and timber quality.

However, the implementation of precision forestry at scale remains challenging, despite the advancements in remote sensing technologies and analytical methods. Some devices often used for assessing forest attributes, such as Terrestrial Laser Scanning (TLS) systems, are highly effective for experiments and conducting small surveys but often lack the scalability needed for the operationalization, as data collection with those might still be time-consuming and resource-intensive (Calders et al. 2020). In other words, some sensors are often unfeasible for collecting fine-scale attributes across large, forested areas.

At the same time, integrating artificial intelligence (AI) into forest management has significantly increased the demand for high-quality datasets, as these models require substantial amounts of data to effectively learn patterns and make accurate predictions. Consequently, the lack of training datasets has been a bottleneck in the deployment of AI-based solutions for forest management (Kattenborn et al. 2021).

Thus, precision forestry must increasingly rely on data collection methods that can provide detailed insights on an operational scale. These methods may combine remote sensing technologies mounted on mobile platforms, the use of georeferenced data from forestry machinery, or synthetic datasets to complement real-world observations. By leveraging such diverse approaches, we can bridge the gap between research-level precision forestry technologies and their large-scale implementation in forest management.

1.1 Remote Sensing in Forestry

Remote sensing is the science and art of extracting information about objects, areas, or phenomena from data collected by sensors that are not in direct contact with them (Lillesand et al. 2015). When it comes to its usage in forestry, remote sensing methods provide means of efficiently and repeatably measuring ecosystems across multiple spatial and temporal scales (Lechner et al. 2020). By doing so, remote sensing has significantly advanced forest monitoring and management capabilities (Fassnacht et al. 2024).

Remote sensing techniques can be broadly divided into passive and active. Passive sensors rely on capturing reflected radiation, commonly using

the sun as the radiation source. Common examples include multispectral and hyperspectral sensors mounted on satellites or airplanes, which can be used to assess conditions such as forest health, species composition, and structure through vegetation indexes and spectral classification (Lechner et al. 2020; Jafarbiglu & Pourreza 2022).

On the other hand, active remote sensing, using techniques such as LiDAR and Synthetic Aperture Radar (SAR), emits their own radiation towards targets and measures the reflected signals. LiDAR has emerged as a promising alternative for forest assessments at different scales due to its ability to capture the three-dimensional (3D) structure of vegetation with high spatial resolution and accuracy (Lovell et al. 2003; Hopkinson et al. 2004). This active remote sensing technique uses light pulses to generate 3D point clouds that can describe different layers of the forest cover, which makes it particularly valuable in forestry, where understanding vertical structure, tree size, and spatial arrangement is essential (Valbuena et al. 2020). Over the past decades, laser scanning has been widely used in forest research, supporting applications from biomass estimation to habitat modeling and structural complexity analysis (Liang et al. 2022).

More recently, developments in platforms for sensors have enhanced the applicability of remote sensing. Unmanned Aerial Vehicles (UAVs) and terrestrial platforms, equipped with optical or LiDAR sensors, bridge the gap between large-area airborne surveys and detailed, site-specific observations. These systems offer high spatial resolution, rapid deployment, and accessibility to remote or challenging terrains, making them increasingly valuable tools for precision forestry practices (Guimarães et al. 2020; Liang et al. 2022; Walker & Dahle 2023).

Nevertheless, all remote sensing and remote sensing-derived measurements are subject to errors and uncertainties that can influence their interpretation and application. For instance, uncertainties may come from, although not limited to, the measurement system and the methods used to process data and translate it into products for different users (Goulden & Hopkinson 2010). For example, LiDAR-derived tree height estimates can be biased by beam divergence and incidence angle of laser pulses on the treetop (Hopkinson 2007). Thus, as precision forestry practices expand, correctly leveraging remote sensing data while accounting for sources of uncertainty becomes integral to improving the efficiency and effectiveness of forest management interventions (Persson et al. 2022).

1.2 Close-range Laser Scanning

Traditionally, forest inventories have been based on attributes that can be efficiently measured manually with simple tools, such as diameter at breast height (DBH), and total height. While foundational to forest inventory and widely used in both research and management, these field-based methods offer a coarse and often simplified representation of tree form and structure. Detailed traits such as taper, crown shape, branching patterns, bark morphology, or leaf traits were typically estimated subjectively, assessed destructively, or simply omitted due to the challenges of measuring them in the field (Liang et al. 2022).

Close-range laser scanning, as well as other close-range remote sensing techniques, come as a paradigm shift in how trees are measured, making it possible to observe fine-scale traits that were not measurable before (Disney 2019). These techniques, also referred to as proximal sensing, can be described as when remote sensing instruments are used from ground-based or low-altitude platforms, standing relatively near the target objects - typically within a range of few meters to a few hundred meters. While there is no universally defined distance threshold, this category of remote sensing generally includes systems like TLS, Mobile Laser Scanner (MLS), and low-flying UAVs. Their usage in forestry has grown significantly, and their potential for forest assessments is well documented in the literature (Liang et al. 2022; Molina-Valero et al. 2025).

Close-range remote sensing also includes passive optical techniques, such as high-resolution RGB imagery. For example, Kim et al. (2022) trained convolutional neural networks (CNNs) to recognize species-specific bark traits from high resolution photography. The CNN classified 42 tree species by bark texture with approximately 90% overall accuracy, identifying traits such as blisters, lenticels, and vertical fissures in the bark as determinant for species identification.

Amongst close range-remote sensing techniques, TLS has become a prominent tool for the characterization of forest structure (Arrizza et al. 2024), timber quality, and availability of fuel in different forest strata (Hillman et al. 2021; Wallace et al. 2022; Olofsson & Holmgren 2023). For instance, Moriguchi (2023) highlighted the potential of multi-view TLS surveys for the precise estimation of a tree's fractal dimension, while Terryn et al. (2020) used quantitative structure models (QSMs), constructed from TLS point clouds, to determine structural features from the tree crowns and

later use those to discriminate between tree species. On a higher level, Yang et al. (2023) highlighted the role of TLS as a rapid and reliable method for measuring leaf angles, revolutionizing the current ability to measure such fine-scale attribute of the forest crown. Rather than single-time measurements, TLS has also been used for continuous monitoring of the diurnal variation of leaf water content (Junttila et al. 2019) and structural and phenological dynamics of forest canopy (Campos et al. 2021).

Despite these capabilities, TLS surveys can be time- and labor-intensive, often requiring similar effort as traditional fieldwork. Thus, Mobile Laser Scanning (MLS) has emerged as a more efficient alternative to static TLS. MLSs leverage mobile platforms, such as ground vehicles, for rapidly acquiring high-resolution data over larger forest areas. These systems offer a trade-off: while they may not reach the same levels of geometric precision as a TLS, they allow for broader spatial coverage with reduced acquisition time (Hunčaga et al. 2020). As such, MLSs are often used for high-resolution forest monitoring of larger areas. Amongst different MLSs, Personal Laser Scanners (PLSs) – laser scanning systems carried in backpacks or handheld devices – are often used for plot-level surveys. These systems allow navigation around trees and understory, producing close-range point clouds that can be used for different purposes, such as tree detection, stem attribute measurement, tree species classification (Liu et al. 2022), and fuel type characterization (Hoffrén et al. 2024).

Because PLS systems are frequently operated in environments where GPS/GNSS signals are obstructed, such as under forest canopy, accurate sensor positioning must rely on other techniques such as Simultaneous Localization and Mapping (SLAM). SLAM (Durrant-Whyte & Bailey 2006) is a technique used to estimate a platform's own position while simultaneously constructing a map of its surroundings relying on onboard sensors, such as Inertial Measurement Units (IMUs), optical cameras and LiDAR (Qian et al. 2017; Wu et al. 2025). It works by identifying and tracking stable geometric features across successive observations, allowing the system to infer both its movement and the surrounding area over time. In other words, SLAM uses the estimated sensor position to build a map, and at the same time it uses the evolving map to infer the sensor's position (Aguiar et al. 2020). As measurements accumulate, small localization errors can result in positional drift. Despite these limitations, modern SLAM implementations have been successfully adapted from indoor and urban

robotics to complex forest environments, enabling accurate georeferencing and map reconstruction without relying on external GNSS input (Holmgren et al. 2017; Kukko et al. 2017; Pierzchała et al. 2018; Hyyppä et al. 2020c).

While SLAM is particularly important in GPS/GNSS denied environments, platforms that operate in more open conditions can benefit from satellite positioning, which tends to be more stable and provides global georeferencing. In this context, researchers have leveraged ground vehicles as platforms for laser scanning systems to further scale up data acquisition. By mounting LiDAR sensors on moving vehicles such as cars, all-terrain vehicles (ATVs), or even tractors and forestry machines, data collection becomes significantly more efficient. Such a combination of sensor and platform enhances data collection capabilities as vehicles can usually cover larger areas in shorter times when compared with PLSs. For instance, instead of measuring scattered field plots, a surveyor could drive along several kilometers of roads through a forest and capture data on thousands of trees in a single day (Pires et al. 2024).

The choices of sensor and platform depend on several factors, such as mission scope, hardware availability, and desired autonomy. For instance, Pierzchała et al. (2018) and Sheng et al. (2024) used consumer grade Velodyne VLP-16 LiDAR scanners on small, unmanned ATVs to extract DBH of individual trees, reaching accuracies from 1.48 cm to 3.48 cm. In parallel, Liang et al. (2018b) and Bienert et al. (2018) mounted survey grade systems on ATV and car, respectively, allowing for heavier and more advanced hardware. In these cases, the system produced point clouds with improved geometric accuracy. However, higher point cloud accuracy is not always a synonym for accurate estimation of tree attributes, with the algorithms used for extracting such variables playing an equally significant role. For instance, even though Bienert et al. (2018) used a professional survey grade MLS for data collection, the method chosen for attribute estimation required a denser point cloud. Thus, the accuracy obtained by using this instrument - 3.7 cm Root Mean Square Error (RMSE) in DBH estimation – was similar to the ones obtained by consumer grade systems. This highlights that both hardware and data processing methods play equally important roles in determining the final accuracy of forest structural metrics.

From a hardware perspective, another important factor influencing the accuracy of LiDAR-derived vegetation and stem measurements is beam divergence, which determines the footprint size of the laser beam at a given

distance. A larger divergence produces a wider footprint, reducing peak pulse power concentration and increasing the chances of a laser beam interacting with multiple surfaces such as foliage, branches, and background (Hopkinson 2007). Beam divergence affects the resolution of fine-scale features and should be carefully considered depending on forest type and application (Calders et al. 2020). In addition, wider footprints caused by either widening the beam or increasing flying altitude can reduce the maximum canopy return heights in tall stands (Hopkinson 2007). These effects arise because reduced pulse power can delay the triggering of returns within vegetation, allowing the laser beam to penetrate deeper into the forest cover before generating a return. Measurement errors are also influenced by surface curvature and angle of incidence, both of which shape the returned signal. Beyond beam geometry and power concentration, the way echoes are detected can affect point cloud accuracy, as detection strategies respond differently to distorted returns from sloped or curved surfaces (Forsman et al. 2018). These sensor- and configuration-related effects can cause systematic differences in measured canopy structure when comparing different datasets, which may be mistaken for real ecological variation if not accounted for during analysis.

In addition to ground-based platforms, UAVs have increasingly been used as aerial platforms for LiDAR and optical sensors in close-range applications (Jaakkola et al. 2017). Their ability to rapidly cover relatively large areas, access difficult terrain, and acquire high-resolution data has made them popular in forestry (Sun et al. 2023), with applications that include forest health monitoring (Ecke et al. 2022), mapping of forest structure (Liu et al. 2018; Almeida et al. 2019) and individual tree detection (Straker et al. 2023). Depending on the flight's altitude and trajectory, UAVs can operate right above or even fly below the canopy to reconstruct tree stems and understory conditions with level of detail comparable to terrestrial methods (Hyyppä et al. 2020c; Kuželka et al. 2020; Puliti et al. 2020). Nonetheless, UAV acquisitions are sensitive to flight stability, GNSS signal quality, and environmental conditions such as wind, all of which can reduce the accuracy of resulting data (e.g. point clouds) and increase variability between missions.

UAV-mounted laser scanners (UAV-LS) and optical sensors have been applied in a wide range of forestry tasks. For example, Kattenborn et al. (2019) used UAV optical data as a semi-automatic reference data acquisition

method to map woody invasive species using Sentinel-1 and 2, concluding that, in certain cases, UAV-based reference data acquisitions can be a promising alternative to traditional field surveys. Additionally, Brede et al. (2022) highlighted the role of UAV-LS to scale Above Ground Biomass (AGB) measurements across large areas with reduced fieldwork requirements, being a promising data collection tool for calibration and validation sites.

In parallel, researchers and practitioners have been exploring the potential of UAV systems that fly below the forest canopy for providing in-situ measurements of different forest attributes. In that regard, Hyyppä et al. (2020a) tested a remotely piloted under-canopy UAV-LS. With the system, the authors detected 84% - 93% of the trees and estimated DBH and stem curves with RMSEs from 0.60 cm - 0.92 cm and 1.2 - 1.4 cm, respectively, depending on the forest type being analyzed. In an attempt to automate data collection even further, Liang et al. (2024) presented a fully autonomous under canopy UAV-LS. The system was used for estimation of tree-level attributes, achieving RMSE of 5.13 cm for DBH and 5.18 cm for stem curves. When comparing these accuracies with the ones obtained by using TLS systems, the authors noticed that the lower performance of UAV-LS was largely due to reduced geometric accuracy of the point clouds. In UAV systems, this can be affected by GPS/GNSS signal quality, flight stability and trajectory, SLAM algorithms, among other factors. In addition, UAV-LS platforms often carry smaller sensors, which may differ from TLS in terms of beam divergence and pulse energy, further influencing measurement precision. Addressing these limitations could significantly improve tree attribute estimation with UAV-LS.

In close-range laser scanning techniques, uncertainties may come not only from sensors and platforms used, but also from the interaction between the laser beam and the forest structures. Occlusion by understory vegetation or nearby trees stems can lead to incomplete point cloud coverage, particularly for lower stem sections and inner crown structures (Hyyppä et al. 2020b). Variations in scanning protocol, such as the number and position of scan locations or the trajectory and speed of MLS/PLS platforms, directly influence point density and coverage of resulting point clouds, affecting tree detection and the accuracy of fine-scale features (Gollob et al. 2019; Torralba et al. 2022). Environmental factors such as branch movement caused by wind can distort how trees are represented in point clouds (Vaaja et al. 2016;

Pyorala et al. 2018). On the processing side, assumptions such as the perfect circularity and straightness of stems in cylinder fitting can bias results in stands with irregular forms or leaning trees.

Addressing these challenges requires acquisition protocols and processing workflows that explicitly account for error sources. For example, Astrup et al. (2014) proposed a methodology for adjusting for occlusion in inventories based on single-scan TLS setups, enabling stand-level volume estimates that are comparable to conventional inventory approaches. Still, the lack of robust, repeatable workflows for processing point clouds, with stable accuracy across different forest conditions, is a barrier for the implementation of close-range technologies in an operational context. In practice, there are nearly as many processing workflows as there are combinations of sensors, platforms, and forest conditions (Liang et al. 2018a). Each study tends to develop its own pipeline, tailored to specific point cloud characteristics, scanner configurations, or target variables, making it difficult to generalize or replicate results across different contexts.

For example, individual tree detection and stem attribute estimation can be approached using a wide variety of methods, ranging from geometric rules to complex data-driven models. Often, tree detection in ground-based point clouds involves shape-based algorithms, such as cylinder fitting, where vertical point clusters are identified and modeled as cylindrical or circular sections, typically at breast height (Olofsson & Holmgren 2016; Hyyppä et al. 2022; Muhojoki et al. 2024). This technique is most effective in sparse, well-structured plots but often struggles with leaning stems, overlapping crowns, or occlusion near the ground (Hyyppä et al. 2020b). Similarly, DBH estimation is commonly performed using single-slice circle fitting (Olofsson et al. 2014), where a cross-sectional cut of the stem at around 1.3 m is analyzed to fit a circle. While efficient and interpretable, these methods can become unreliable when stems are obscured by understory vegetation, or when point density is insufficient. Additionally, more advanced approaches such as QSMs fit a series of cylinders along the full stem and branches, enabling the estimation of DBH, taper, and volume simultaneously (Raumonen et al. 2015; Brede et al. 2019; Bornand et al. 2023).

As an alternative to heuristic methods, deep learning has increasingly been used for processing point clouds. This branch of machine learning, based on artificial neural networks, passes information through multiple layers that learn progressively more abstract representations of the input. By

employing many hidden layers and connections, these architectures can capture complex relationships in the data. Such capabilities make deep learning a powerful tool in remote sensing of forests, where learning spatial patterns from data is essential. (Kattenborn et al. 2021; Hamedianfar et al. 2022). For instance, semantic segmentation models can be used to classify each point into classes like stem, leaves, branches, and ground, while instance segmentation models separate the forests into individual tree point clouds (Wielgosz et al. 2024).

Recent advancements include frameworks such as ForAINet (Xiang et al. 2024), which performs both semantic and instance segmentation of airborne LiDAR data accurately distinguishing tree components. The model achieved an F1-score above 85% for individual tree detection and a mean Intersection over Union (IoU) of over 73% across five semantic classes: ground, low vegetation, stems, live branches, and dead branches. From these segmentations, it was possible to derive accurate biophysical parameters such as tree height, crown diameter, crown volume. In parallel, SegmentAnyTree (Wielgosz et al. 2024) was developed as a sensor-agnostic model for individual tree segmentation, transferable across UAV-LS, TLS, and MLS datasets. The model showed consistent performance for point clouds with densities above 50 points/m² and remained effective down to 10 points/m² using random subsampling as an augmentation strategy. Together, such models show how deep learning enables scalable, flexible, and high-resolution analysis of 3D forest structure.

Given such a variety of ways of processing point clouds, there is a growing effort within the research community to make processing tools more accessible and user-friendly. For instance, Murtiyoso et al. (2024) identified 24 tools designed for processing ground-based point clouds in forest applications, of which 20 are open source and 2 are freely available as compiled software. One example is 3DFin (Laino et al. 2024), a cross-platform, open-access tool designed for automatic forest inventories using TLS, MLS, or photogrammetric point clouds. It allows users to extract key features such as DBH, total height, and tree position with high accuracy, and can be integrated as a plugin in other software or used as a standalone application.

1.3 Operational Machinery as a Data Source for Precision Forestry

Mechanized forest operations produce large volumes of potentially valuable data. However, the information collected daily in operations such as harvesting is sometimes underused as reference data for remote sensing applications. For example, harvester production reports (HPRs) contain detailed records of harvested trees, including species, stem diameter and length, assortments, taper, and even indications of tree health or damage. These data are gathered as part of routine operations and could be more integrated into remote sensing-based modelling, as the precision and consistency of harvester data make it a potentially rich source of ground truth.

In the last decade, studies have demonstrated the practical value of integrating harvester data with remote sensing for forest modelling (Holmgren et al. 2012). More recently, Saukkola (2019) used tree-level data recorded by harvesters in Southern Finland to developed models to predict forest inventory attributes using ALS (Aerial Laser Scanning) and aerial imagery. By locating trees through harvester head positioning, they achieved accurate predictions of basal area-weighted mean diameter and height (RMSEs ranging from 10-11% and 6-8%, respectively), demonstrating the use of harvester data as reliable ground truth. Similarly, Noordermeer et al. (2023) used harvester data as reference to impute stem frequency distributions through various ALS-based inventory approaches. They found that area-based methods yielded the highest accuracies for key variables like DBH, tree height, and volume distributions. In a fully operational context, Söderberg et al. (2021) used standardized harvester outputs from cut-to-length (CTL) machines in Sweden, combined with ALS data, to predict stand-level forest metrics such as stem volume and basal area. Their approach achieved RMSEs between 3% and 15% and generated stem diameter distributions, useful for applications such as yield prediction and bucking simulations. Finally, Suvanto et al. (2025) used data from over 10,000 clear-cut stands in Finland to model and map the risk of Norway spruce (*Picea abies* (L.) H. Karst.) root rot. By linking rot indicators derived from bucking patterns recorded by harvesters with spatial environmental data, they identified key drivers of rot occurrence and produced risk maps for operational use.

Together, these studies illustrate how HPRs can serve as a powerful and scalable data source for precision forestry when properly integrated with remote sensing. Nevertheless, measurement precision in harvester systems can vary with machine calibration, operator, and log handling, which means that such datasets can carry their own uncertainties. For example, variation in how logs are positioned in the harvester head can introduce errors in diameter and length measurements, which may propagate into any models.

More advanced approaches, such as mounting LiDAR sensors on forestry machinery, hold significant potential for real-time decision support (Pohjala et al. 2025). The integration of remote sensing into operational machinery can transform conventional activities into surveys, maximizing data collection (Faitli et al. 2024). For example, Gollob et al. (2023) successfully tested a LiDAR scanner mounted on a cable yarder carriage during logging operations in mountainous terrain. By scanning from the moving carriage, they automatically detected over 92% of trees within typical harvesting corridors, achieving RMSEs in DBH estimation ranging from 1.59 cm to 2.23 cm, depending on site conditions. Similarly, Sagar et al. (2024) introduced the use of onboard LiDAR integrated into CTL harvesters to detect stem defects. Their trials demonstrated high accuracy despite using only few real-world trees, showing that integrated LiDAR sensors can act as complementary technology for near real-time decision making, facilitating the work of the machine operator and forest managers.

Despite the most recent advancements, fully leveraging operational machinery for data collection still requires further development. For instance, robust and cost-efficient hardware that can withstand harsh environments is necessary if integrating LiDAR sensors into e.g. cable yarding. In addition, efficient protocols for data integration, analysis, and decision support systems tailored specifically for precision forestry are needed to effectively use the generated information. As these technological and methodological challenges are addressed, machinery-integrated solutions could represent an additional step towards achieving a precision state in forest management.

1.4 Synthetic Data Generation

Synthetic data refers to data that is simulated or generated based on a set of predefined assumptions or rules, with the aim of replicating or approximating real-world scenarios. This is especially relevant for supervised learning, where the scarcity of real-world data can hinder model training (Westling et al. 2021; Schäfer et al. 2024). Through simulations, virtual trees or forests can be created with predefined characteristics, allowing researchers to generate extensive, controlled datasets without costly or logistically demanding field campaigns (Lines et al. 2022; Kulicki et al. 2025).

Synthetic laser scanning simulations can be broadly categorized into different types. The so-called physical models simulate the laser and target interaction, making them suitable for studying the influence of instrument settings such as beam divergence or pulse repetition frequency. Geometrical models attempt to replicate tree and forest structure using mathematically defined shapes, such as cylinders, allowing precise control over structural parameters. Statistical models generate vegetation structure based on probabilistic distributions of different attributes, often calibrated from field or inventory data. Finally, imputation models insert real-world measurements of trees or forests into simulated scenes, preserving realism in structure while allowing experimental control. Many modern simulators combine these approaches. For example, Winiwarter et al. (2022) presented HELIOS++, a simulation framework that combines 3D scenes with modular scanner and platform models to replicate TLS, MLS, UAV-mounted or ALS data acquisitions. Such framework allows users to configure parameters such as beam divergence, scan pattern, platform trajectory, and pulse repetition rate. Thus, HELIOS++, as well as other laser scanning simulators, can produce virtual point clouds that can be used for applications ranging from data acquisition planning to algorithm testing. Similarly, Kukko and Hyyppä (2009) developed a simulation method that integrates spatial and radiometric modelling to produce waveform and point cloud data by modelling both light–object interactions and the characteristics of specific scanning systems.

In this context, recent studies have demonstrated the utility of synthetic laser scanning data. Bryson et al. (2023) used a synthetic tree simulator to generate training data for deep learning-based stem segmentation in LiDAR point clouds. Their synthetic-data-trained segmentation models performed similarly to models trained exclusively on real-world data, achieving

improvements in IoU ranging from 1% to 7%. Analogously, Schäfer et al. (2023) compared synthetic ALS data against actual ALS data. They found that the canopy cover and height distributions extracted from synthetic data were comparable to the ones extracted from real LiDAR data, still biomass models trained on the synthetic datasets showed a slight reduction in accuracy compared to those trained on field data.

In addition to overcoming data scarcity, synthetic LiDAR data enables precise experimental control, as users can systematically vary parameters such as tree species composition and canopy structure, to isolate their effects on model outcomes. Such controlled environment helps researchers better understand different phenomena without the unexplained variability common in real-world data. For instance, Fassnacht et al. (2018) generated synthetic canopy height models by combining a forest growth simulator with realistic 3D representations of individual trees derived from actual LiDAR point clouds. This allowed them to simulate forests under known conditions and systematically test how plot size affects model performance. Similarly, Bester et al. (2023) used synthetic TLS data to compare machine-learning models and point-cloud processing strategies for volume estimation. By removing uncontrolled variability and measurement noise, they were able to identify the best method choice for volume estimation in ideal conditions.

Despite these advantages, using synthetic LiDAR data for modelling has limitations. Simulations often simplify real-world complexity, potentially introducing biases or inaccuracies, especially if forest structure or sensor characteristics are highly simplified (Schäfer et al. 2023). Therefore, simulations are often seen as complimentary to real-world data, being particularly useful for method development, initial model training, or hypothesis testing, after which fine-tunning and validation against field-collected data might still be necessary. In summary, synthetic laser scanning data provides a powerful and flexible strategy for forestry modelling, enabling controlled experiments and generation of training datasets. While they may not fully replicate the complexity and variability of field data, simulated point clouds are a valuable data source for advancing remote sensing applications in forestry.

1.5 Objectives

The overall objective of this thesis is to develop and evaluate methods for generating tree-level reference data to improve predictive modelling in remote sensing-based forest inventories. For that, the thesis summarizes different studies in order to illustrate how they together contribute to addressing current challenges in acquiring tree-level information. The objectives of each study are:

Paper I: To develop an algorithm for individual tree detection, DBH, stem profile, and volume estimation from car-mounted MLS data, and to evaluate the effect of distance from the roadside on estimation accuracy.

Paper II: To compare ALS-based DBH and stem volume models trained with car-mounted MLS data against those trained with traditional field inventory data, assessing the potential of MLS as an alternative reference data source.

Paper III: To propose a method for automatically annotating ALS data at the single-tree level using HPRs, and to use these annotated datasets for training a tree species classification CNN across ALS datasets with varying spectral and spatial resolutions.

Paper IV: To propose a simulation pipeline for generating synthetic crooks on TLS-derived tree stems, and to evaluate the performance of a crook detection CNN trained on the synthetic dataset.

2. Material and Methods

This thesis is composed of four studies, each utilizing different data sources, methodologies and reaching different outcomes. Table 1 provides an overview of the studies, summarizing the main data sources, target variables, and analysis carried out in each case. While each study addresses a specific research question, together they demonstrate how alternative data sources, beyond traditional field inventories, can be used to estimate tree-level attributes in a scalable manner. The table allows for a quick comparison of the different data (e.g., MLS, TLS, ALS, synthetic data), processing workflows, and modelling strategies applied, and how these relate to the respective study objectives and outcomes.

Table 1. Overall description of Papers I-IV.

Paper	Main Data Source(s)	Main Target Variable(s)	Main Method(s)	Validation Data	Main Contribution to Data Availability and Estimation of Tree-level Attributes
I	ALS[1] and car-mounted MLS[2]	Stem count, DBH[3], stem curves and volume	Arc detection through RANSAC[4] circle fitting and taper modelling	Target variables extracted from TLS[5] data	Developed and evaluated an algorithm for stem detection and attribute estimation using car-mounted MLS
II	ALS + MLS ALS + field inventory	DBH, stem volume	ALS tree segmentation + linear regression	Target variables measured in a field inventory	ALS models trained with MLS-derived reference data achieved accuracy comparable to those trained with field plots
III	Dual-wavelength ALS + HPR[6]	Tree species classification	Automated ALS-HPR matching + CNN[7]-based species classification	Cross validation (Leave-one-stand-out)	Accurate species classification without manual labelling; performance varied according to ALS datasets with different spatial and spectral resolutions
IV	Synthetic TLS	Stem crook detection	CNN-based object (crook) detection	Crooks annotated in real-world TLS data	Demonstrated a pipeline for crook simulation and evaluated the performance of models trained on simulated data for detecting crooks in real-world stem point clouds

Note. [1]Aerial Laser Scanning. [2]Mobile Laser Scanning. [3]Diameter at Breast Height. [4]Radom Sample Consensus. [5]Terrestrial Laser Scanning. [6]Harvester Production Report. [7]Convolutional Neural Network.

2.1 Paper I: Individual tree detection and estimation of stem attributes with mobile laser scanning along boreal forest roads

Paper I presented a methodology for detection of tree stems and estimation of stem attributes using car-mounted MLS data acquired along forest roads, the overall processing workflow is shown in Figure 1. The study took place in Remningstorp, in southern Sweden (lat. 58.5° N, long. 13.6° E). The area is dominated by Norway spruce, followed by Scots pine (*Pinus sylvestris* L.), and birch (*Betula* spp.), with tree density of 580 trees/ha.

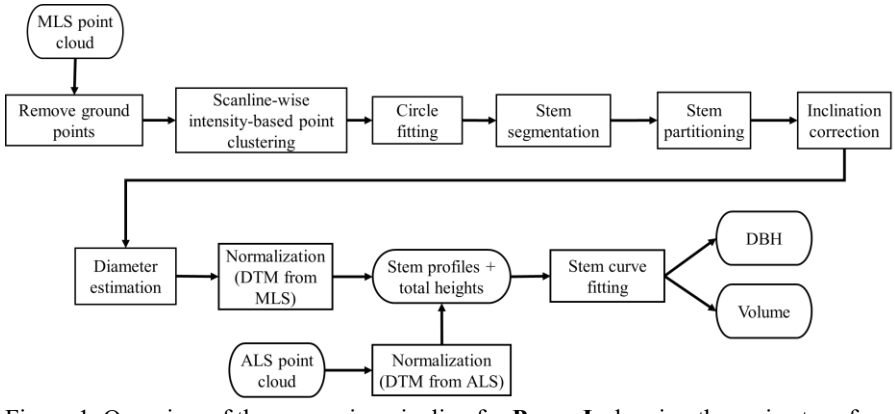

Figure 1. Overview of the processing pipeline for **Paper I**, showing the main steps from extraction of tree-level attributes from car-mounted Mobile Laser Scanning (MLS). DTM = Digital Terrain Model. ALS = Aerial Laser Scanning. DBH = Diameter at Breast Height.

The ALS data used in **Paper I** was collected in October 2019 using a Leica TerrainMapper-LN sensor operating at a pulse frequency of 1600 Hz and a field of view of 30°. The system was flown at an approximate altitude of 1450 meters, with the airplane maintaining an average speed of 213 km/h (equivalent to 115 knots). This configuration produced a footprint size of about 35 cm and yielded a mean point density of 22 points/m^2 across the study area.

In this study, the main data source used a car-mounted MLS system composed by a RIEGL VUX-1LR (RIEGL Laser Measurement Systems

GmbH, Horn, Austria), a GNSS and an IMU. The data collection was done in November 2019, covering approximately 7 kilometers of forest roads, with both sides of the road scanned at a driving speed of 8 km/h. The LiDAR sensor, operating in the near-infrared wavelength (1550 nm), was mounted at an angle of 30° from the horizontal plane, oriented upwards and turned towards the front of the vehicle. This configuration was chosen to reduce the influence of GNSS/IMU positioning errors on stem diameter estimation, as the stem curvature could be observed in a single scan sweep (as in a horizontal mount) while still capturing some ground information (as in a vertical mount). In addition, the scanner's sweep frequency was reduced compared to standard settings to achieve denser sampling within each scan line for more accurate diameter estimation, while accepting greater spacing between consecutive lines. The sensor emitted pulses at a frequency of 820 Hz and featured a 330° field of view, producing an angular step width of 0.0066°. At a distance of 100 m, the pulse footprint measured approximately 5 cm. The system recorded up to three returns per emitted pulse and achieved a ranging accuracy of 1.5 cm at 150 m. A sample resulting point cloud is shown in Figure 2.

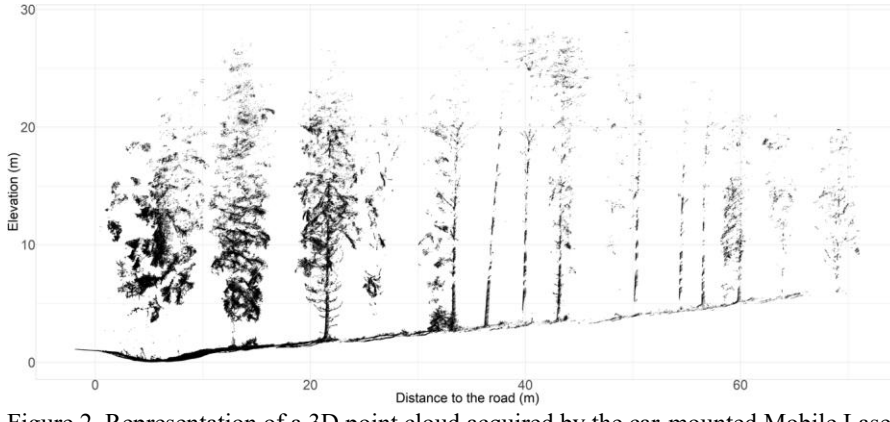

Figure 2. Representation of a 3D point cloud acquired by the car-mounted Mobile Laser Scanning system. The left side is closer to the sensor than the right side and has more points in the canopy and on the stem compared to the trees on the right side of the figure.

Finally, TLS data was used as validation for the stem curve and DBH estimates from the car-mounted MLS system. In this case, a Trimble TX8 scanner was used. This system operates in the near-infrared wavelength (1500 nm) and emits one million points per second. The sensor had a full

360° horizontal and 317° vertical field of view. At a distance of 100 m, the point spacing was approximately 4 cm, while the beam footprint expanded to 3.4 cm. Stem profiles were extracted from the TLS point cloud following the method described by Olofsson and Holmgren (2016).

2.1.1 Paper I: Methodology

Due to the scanning configuration, with high pulse repetition rate and low scanning frequency, the point cloud had high spatial resolution within scan lines (point spacing of approximately 0.5 cm at 40 m) and wider gaps between two consecutive lines (approximately 17 cm at 40 m). Such configuration resulted in stems being represented not as continuous cylindrical surfaces but as discrete cross-sectional arcs (Figure 3), guiding the detection algorithm which detects circles – or arcs - scan line-wise.

Stem arc detection within each scan line began with spatial clustering of neighboring points. The clustering threshold was derived from the sensor's angular step width and range accuracy. In practice, this meant calculating the expected spacing between consecutive echoes on a flat surface at a given range from the sensor, then adding a margin to account for the sensor's ranging uncertainty and surface curvature. Points within the same scan line that were closer than this adaptive threshold were grouped as belonging to the same object. This approach allowed stem points to be clustered consistently, regardless of their distance from the scanner.

Once clusters were formed, an intensity-based filter was applied to reduce the number of partial returns – as observed by Forsman et al. (2018). For each cluster, points with intensity < 70% of the 95th percentile of return intensity in that cluster were excluded. This step served to prioritize echoes from solid surfaces, excluding low intensity returns often associated with foliage and edges.

To determine if a cluster corresponded to a stem arc, circles were fit to the filtered point clusters using a modified RANSAC (Random Sample Consensus) approach. The procedure went as follows: in each iteration, three points were randomly sampled from a cluster to define a candidate circle. A circle was accepted as a potential stem arc if it maximized the number of inliers - points lying within a tolerance distance (equal to the sensor's range accuracy at 150 m, 1.5 cm) from the circle perimeter. An additional constraint was applied: candidate circles containing a significant number of interior outliers were rejected, since true laser returns should lie only on or

outside the stem surface. The circle with the largest inlier count amongst valid candidates was selected as the best fit, and its center, radius, and average height were recorded.

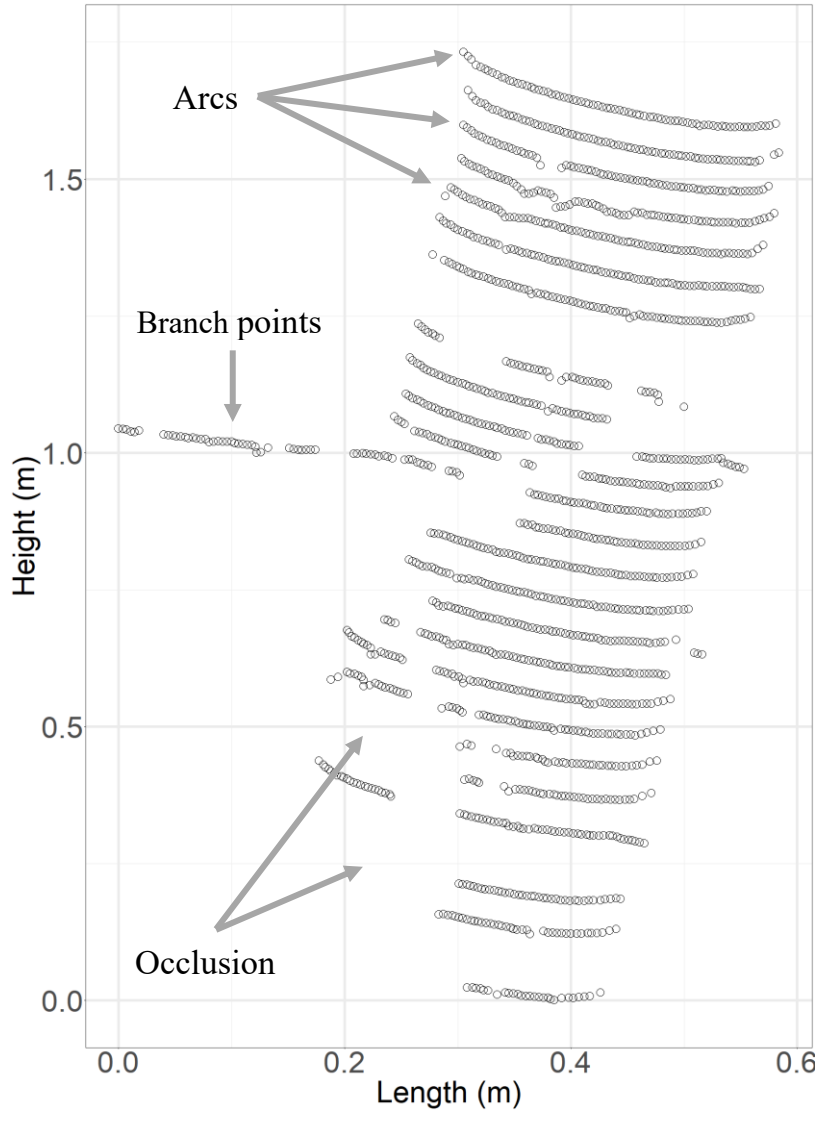

Figure 3. Representation of a stem section in the car-mounted Mobile Laser Scanning (MLS) point cloud. The stem is represented as a collection of arcs. It is possible to notice branches and shaded areas (occlusion). Individual tree detection begins with identifying these arcs within each scan line.

Since arcs were detected independently in each scan line, they were aggregated vertically to form the full stems. For that, the centers of arcs within a fixed horizontal neighborhood (here defined as 50 cm) were used to estimate a local stem direction vector, as in the study by Holmgren et al. (2019). This strategy aimed at grouping arcs that corresponded to the same physical stem even in the presence of gaps due to occlusion.

After stem reconstruction, each tree was divided into vertical sections (formed by multiple arcs) to estimate stem profiles. For each section, diameters were then estimated using a second RANSAC-based circle fitting procedure. In this step, the circles were fit using a two-step process: a preliminary circle was fit using the same RANSAC criteria as before, and its radius and center are used to select a refined subset of points located within a tolerance band (e.g., 1.1 times the estimated radius). A final least-squares fit on this subset provides the segment's diameter.

The extracted diameter values and their respective heights were used to fit a taper curve to each tree. In this step, a composite model averaging a quadratic taper and a square root function was applied, providing a smooth, robust stem profile even when only a few measurements (arcs) were available. For more details on the taper curve methodology, equations and thresholding used, we refer to **Paper I**. Total tree heights were retrieved for each tree from ALS data over the study area, as the highest return within a small radius (30 cm) of the stem base. Stem volume values were obtained by integrating the taper curve, and DBH values were determined using the diameter value extracted from the taper curve at 1.3 m.

Stem detection was validated against field inventory data, and the extracted DBH, stem curves and stem volumes were validated against TLS reference data. The validation was carried independently in six distance zones, extending from the forest road into the stand: 0–10 m, 10–20 m, 20–30 m, 30–40 m, 40–50 m, and 50–60 m. For each zone, MLS-detected tree positions were matched to field-measured stem positions within a 30 cm search radius. Matched stems were treated as true positives, unmatched MLS detections as commission errors, and unmatched field-measured stems as omissions. Based on these, standard metrics of precision (P - Equation 1) and recall (R – Equation 2) were computed for each distance band to assess detection performance.

(1) $$Precision_p = TP_p/(TP_p + C_p)$$

(2) $$Recall = TP_p/(TP_p + O_p)$$

where TP_p is the number of trees correctly detected trees (true positives), C_p and O_p are the number of commission and omission errors in zone p, also known as false positives and false negatives, respectively.

For the correctly detected trees, MLS-derived DBH, stem profiles, and volume estimates were compared to TLS-derived values using Root Mean Square Error (RMSE – Equation 3) and bias (Equation 4). For that, stem profiles were extracted from the TLS point cloud as described by Olofsson and Holmgren (2016). Later, DBH and volume were estimated using TLS-derived stem profiles under the same methodology as for MLS-derived data. This zone-wise validation design allowed for an assessment of how both detection rates and attribute accuracy were influenced by the increasing distance between trees and the MLS trajectory – i.e. distance to the road.

(3) $$RMSE = \sqrt{\sum_{i=1}^{n}(\hat{y}_i - y_i)^2/n}$$

(4) $$bias = \sum_{i=1}^{n}(\hat{y}_i - y_i)/n$$

where n is the number of trees. $\hat{y}_i$ and y_i are target variable's predicted and observed values for tree i.

2.2 Paper II: Mobile laser scanning as reference for estimation of stem attributes from airborne laser scanning

The main objective of **Paper II** was to assess the suitability of the car-mounted MLS described in **Paper I** as an alternative to traditional field inventory for collecting reference data in a tree-level forest inventory based on remote sensing. Specifically, the study aimed at estimating DBH and stem volume at the individual tree-level from ALS data, using reference – or training - datasets derived either from conventional field measurements or from MLS data. The motivation for this analysis is the potential efficiency gains in forest inventories and the opportunity to increase the amount of collected data compared to traditional methods.

Paper II was conducted in Remningstorp (Figure 4 A - lat. 58.5° N, long. 13.6° E). The ALS data used is described in section 2.1. The aerial point clouds were first segmented into individual tree crowns using the two-

dimensional segmentation algorithm by Holmgren et al. (2022). The resulting segments were considered individual trees.

As previously stated, two reference datasets were collected in the study area using different data collection methods. The first was obtained through conventional field inventory, namely the "field inventory dataset", or simply "FI dataset". The survey consisted of 265 circular plots with a 10 m radius, systematically distributed across the study area with 200 m spacing between plot centers (Figure 4 A). In each plot, all living trees with DBH ≥ 4 cm were recorded, including DBH and stem position using a DP POSTEX system (www.haglofsweden.com). A co-registration algorithm was used to align field-measured tree positions with the ALS-derived crown segments, following the method described by Olofsson et al. (2008). This algorithm uses cross-correlation of images created from positions and tree sizes as measured by ALS and field inventory, respectively. Since ALS-derived segments were treated as individual trees, if multiple field-recorded trees were assigned to the same segment, the tree with the largest DBH was retained. Unmatched field trees were treated as omission errors, while unmatched ALS segments were treated as commission errors. A total of 181 plots remained in the final field inventory dataset, corresponding to 3023 individual trees that were successfully matched to their respective ALS segments (Figure 5). For further details on the field inventory dataset, we refer to **Paper II**.

The second reference dataset used was collected using the MLS system described in **Paper I** (section 2.1) and is referred to as the "MLS dataset". The tree detection and attribute estimation methodology followed all steps previously described in section 2.1.1. However, data collection was restricted to trees located between 20 to 40 m from the roadside to avoid biases associated with edge effects and tree detection errors. This distance range had previously demonstrated the best balance between stem attribute accuracy and detection rates (Pires et al. 2022). Within this range, the survey covered approximately 28 ha of forest. MLS-derived tree positions showed a systematic displacement of approximately 1.5 m relative to ALS segments, so tree positions were manually adjusted to ensure alignment. In total, the position of 6432 MLS-derived trees matched corresponding ALS crowns (Figure 5).

Before training the models to estimate stem attributes based on the FI and MLS datasets, the trees in the FI dataset were divided into training and

validation groups according to their field plots, thereby creating a benchmark dataset for both MLS- and FI-derived models. Specifically, 70% of the plots in the FI dataset (2050 trees) were used for training, while the remaining 30% (973 trees) were reserved for validation (crosses in Figure 4 A). Consequently, the FI-based models were trained on 70% of the FI dataset, whereas the MLS-based models were trained using the entire MLS dataset. All models were then validated against the 30% validation portion of the FI dataset.

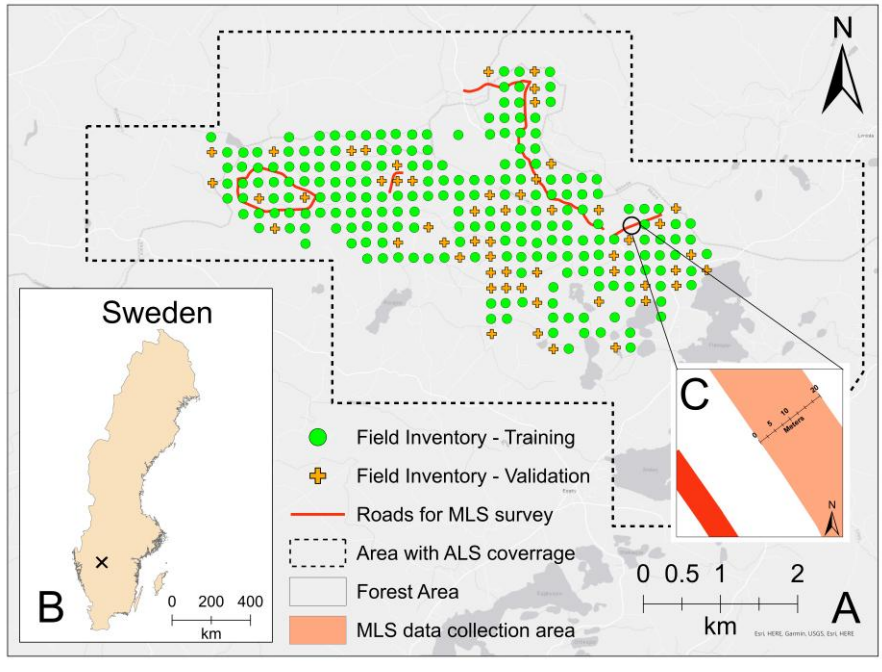

Figure 4. (A) Overview of the study area used in **Papers I** and **II**, with field plots used for training showed as green circles, the field inventory plots used for validation shown as orange crosses and the roads scanned by Mobile Laser Scanning (MLS) survey in red. (B) Position of the study area in Sweden. (C) Close-up on the area from which MLS data was collected, considering the 20-40m distance range to the roadside.

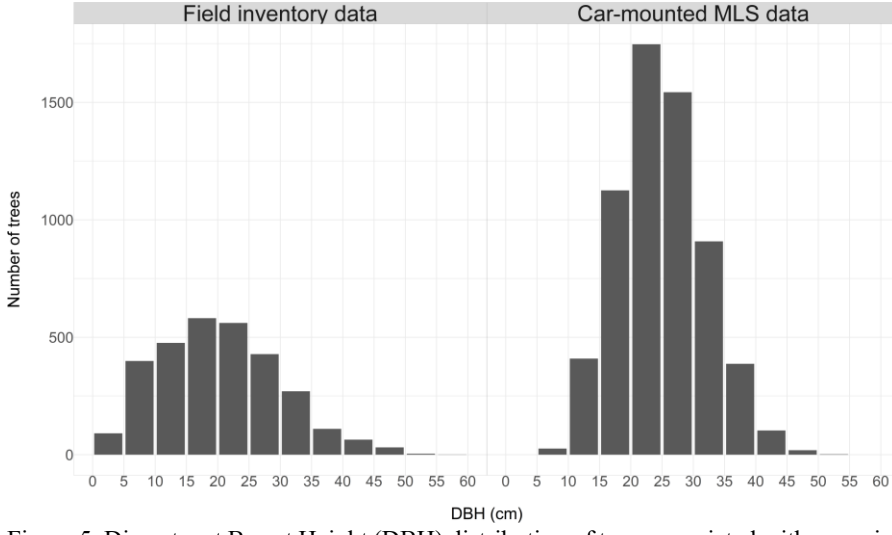

Figure 5. Diameter at Breast Height (DBH) distribution of trees associated with an aerial laser scanner-derived tree crown in the field inventory and car-mounted Mobile Laser Scanning (MLS) datasets.

2.2.1 Paper II: Methodology

In **Paper II**, a set of metrics was derived from the segmented ALS data, such as height percentiles, intensity percentiles, and crown-related attributes (Table 2). These metrics served as predictors in subsequent statistical models.

Table 2. Description of the Aerial Laser Scanning (ALS)-based metrics used as independent variables in **Paper II**.

Metric	Description
$h_{10} - h_{99}$	10th to the 99th height percentiles
$i_{10} - i_{99}$	10th to the 99th intensity percentiles
$mean_i$	Mean of intensity values
std_i	Standard deviation of intensity values
$skew_i$	Skewness of intensity values
kur_i	Kurtosis of intensity values
CR	Crown radius
CA	Crown area
CE	Extent of crown polygon
$CRh95$	$CR \cdot h_{95}$
CR^2h95_{sqrt}	$\sqrt{\mathrm{CR}^2 \cdot h_{95}}$

Once the reference datasets with target variables were defined, models predicting DBH and stem volume from ALS-derived metrics were trained separately using each of the two reference datasets. For that, regression coefficients were estimated using ordinary least squares (OLS), and the optimal combination of predictor variables was selected using a backward elimination method to minimize collinearity. During stem volume estimation, a logarithmic transformation was applied to both stem volumes and ALS-derived metrics to enhance linearity. Biases introduced by this transformation were corrected using a ratio estimator based on the sum of observed and predicted volumes (Holm 1977).

The performance of the two sets of predictive models, one trained on FI data and the other on MLS data, was validated against an independent subset of the FI dataset, not used in training (crosses in Figure 4 A). Validation was done at tree- and plot-levels in terms of RMSE and bias (Equations 3 and 4, respectively). Individual tree-level DBH and stem volume estimates were compared directly against field measurements, while plot-level stem volume estimates were derived by summing individual tree predictions within each validation plot.

2.3 Paper III: Boreal tree species classification using airborne laser scanning data annotated with harvester production reports, and convolutional neural networks

Paper III explored the use of HPRs as an alternative data source for automatic tree-level annotation of ALS data. Linking ALS data with spatially explicit HPRs, containing species and GNSS-based tree positions, provided rapid and nearly cost-free training data for CNN-based tree species classification. In addition, we evaluated how both spatial and spectral characteristics of ALS data affect tree species classification performance under the proposed methodology.

The analysis in **Paper III** was conducted in the municipality of Hällefors, in Southern Sweden (lat. 59.46° N, long. 14.31° E) in Norway spruce–dominated production forests. In total, 17 stands were included in the study, with areas ranging from 3.7 to 16.8 hectares. The stands were selected based on their planned harvesting dates, which occurred between 2021 and 2022.

In the harvested stands, Norway spruce was the dominant species (~79%), followed by Scots pine (~11%) and birch species (*Betula* spp.; ~10%).

In this paper, the ALS data collection was done using a dual-wavelength system, developed by the Finnish Geospatial Institute (FGI) and described by Hakula et al. (2023). The setup consisted of two single-wavelength LiDAR sensors: a RIEGL miniVUX-1UAV (~100 points/m²) operating at 905 nm (near-infrared) and a RIEGL VUX-1HA (~875 points/m²) operating at 1550 nm (shortwave infrared). These sensors were mounted on a helicopter flown at an altitude of 100 meters at a speed of approximately 50 km/h. Although the system was originally equipped with a third (green-wavelength) scanner, data from that channel was unavailable due to technical problems, and only the near- and shortwave infrared returns were used to generate the final dual-wavelength point cloud.

2.3.1 Paper III: Methodology

In forest environments, point clouds with higher point density often provide greater sampling of crown surfaces, allowing fine-scale differences in crown shape, branch structure, and canopy texture to be more clearly observed, features critical for species discrimination. Another important factor is the laser beam footprint, defined by the beam's divergence and distance to the target, which determines the area illuminated when the beam hits a surface. This property affects how leaves, branches, and canopy gaps are represented in the point cloud, as a smaller footprint can capture narrower branches and smaller gaps more clearly, while a larger footprint tends to blur finer details.

Beyond spatial properties, the wavelength of the emitted pulses also plays a key role in describing forest environments, as different wavelengths interact differently with vegetation. Using multiple wavelengths can therefore provide complementary information on canopy structure and species traits, supporting more accurate classification.

To compare the impact of both spectral (wavelength) and spatial (point density and footprint) resolutions on the classification performance, three ALS datasets were derived from the data collection (Table 3): (1) the miniVUX dataset (905 nm, lower point density, larger footprint), (2) the VUX dataset (1550 nm, higher point density, smaller footprint), and (3) a dual-wavelength dataset combining co-registered returns from both sensors (higher spatial and spectral resolutions).

Table 3. Description of the Aerial Laser Scanning (ALS) datasets used for tree species classification.

	ALS dataset		
	MiniVUX (1)	**VUX (2)**	**Dual-wavelength (1+2)**
Sensor(s)	miniVUX-1UAV	VUX-1HA	miniVUX-1UAV (1) + VUX-1HA (2)
Footprint at 100 m from the target (cm)	16 x 5	5	16 x 5 (1) + 5 (2)
PRR[1] (kHz)	100	1017	100 (1) + 1017 (2)
Scan speed (revolutions/s)	100	143	100 (1) + 143 (2)
Point density (points/m^2)	100	875	975 (1+2)
Wavelength (nm)	905	1550	905 (1) + 1550 (2)

Note. [1]Pulse Repetition Rate.

A total of 69,253 trees were harvested between November 2021 and October 2022 across 17 stands using a CTL harvester equipped with a GNSS-based positioning system. This system combined two GNSS receivers on the harvester cabin with built-in sensors that recorded boom angle and extension at the time of felling, allowing estimation of each tree's position. From the HPRs, each tree's species, DBH, and log lengths were extracted. Tree species were grouped into three classes: Norway spruce, Scots pine, and a combined "Deciduous" class merging birch and other broadleaves.

To generate training labels, individual tree crowns were first segmented from the dual-wavelength ALS point cloud using the two-dimensional segmentation algorithm by Holmgren et al. (2022). Tree-level annotation was performed by matching each HPR-recorded tree position to the nearest ALS-derived tree segment, using the distance and similarity in tree height as matching criteria. This matching procedure avoided the need for extensive visual interpretation. For further details on the annotation procedure, we refer to **Paper III**.

Altogether, 45,516 tree positions were linked to an ALS-derived segment, representing 65.7 % of all harvested trees. Of those, 36,162 trees (79.4 %) were Norway spruces, 5,397 trees (11.9 %) Scots pine, and 3,957 (8.7 %) were deciduous trees. Finally, the number of labeled trees in each class was downsampled to the number of trees in the class with least instances ("deciduous"). After downsampling, a brief quality-control step was

conducted to ensure label reliability. Segments that clearly did not correspond to trees (e.g., artifacts from segmentation) were assigned to a separate "Noise" class across all ALS datasets. Additionally, 228 trees (0.5% of matched cases) with evident species-label inconsistencies, likely due to harvester annotation errors or mismatches in spatial alignment, were excluded to avoid using incorrect labels for training the model. Thus, the final dataset was composed by 3772 "Pine", 3559 "Spruce", and 3459 "deciduous" trees, with 853 segments being sorted as "Noise".

After sorting the tree segments into classes, each tree point cloud was converted into a set of two-dimensional raster images. Converting the point clouds into 2D allowed leveraging state-of-the-art CNN architecture without requiring voxelization or point-based models. To increase the number of representations for each tree, side-view projections were created by rotating the point cloud around the vertical axis (Z) in 45° intervals, resulting in four projections per tree. For each rotation, points were projected onto a vertical (X vs. Z) plane and rasterized into a grayscale or RGB images, depending on the ALS dataset used.

In the miniVUX and VUX datasets (single-wavelength), grayscale images were created with pixel values representing the point density, i.e., the number of returns within each pixel. No intensity or spectral information was used in these cases. In contrast, images derived from the dual-wavelength dataset were created as RGB false-color composites. The red channel was assigned the mean intensity of NIR points, the green channel the mean intensity of SWIR points, and the blue channel the Normalized Difference Infrared Index (NDII – Equation 5), considering all returns. In both cases, the pixel and image sizes were defined based on the tree's size and the point density, ensuring an even representation of structure without cropping the trees or leaving blank spaces. For further details on the rasterization of point clouds and image generation, we refer to **Paper III**.

(5) $$NDII_k = \frac{nir_k - swir_k}{nir_k + swir_k}$$

where *nir* is the mean intensity of the returns from the miniVUX dataset, and *swir* is the mean intensity of the returns from the VUX dataset for pixel *k*.

For the classification task, we used a CNN from the YOLO family - YOLOv8s-cls - due to its performance in classification problems and its user-friendly PyTorch implementation (Jocher et al. 2023). The model was trained

for 15 epochs using default settings. Because each tree was represented by four side-view images, each species class was composed of approximately 14,000 images. The dataset was split into 70% for training and 30% for validation. To prevent a tree from being used in both sets, each tree was assigned exclusively to one set, so that all four views of a given tree were used either for training or for validation. YOLO networks have proven effective in forestry-related applications such as tree detection and wood defect identification (Fang et al. 2021; Straker et al. 2023), making YOLOv8 an ideal choice for species classification in this context.

The testing procedure followed a leave-one-stand-out cross-validation design: in each round, one stand was excluded from the training and validation datasets and used for testing, allowing a realistic accuracy assessment across different areas. Tree-level predictions were aggregated across views by averaging class probabilities, and the highest-probability class was assigned as the final label. Model performances were evaluated using confusion matrices and standard metrics: overall accuracy (OA – Equation 6), F1-score (Equation 7), precision (P - Equation 1) and recall (R - Equation 2), and macro F1-score, which is the average of each class's F1-score.

(6) $$OA = TP/N$$

(7) $$F1_C = 2 \cdot P_C \cdot R_C/(P_C + R_C)$$

where TP is the number of true positives, and N represents the number of trees analyzed in this study. P_C is the precision, and R_C is the recall of class C.

2.4 Paper IV: Stem crook detection in terrestrial laser scanning data using semi-empirical simulations

Paper IV presented a semi-empirical method for generating synthetic crook deformations on TLS-derived stem point clouds, which were then used to train a CNN for crook detection. This study was motivated by the lack of labeled data for stem defects such as crooks, which limits the training and testing of methodologies for detecting such defects, especially using machine learning models.

The analysis in **Paper IV** was conducted in northern Sweden, in Scots pine–dominated forests located near Sävar (Figure 6 A - lat. 64° N, long. 20.6° E) and Tribladsberget (Figure 6 B - lat. 64.3° N, long. 19.8° E). The TLS surveys were performed using a Leica RTC360 system, which operates at a wavelength of 1550 nm. The scanning mode provided point spacing of approximately 6 mm at 10 m range. The system captures up to 2 million points per second, with a full 360° horizontal and 300° vertical field of view. The range accuracy is 1.9 mm at 10 m.

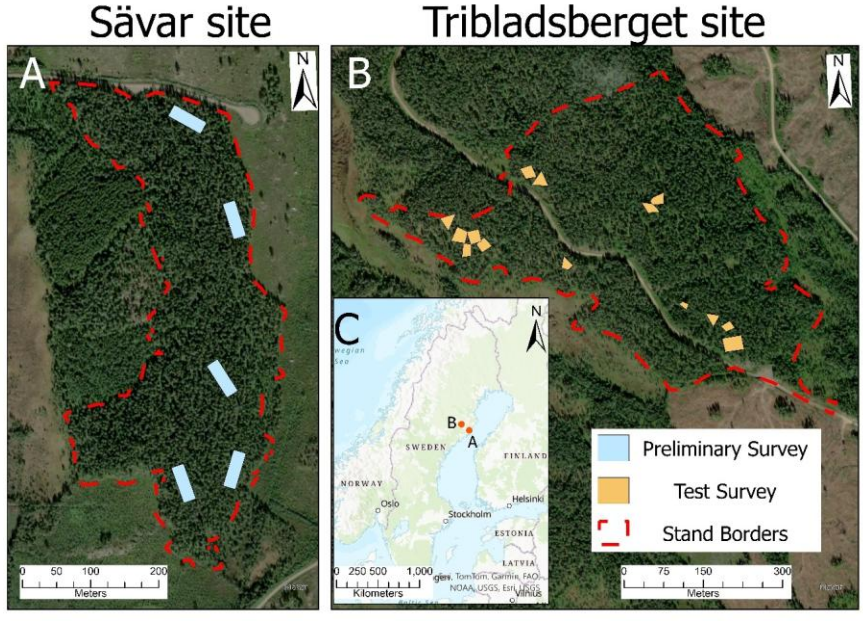

Figure 6. (A) Overview of the Sävar site, and the field plots where a preliminary survey to collect model stems was conducted. (B) Overview of the Tribladsberget site, and the field plots where the test survey was conducted. (C) Position of the Sävar and Tribladsberget sites in Sweden.

A preliminary survey was first conducted at the Sävar site, in a Scots pine-dominated stand (Figure 6 A). Data were collected in five 15 × 50 m plots. There, the multi-scan TLS acquisition was performed by placing the scanner along the plot perimeter every 5–10 m, requiring 15–20 scans per plot. In total, 287 stems were extracted from the five plots. Of these, seven crooked trees were marked in the field and manually identified in the point clouds, providing reference examples to guide the simulation of crooks.

A second survey was later carried out at Tribladsberget in areas with high concentrations of crooked trees (Figure 6 B). Like the Sävar site, the stand was also Scots pine-dominated. However, in this survey plots had no fixed size. Instead, the scanning focused on crooked trees, with 4-10 TLS scans collected around individual trees or clusters across 14 plots. Black-and-white reflective targets were placed at the plot corners, and their coordinates were measured with GNSS. These targets were used both to georeference the TLS data and to define the plot boundaries, which were delineated by connecting the target positions into closed polygons. Altogether, the mapped area covered 0.622 ha, from which 310 stems were extracted.

2.4.1 Paper IV: Methodology

The analysis in **Paper IV** started with setting the definition of crooks based on Swedish log grading guidelines and field observations (Biometria 2025). In these guidelines, crooks are described as noticeable deviations from vertical growth, often abrupt and visually distinctive (Figure 7). To inform simulation parameters, we carried out inspections in the Sävar site (Figure 6 A) and at the Sävar sawmill. Observations from these visits guided the dimensions and shapes of the crooks ultimately simulated in the study. Synthetic crooks were created by deforming stem point clouds of Scots pine trees captured during the TLS survey on the Sävar site. A total of 280 defect-free model stems were segmented using 3DFin (Laino et al. 2024) up to a height of 25 m and used as the basis for simulation. Crooks were generated by modifying the X-coordinates of points along the stem using cubic smoothing splines, while keeping the Y and Z coordinates fixed. Two crook types were implemented: (1) a single-direction bend (*1dir*), and (2) a double-direction bend with an inflection point (*2dir*), each parameterized by crook length (l), starting height (s), horizontal deviation (d), and, for *2dir* crooks, the inflection position (ip) and the inflection extension (ie). Figure 8 illustrates the types of crooks that were modelled. These parameters were defined based on crook characteristics observed during visits to the sawmill and forest site and were then randomly sampled within those observed ranges (Table 4). For each stem, 50 unique deformations were generated, resulting in a total of 14,000 simulated crooks. For further details on the crook simulation, we refer to **Paper IV**.

Figure 7. Example of a crook in a standing tree (photo by Nils Lindgren, used with permission).

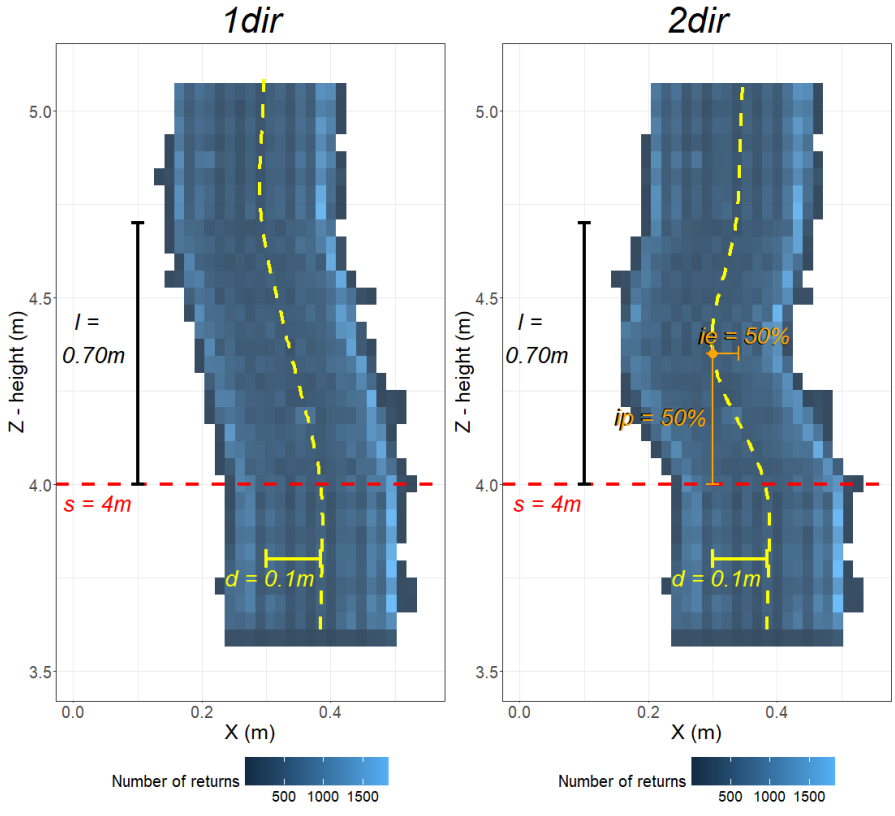

Figure 8. Schematic representation of the one (*1dir*) and two directional (*2dir*) crooks in a model Scots pine (*Pinus sylvestris* L.) stem. All points along the predefined crook length (*l*) are shifted according to the smooth spline (dashed yellow line). *s* = crook starting height, *d* = crook deviation, *ip* = inflection position, *ie* = inflection extension.

Table 4. Parameter ranges used for simulating crook deformations in synthetic stem point clouds.

Parameter	Minimum	Maximum	Increment
Crook length (*l*)	30 cm	120 cm	2 cm
Crook deviation (*d*)	5 cm	25 cm	2 cm
Inflection position (*ip*)	25%	50%	2%
Inflection extension (*ie*)	50%	100%	2%
Starting height (*s*)	30 cm	90th height percentile	25 cm

Prior to crook detection, the 3D point clouds were converted into 2D binary raster images. Each stem was divided into vertical sections of 2 m

height, with a 0.5 m overlap between adjacent sections. Each section was then rotated around the vertical axis in 20° increments (from 0° to 160°), producing nine views per section. Each view was rasterized into a 192 × 96 binary raster, where pixels encoded presence (1) or absence (0) of points in the corresponding spatial region.

The rasterized stem images were then used as training input to a CNN for crook detection. In this study, we used YOLOv8s (Jocher et al. 2023), a version of the YOLO (You Only Look Once) object detection architecture. YOLOv8s was selected due to its efficient performance and suitability for small, single-class detection problems, as well as its accessible implementation in PyTorch. The model consists of a backbone for feature extraction, a neck for multi-scale feature fusion, and a prediction head for bounding box regression. The model was trained for 15 epochs with a batch size of 128 and a dropout rate of 0.25 to reduce overfitting. The dataset was randomly split into training and validation subsets, with 30% of the images reserved for validation at the end of each epoch. To ensure independence between the subsets, all viewpoints from the same simulated stem were assigned exclusively to either training or validation.

The survey on Tribladsberget (Figure 6 B) was used to test the crook detector. All 310 stems were visually inspected for crooks by dividing each stem into consecutive 2 m sections with 0.5 m overlap, ensuring continuous assessment. Crooks were annotated following Biometria's guidelines as visible deviations from vertical growth, including both gradual shifts and abrupt bends, with epicormic branches or stem wounds often serving as cues. For each crook, start and end points were marked where the deviation began and where the stem resumed straight growth, resulting in 65 annotated crooks.

For inference, stems from Tribladsberget site were rasterized using the same procedure as for training. The trained CNN was applied independently to each raster view, and for each stem section, bounding boxes from different views were merged by averaging center coordinates and box sizes. A prediction was considered a true positive if its intersection-over-union (IoU – Equation 8) with a ground-truth crook exceeded a given threshold. Omission and commission were also recorded.

(8) $$IoU = Area\ of\ Intersection\ /\ Area\ of\ Union$$

The final accuracy assessment was based on standard object detection metrics: precision (Equation 1), recall (Equation 2), and F1-score (Equation 7). In addition, a sensitivity analysis was performed across multiple IoU thresholds ($IoU \in [0.01,1]$) to assess how detection performance responded to varying levels of spatial agreement between predictions and visual assessments. This approach ensured that the model's ability to generalize from synthetic training data to real-world data was evaluated under different levels of localization tolerance.

3. Results

3.1 Tree detection and attribute estimation from car-mounted MLS (Paper I)

In **Paper I**, tree detection accuracy varied with the distance to the roadside (Table 5). In this study, the best tree detection performance occurred between 10 m and 40 m distance to the roadside, with both precision and recall exceeding 92%. On the other hand, accuracy declined closer to the road (0-10 m range), due to a high presence of commission errors, likely caused by misclassified large branches and understory vegetation, and beyond 40 m, where increasing stem occlusion and decreasing point density likely led to omissions errors, i.e. lower recall.

Table 5. Individual tree detection precision and recall according to the distance range from the road.

Zone	Precision	Recall
0 – 10 m	82.8%	85.7%
10 – 20 m	96.5%	96.7%
20 – 30 m	98.8%	94.2%
30 – 40 m	92.5%	92.5%
40 – 50 m	98.0%	86.1%
50 – 60 m	100.0%	62.7%

DBH and stem volume estimates derived from MLS were compared to TLS references (Figure 9 and Figure 10). RMSEs for DBH ranged from 1.82 cm to 4.84 cm, also depending on distance to the roadside, while bias remained low and stable across zones (< 3%). MLS-derived stem profiles were also consistent with TLS reference values, particularly within 20–40 m from the roadside (Figure 11).

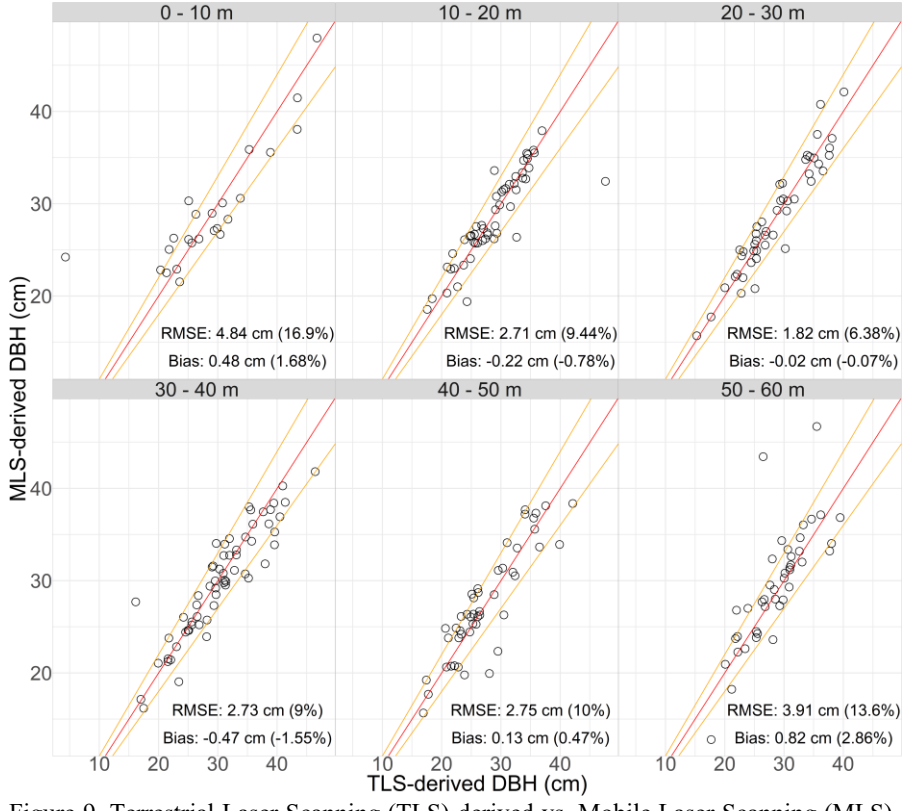

Figure 9. Terrestrial Laser Scanning (TLS)-derived vs. Mobile Laser Scanning (MLS)-derived Diameter at Breast Height (DBH), in cm. The red line is the 1:1 line, where reference and estimated values are equal. The orange lines represent a 10% deviation from the 1:1 line. RMSE = Root Mean Square Error.

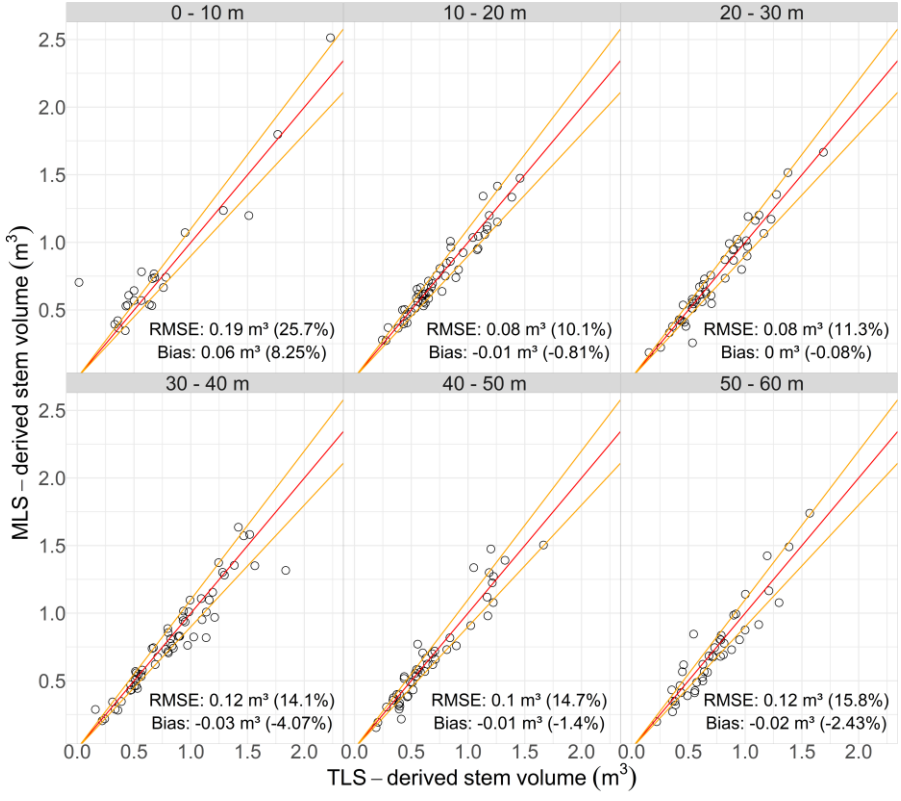

Figure 10. Terrestrial Laser Scanning (TLS)-derived vs. Mobile Laser Scanning (MLS)-derived stem volume, in m^3. The red line is the 1:1 line, where reference and estimated values are equal. The orange lines represent a 10% deviation from the 1:1 line. RMSE = Root Mean Square Error.

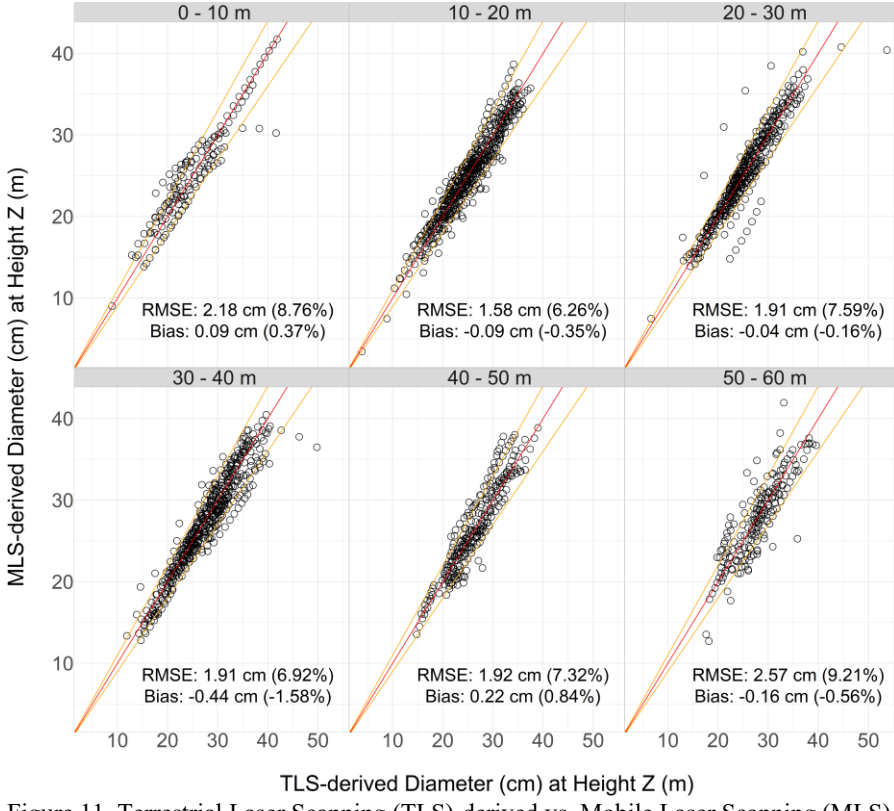

Figure 11. Terrestrial Laser Scanning (TLS)-derived vs. Mobile Laser Scanning (MLS)-derived stem profiles, in cm. The red line is the 1:1 line, where reference and estimated values are equal. The orange lines represent a 10% deviation from the 1:1 line.

3.2 ALS-based Estimation of Tree Attributes Using Field and MLS References (Paper II)

The results of **Paper II** showed that ALS-based models trained on MLS-derived reference data achieved equivalent performance to those trained on traditional field inventory (FI) data. Norway spruce trees' DBH estimates had RMSEs of 3.97 cm and 4.06 cm when using the MLS and FI datasets as reference, respectively (Figure 12). Tree-level stem volume estimation for the same species yielded RMSE values of 0.176 m³ for the MLS- and FI-based models in the same species group (Figure 13). However, while the estimates based on the MLS data had negligible biases, the FI-based estimated had bias of -5.71%.

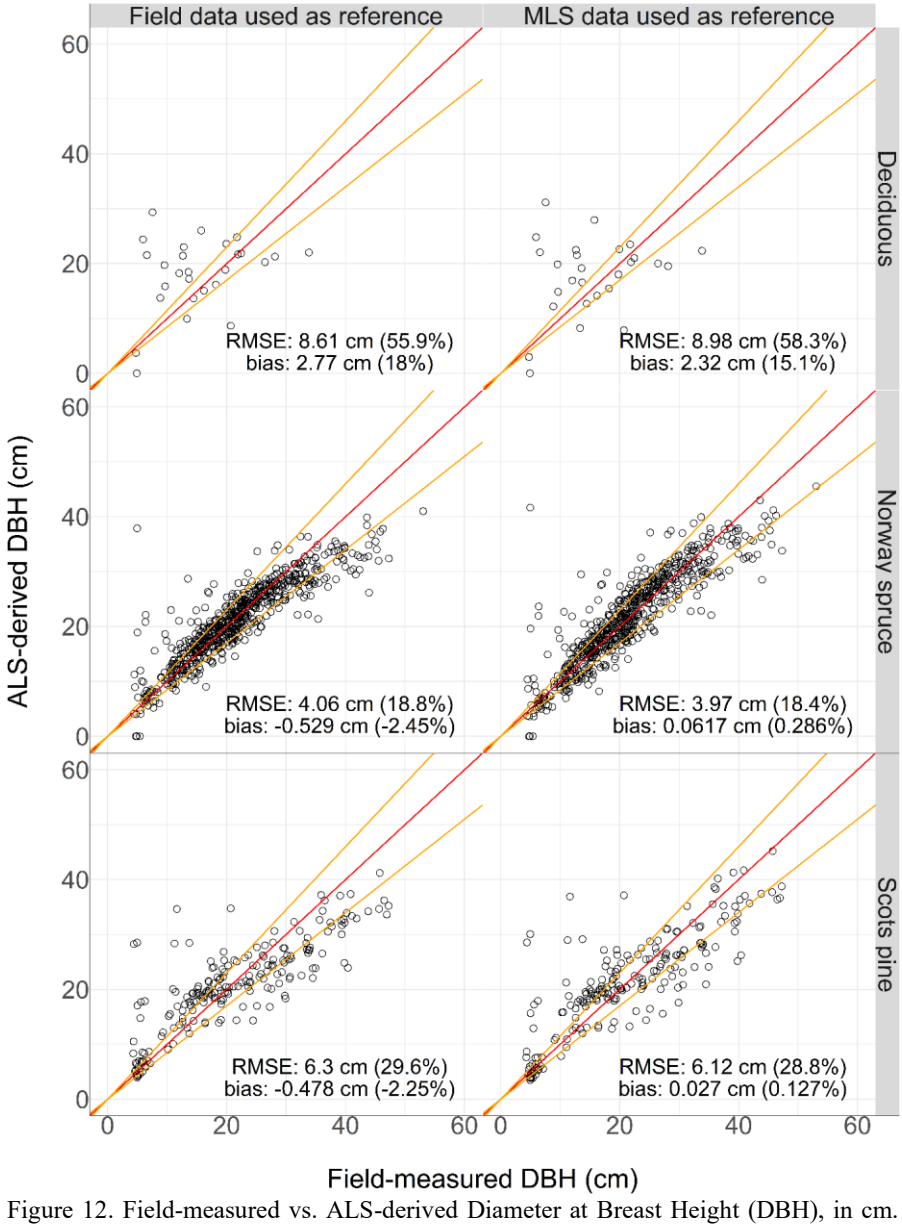

Figure 12. Field-measured vs. ALS-derived Diameter at Breast Height (DBH), in cm. The columns represent different reference datasets, and the rows represent the different species groups. The red line is the 1:1 line, where field-measured and ALS-derived values are equal. The orange lines represent a 15% deviation from the 1:1 line. RMSE = Root Mean Square Error.

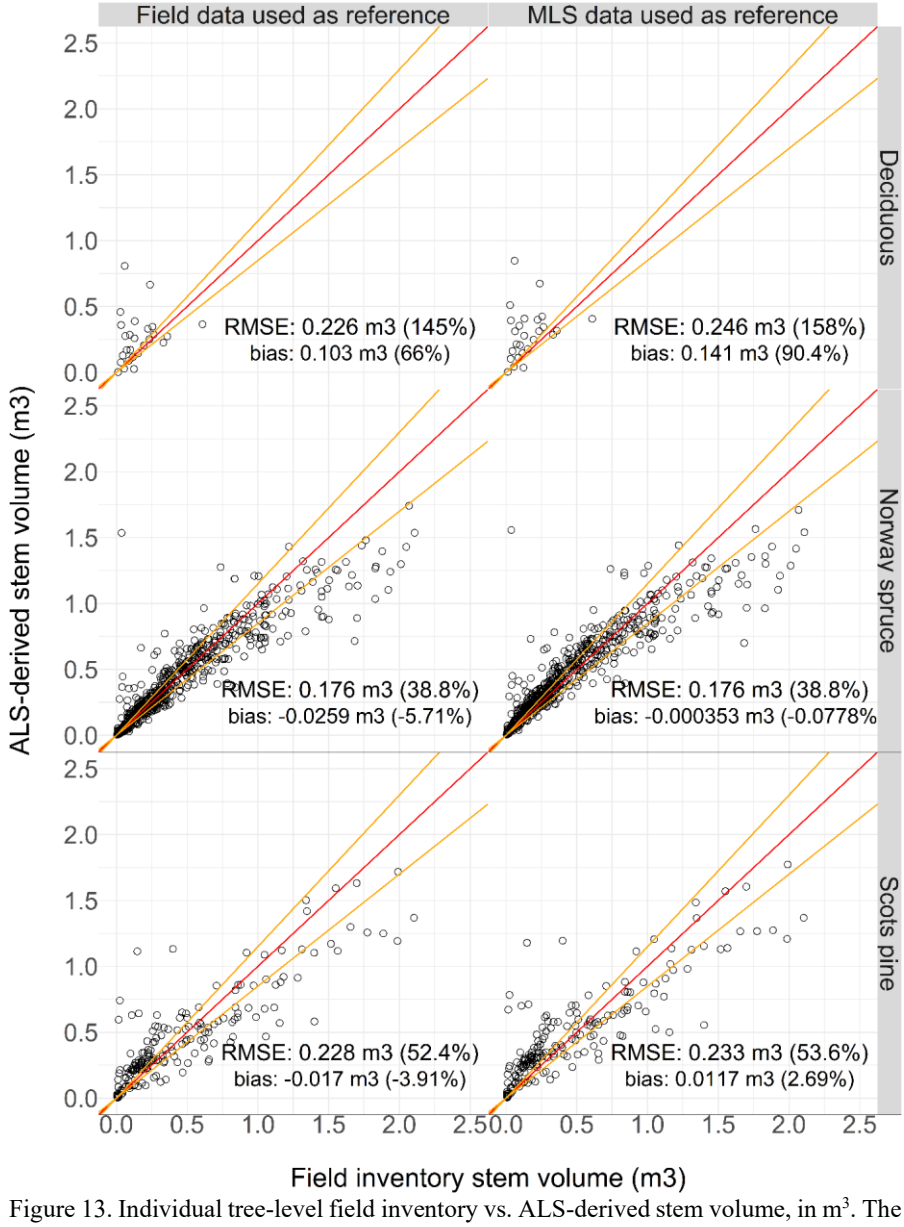

Figure 13. Individual tree-level field inventory vs. ALS-derived stem volume, in m^3. The columns represent different reference datasets, and the rows represent the different species groups. The red line is the 1:1 line, where the field inventory and ALS-derived values are equal. The orange lines represent a 15% deviation from the 1:1 line. RMSE = Root Mean Square Error.

At the plot level, stem volume predictions showed similar accuracy regardless of training source. The RMSE was 43.7 m³ (18.7%) with FI dataset and 46.2 m³ (19.8%) when using MLS dataset for training. Relative biases were -4.92% and 1.07% for the FI and MLS-based models, respectively (Figure 14).

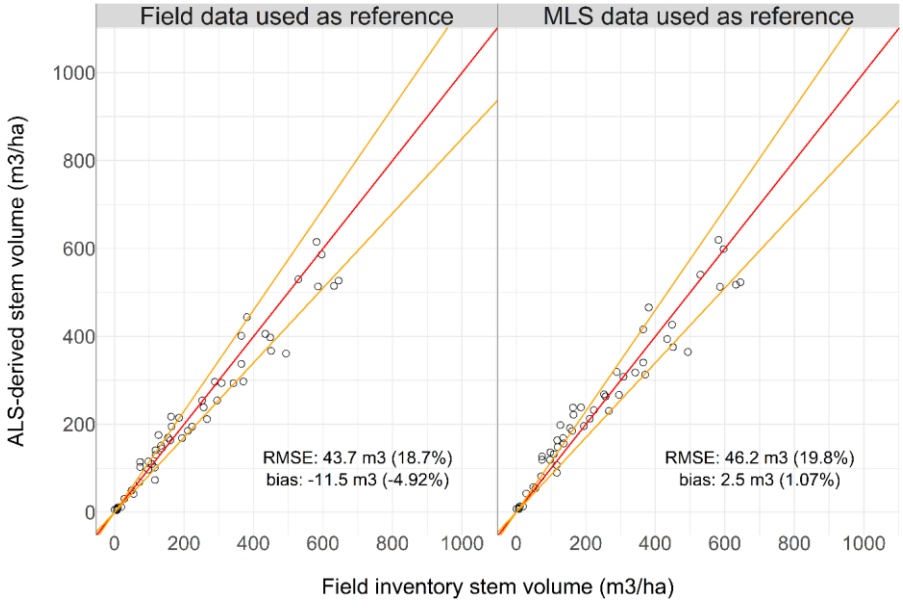

Figure 14. Plot-level field inventory vs. ALS-derived stem volume, in m³. The columns represent different reference datasets. The red line is the 1:1 line, where the field inventory and ALS-derived values are equal. The orange lines represent a 15% deviation from the 1:1 line. RMSE = Root Mean Square Error.

The variable selection step had similar outcomes regardless of the reference dataset used, prioritizing ALS height percentiles and crown-related metrics (Tables 6 and 7), with only minor differences in selected predictors. In both training scenarios, models with two predictors yielded the highest adjusted R^2. For DBH estimation (Table 6), the FI-based model relied on *h95* and *CA*, while the MLS-based model achieved best performance using *h95* and the crown ratio derived from *h95* (*CRh95*). For stem volume prediction (Table 7), both datasets led to the same variable combination: *h95* and *CA*. This consistency across models suggests that ALS-derived structural metrics related to tree height and crown size are strong predictors of stem dimensions, regardless of the reference source used.

Table 6. Models with one, two and three independent variables for Diameter at Breast Height (DBH) estimation using the forest inventory (FI) or car-mounted Mobile Laser Scanner (MLS).

N° of Predictors	FI dataset		MLS dataset	
	Model	Adj. R^2	Model	Adj. R^2
1	$DBH_{FI} = \alpha_1 \cdot h_{95}$	0.93	$DBH_{MLS} = \alpha_1 \cdot CRh95$	0.96
2	$DBH_{FI} = \alpha_1 \cdot h_{95} + \alpha_2 \cdot CR^2h95_{sqrt}$	0.94	$DBH_{MLS} = \alpha_1 \cdot CRh95 + \alpha_2 \cdot h_{95}$	0.98
3	$DBH_{FI} = \alpha_1 \cdot h_{95} + \alpha_2 \cdot CR^2h95_{sqrt} + \alpha_3 \cdot skew_i$	0.94	$DBH_{MLS} = \alpha_1 \cdot CRh95 + \alpha_2 \cdot h_{95} + \alpha_3 \cdot i_{90}$	0.98

Note. Adj. R^2 stands for the adjusted coefficient of determination (R^2).

Table 7. Models with one, two and three independent variables for stem volume estimation using the forest inventory (FI) or car-mounted Mobile Laser Scanner (MLS).

N° of Predictors	FI dataset		MLS dataset	
	Model	Adj. R^2	Model	Adj. R^2
1	$\hat{v}_{FI} = e^{\beta_0+\beta_1 \cdot ln\, h_{95}}$	0.78	$\hat{v}_{MLS} = e^{\beta_0+\beta_1 \cdot ln\, h_{95}}$	0.74
2	$\hat{v}_{FI} = e^{\beta_0+\beta_1 \cdot ln\, h_{95}+\beta_2 \cdot ln\, CA}$	0.80	$\hat{v}_{MLS} = e^{\beta_0+\beta_1 \cdot ln\, h_{95}+\beta_2 \cdot ln\, CA}$	0.79
3	$\hat{v}_{FI} = e^{\beta_0+\beta_1 \cdot ln\, h_{95}+\beta_2 \cdot ln\, CA+\beta_3 \cdot ln\, h_{10}}$	0.80	$\hat{v}_{MLS} = e^{\beta_0+\beta_1 \cdot ln\, h_{95}+\beta_2 \cdot ln\, CA+\beta_3 \cdot ln\, mean_i}$	0.79

Note. Adj. R^2 stands for the adjusted coefficient of determination (R^2). $\hat{v}$ is the estimated stem volume before bias correction.

Overall, results show that MLS data can be a reliable reference data collection method in remote sensing-based forest inventory. When used for ALS-based model training at tree-level, the data derived from this close-range remote sensing technique can pose as an alternative or complement to traditional field plots.

3.3 Tree Species Classification from ALS and HPR files (Paper III)

The resolution of the 2D images generated from the ALS point clouds played a significant role in the species classification performance. As shown in Table 8, image resolution varied across ALS datasets. Images created from the miniVUX dataset had the lowest average resolution, with a mean pixel size of 27.6 cm, often failing to capture fine crown details. In contrast, the VUX and dual-wavelength datasets produced images with significantly

higher resolution - 10.1 cm and 9.5 cm average pixel sizes, respectively – often preserving structural traits such as trunk and crown shape (Figure 15).

Table 8. Average pixel size (cm) for the tree species classes and noise class (± standard deviation). Different letters in the last row denote statistically significant differences according to Student's t-test at a 95% confidence level.

Class	MiniVUX	VUX	Dual-wavelength
Pine	26.7 (± 5.88)	9.23 (± 2.1)	8.76 (± 1.98)
Spruce	27 (± 6.04)	9.61 (± 2.3)	9.11 (± 2.17)
Deciduous	27.5 (± 6.43)	10.5 (± 2.83)	9.88 (± 2.62)
Noise	38.9 (± 11.8)	16.4 (± 5.57)	15.4 (± 5.14)
All classes	**27.6 a (± 7.04)**	**10.1 b (± 3.07)**	**9.52 c (± 2.86)**

Tables 9, 10 and 11 show the species classification results for the miniVUX, VUX and dual-wavelength datasets, respectively. The best performance was achieved using the dual-wavelength dataset, where the model reached an overall accuracy of 92.3% and a macro F1-score of 0.896. The VUX dataset, despite its lower spatial and spectral resolutions, still achieved 91.6% accuracy and 0.894 macro-F1. The miniVUX dataset, with the lowest spatial resolution, achieved 85.4% accuracy and 0.835 macro-F1. These results suggest that, for the species groups analyzed in this study, both spectral and spatial resolution influenced classification performance. While combining wavelengths as in the dual-wavelength dataset added value, the ability to preserve crown structure in the raster images – affected by increasing point density and smaller footprint sizes - was critical for accurate species identification. It should be noted that these results are based on the analysis of three dominant species groups in managed, mature forests. Thus, they could differ significantly in more diverse forest types or in areas with higher species diversity.

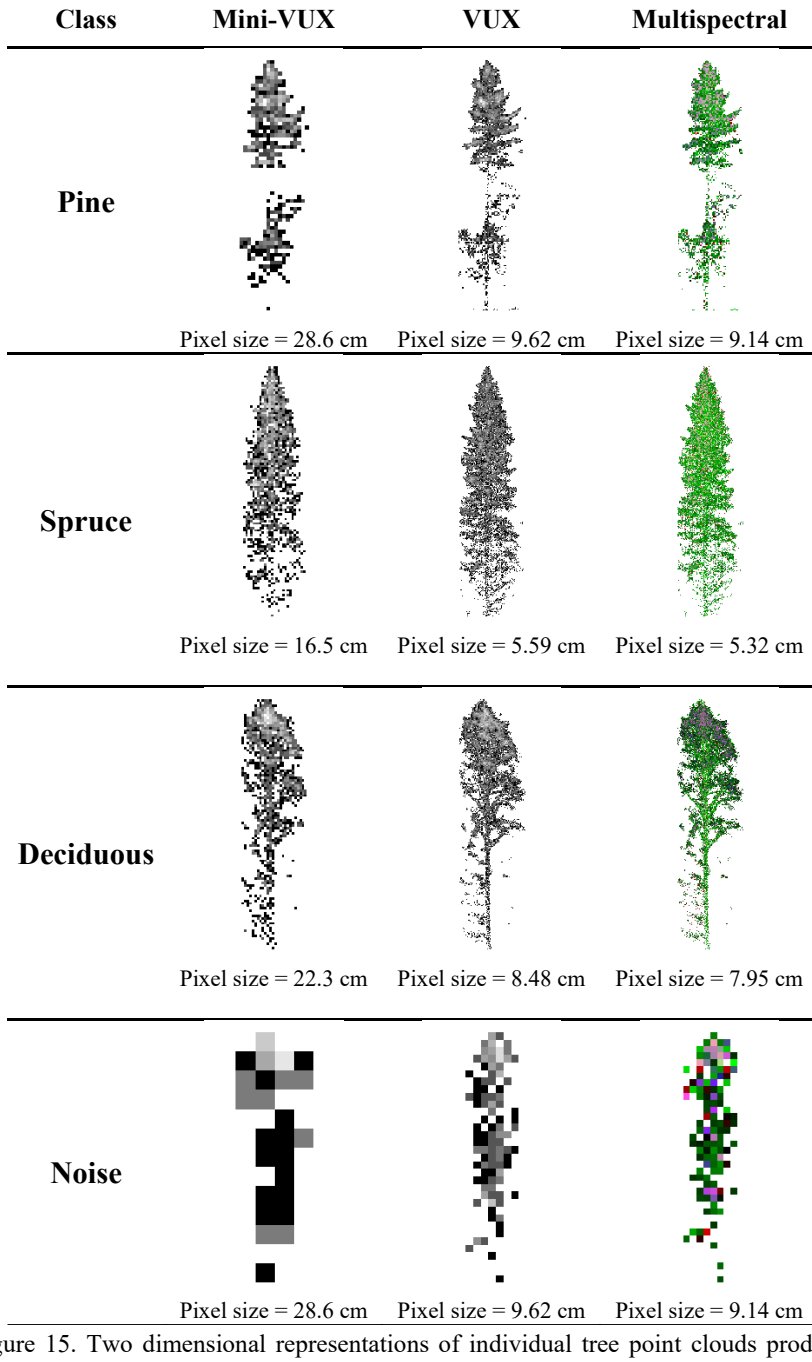

Figure 15. Two dimensional representations of individual tree point clouds produced with different aerial laser scanning datasets.

Table 9. Confusion matrix of predictions made using miniVUX-based images.

		Observed Species				Precision	F1-score
		Pine	Spruce	Deciduous	Noise		
Predicted Species	Pine	3190	137	292	17	87.7%	0.867
	Spruce	245	3233	206	97	89.8%	0.876
	Deciduous	257	158	2886	114	84.5%	0.840
	Noise	30	71	75	625	78%	0.756
Recall		85.7%	87.6%	83.4%	73.3%	**OA[1] = 85.4%**	**macro-F1[2] = 0.835**

Note. [1]Overall Accuracy. [2]Arithmetic mean of F1-scores.

Table 10. Confusion matrix of predictions made using VUX-based images.

		Observed Species				Precision	F1-score
		Pine	Spruce	Deciduous	Noise		
Predicted Species	Pine	3409	85	57	5	95.9%	0.937
	Spruce	203	3362	109	80	89.6%	0.914
	Deciduous	94	76	3207	85	92.6%	0.928
	Noise	16	76	86	686	79.4%	0.798
Recall		91.6%	93.4%	92.7%	80.1%	**OA[1] = 91.6%**	**macro-F1[2] = 0.894**

Note. [1]Overall Accuracy. [2]Arithmetic mean of F1-scores.

Table 11. Confusion matrix of predictions made using dual-wavelength images.

		Observed Species				Precision	F1-score
		Pine	Spruce	Deciduous	Noise		
Predicted Species	Pine	3455	103	87	9	94.6%	0.937
	Spruce	198	3392	60	100	90.4%	0.923
	Deciduous	45	43	3242	97	94.6%	0.942
	Noise	24	61	70	650	80.8%	0.783
Recall		92.8%	94.2%	93.7%	75.9%	**OA[1] = 92.3%**	**macro-F1[2] = 0.896**

Note. [1]Overall Accuracy. [2]Arithmetic mean of F1-scores.

3.4 Crook Detection Using Synthetic Training Data (Paper IV)

In **Paper IV**, crook detection accuracy varied depending on the IoU threshold used to decide if a detection was correct. As shown in Figure 16, the model achieved high sensitivity to the presence of crooks at low

thresholds, with F1-scores exceeding 0.60 for IoU < 0.3 and with recall exceeding 0.80. These figures dropped substantially at stricter thresholds. At the commonly used IoU = 0.5, the F1-score fell to approximately 0.45, with a recall of approximately 0.55 and precision of 0.35. This indicates strong detection capabilities but poor placement of the bounding box around the crooks.

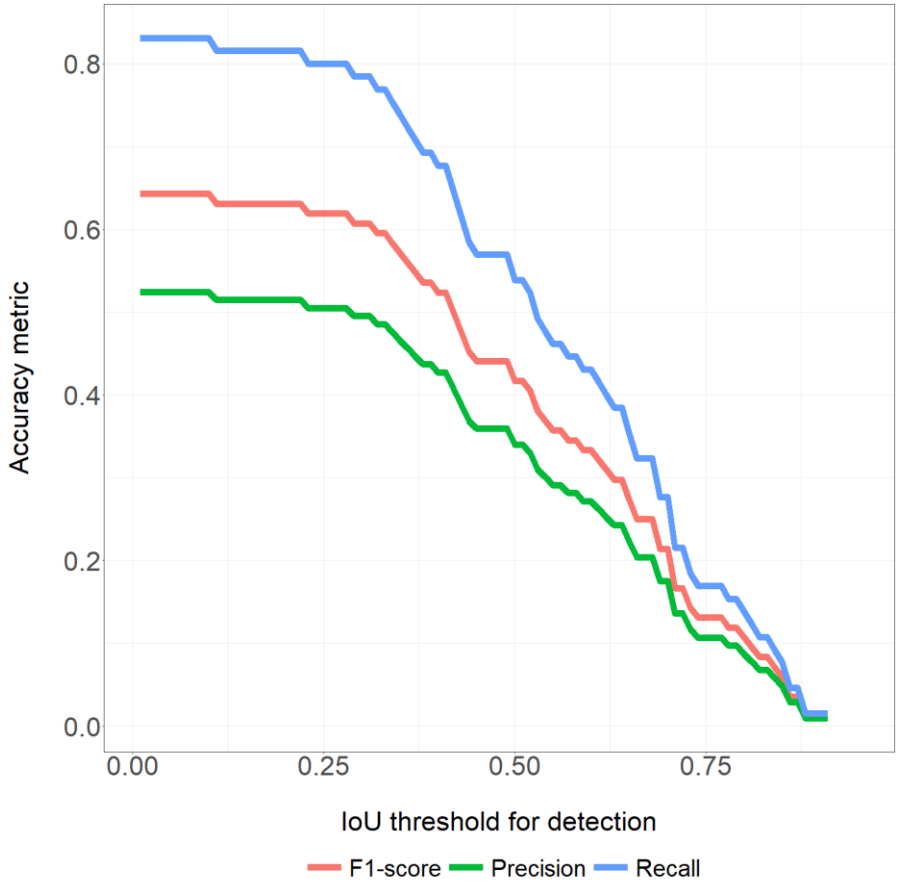

Figure 16. Accuracy of the crook detection model across varying Intersection over Union (IoU) thresholds. The plot shows F1-score (red), precision (green), and recall (blue) as a function of the IoU threshold used to define true positives.

In addition, systematic detection errors were observed (Figure 17). At the IoU threshold of 0.25, most true positives occurred between 3 m and 8 m above ground. However, commission errors were common above 10 m,

likely due to low point density and increasing structural complexity of the crown. On the other hand, omission errors were mostly observed below 2.5 m, possibly due to irregular basal stem shapes that were underrepresented or less realistically modeled during simulation. Together, these results demonstrate that a model trained only with synthetic data can generalize to real-world TLS for crook detection when flexible spatial thresholds are allowed. However, accurate localization and detection across the full stem profile is a challenge, particularly in regions with occlusion, low sampling density, or geometric variability. The results highlight both the opportunities and challenges that come associated with using simulation-based training for rare stem defect detection.

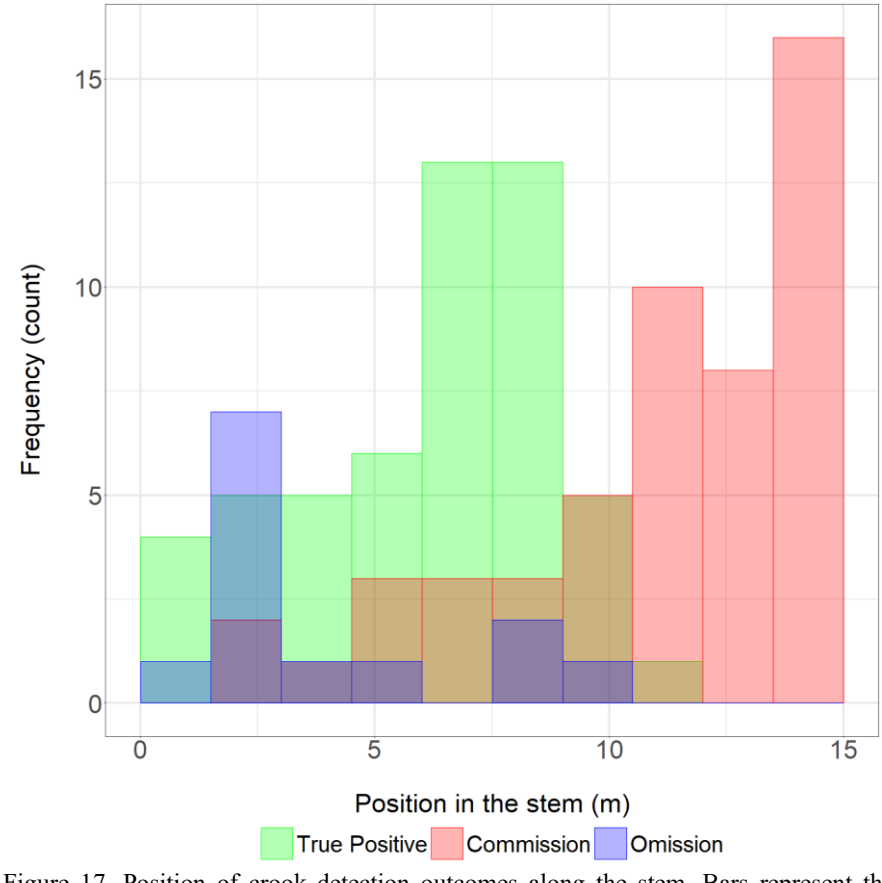

Figure 17. Position of crook detection outcomes along the stem. Bars represent the number of crooks detected (true positives, green), commission (red), and omission (blue) errors across stem height intervals.

4. Discussion

This thesis explores how multiple data sources, from close-range remote sensing technologies to harvester production reports and simulations, can enhance data availability for tree-level forest inventories based on remote sensing. Across **Papers I** to **IV**, different datasets, analytical techniques and algorithms are used to estimate forest attributes. While each study has a different objective, together they demonstrate that emerging data collection strategies can enhance the scalability, efficiency, and automation of forest monitoring workflows.

In **Papers I** and **II** we propose car-mounted MLS as an operationally viable alternative to traditional field-based reference data collection. The results show that tree attributes such as DBH and stem volume can be accurately estimated from car-mounted MLS datasets, achieving comparable accuracy to TLS. More importantly, the system can provide reference data in sufficient quality and quantity to precision forestry related applications, such as tree-level modelling, by taking advantage of road networks. In practice, the approach enabled the measurement of over 6000 trees within a two-hour survey, highlighting its potential to substantially increase data collection efficiency compared to conventional fieldwork. **Paper II** further confirms that these MLS-derived measurements can be used to train ALS-based models at tree-level, yielding similar results to models trained on conventional field-plot data. These findings are particularly relevant for large-scale forest inventories, where the cost and labor intensity of traditional field surveys often limit the data collection capabilities. By enabling rapid and consistent data acquisition, MLS-derived ground-truth data can support model training for remote sensing–based forest monitoring, at tree-level.

Paper III addresses another limitation often faced in forest remote sensing workflows: data annotation. By integrating HPRs with ALS data, we proposed an automatic annotation pipeline that minimizes manual interpretation and provides a reference dataset for tree species classification. As HPRs are a routine by-product of mechanized harvesting, they represent a source of information that can be repurposed for modelling without requiring extra data collection. For the species groups analyzed under the same forest conditions, our comparative analysis of ALS datasets with different spectral and spatial resolutions showed that spatial resolution, here denoted by a combination of footprint size and point density, has a strong

impact on classification accuracy. These findings suggest that ALS-based species classification can be made more efficient both through sensor choice and the use of such operational by-products.

Finally, **Paper IV** proposes the usage of synthetic data as a way to overcome the lack of training data for rare stem defects detection, specifically crooks. The framework for generating synthetic crook deformations proved effective for training a CNN, though its ability to generalize to real-world data was limited. While localization accuracy was limited, the study illustrates how simulation-based training can support defect detection where annotated real-world data is rare or difficult to obtain. Future work should focus on increasing simulation realism and in strategies to reduce problems related to domain shift.

Nevertheless, shifting from traditional data collection methods to alternative or novel data sources introduces new uncertainties into modelling. For instance, in **Paper I**, estimate's accuracy varied according to how far from the sensor trajectory (i.e. roadside) the trees were, with a high number of commissions from 0-10 m from the roadside, while omissions were prominent beyond ~40 m. In **Paper II**, even though models trained on MLS references produced estimates comparable to those trained on field plots, it remains important to assess how adopting such estimates as inputs may influence downstream forest planning decisions and constraints. In **Paper III**, even though the automatic labeling removed much of the manual work required in annotation, key uncertainties can come from the HPR side, such as operator annotation errors and imperfect HPR–to–ALS matching. Finally, in **Paper IV**, training a crook detector only on synthetic data yielded weak localization at stricter IoU thresholds and height-dependent errors (varying with crook position along the stem), underscoring a possible synthetic-to-real domain gap.

Despite these shortcomings, this thesis advances precision forestry by addressing challenges related to data availability and scalability of detailed (i.e. tree-level) forest inventories. In that sense, Hyyppä et al. (2022) proposed a transition towards direct laser-based measurements of stem form and volume – in line **Papers I** and **II**. In contrast to the ground-based platform in **Paper I**, Hyyppä et al. (2022) used a helicopter-mounted system for stem attribute derivation, which achieved a lower tree detection rate yet allowed coverage of a larger area. More broadly, aerial platforms such as the one used by Hyyppä et al. (2022) or Puliti et al. (2020) can cover larger areas

and are not bound to the road network or terrain accessibility, which may be more scalable than car- or ATV-mounted systems. At the same time, ground-based systems present a different set of trade-offs. Costs and operational risks are substantially lower compared to aerial platforms, making them attractive for detailed local inventories. However, their dependence on the road network or terrain accessibility introduces limitations, as inaccessible forest patches may remain unsampled, leading to potential design biases.

Paper II builds on this discussion by addressing the research gap pointed out by Hyyppä et al. (2022), namely whether laser scanning-based stem attribute estimates can serve as reliable reference data for training individual-tree-level models. Our comparison of MLS- and FI-derived datasets revealed both advantages and limitations of using laser scanning as reference. The MLS dataset provided a larger sample size, which can strengthen model calibration. However, model performance does not necessarily improve once a threshold in sample size is reached (Fassnacht et al., 2014; Lisańczuk et al., 2020), and adequate representation of attribute variability across the study area often plays a more important role than the absolute number of samples (Junttila et al., 2013; Li et al., 2023).

In their review study, Liang et al. (2022) emphasize that close-range remote sensing technologies hold great promise for forest observation, but their operational deployment depends on improvements in data acquisition protocols, calibration and validation. In this sense, the thesis tested and validated the use of MLS, TLS and low-flying ALS as a step towards addressing this gap, providing examples of how such information could support forest inventory practices. Rather than focusing on single-sensor solutions or controlled conditions, the work illustrates how scalable inventory methods may gradually be developed by leveraging diverse close-range data.

Beyond operational inventory applications, Valbuena et al. (2020) suggest that structural traits such as height, cover, and complexity can provide a useful bridge between 3D data and ecological understanding. The work presented in this thesis offers some insights in this direction by showing how attributes like DBH and stem volume (**Papers I** and **II**), tree species (**Paper III**), and shape anomalies (**Paper IV**) can be derived from close-range remote sensing data. While the thesis focus was on tree size and shape, it may also support the mapping of other structural metrics relevant to

ecological studies. With further development, these approaches could contribute to broader trait-based assessments of forest ecosystems.

Disney (2019) emphasizes TLS's capacity of describing plant structure and function, particularly architectural traits and form-function relationships. Some of the methods described in the thesis, such as the reconstruction of stems (**Papers I** and **II**) and the detection of deformations like crooks (**Paper IV**), may offer some contribution in that direction. These approaches were not designed with ecological modelling in mind, but they demonstrate how structural detail captured with close-range sensors can be processed and interpreted in scalable ways.

In addition to enhancing data availability, close-range remote sensing has been tested both as auxiliary information in probability-based estimators and as a practical extension to national forest inventories (NFIs). Molina-Valero et al. (2025) showed that incorporating TLS and/or UAV-LS as auxiliary information significantly reduced the standard error of stand volume estimates. The study also showed that simply using TLS-derived values of DBH, height, or volume does not guarantee variance reductions because single-scan TLS can introduce occlusion-related bias and increased plot-level variability. At NFI scale, practice-oriented pilots in France, Finland, and Switzerland reached a complementary conclusion: close-range laser scanning such as TLS and MLS should complement existing survey protocols, with the goal of expanding what is measured in each plot, as vertical structure, regeneration, and lying deadwood, rather than replacing standard measurements (Holvoet et al. 2025).

At the same time, making full use of alternative data collection tools also requires changes in the systems that support forest planning. Most planning frameworks use fixed stands as the main management unit, but maps based on sources such as close-range LiDAR or HPRs may contain information that would be lost or underused when aggregated to stand level, for example tree-level stem defects. Such aggregation can reduce the value of the data and lead to suboptimal planning decisions (Maleki et al., 2024). To better capture this type of detail, planning frameworks need to allow more flexible units. Dynamic treatment units are one example, where harvest blocks are formed by grouping small spatial units, adapting to local variation instead of following fixed stand boundaries (Pascual et al., 2016; Wilhelmsson et al., 2021).

Building on the examples tested in this thesis, future research should continue to explore how complementary data collection tools can expand the range of attributes captured in forest inventories. Close-range laser scanning and HPRs, in particular, can describe attributes that are costly or impractical to measure through conventional means, such as regeneration density, lying deadwood, crown architecture, and stem form. Further work is needed to determine how such tools can be incorporated into inventory protocols, not as replacements for established measurements, but as additions that increase the relevance of forest inventories. Second, future studies should investigate how the derived information can be integrated into decision support systems, and which types of management or planning decisions it can effectively support. For instance, while estimating attributes such as regeneration or deadwood at large scale is valuable in itself, their real impact lies in clarifying how such information can guide operational and strategic choices.

5. Conclusion

Reliable reference data are essential in remote sensing-based forest inventories, providing the foundation for model training and validation. Yet, the collection of such data remains a bottleneck, particularly in cases where extensive reference datasets are needed, e.g. for training neural networks, or where the target variables cannot be easily or reliably measured through traditional manual fieldwork. This thesis contributes to addressing this challenge by exploring how multiple data sources and techniques can expand the availability of tree-level information, thereby supporting scalable and more detailed forest inventories.

The results show that:

- Mobile laser scanning from cars can measure stem attributes with accuracy comparable to stationary laser scanning, while enabling data acquisition at greater speed, offering a viable alternative to conventional manual field inventories.
- By linking ALS data with HPRs, we demonstrated that operational by-products of mechanized harvesting can be repurposed to create automatically annotated reference datasets, reducing manual interpretation and ensuring consistency in tree species classification.
- Synthetic laser scanning data can be used to train neural networks for the detection of rare defects, such as stem crooks, implying that semi-empirical simulation approaches can overcome data scarcity in tasks where large, annotated datasets are impractical to obtain.

Together, these studies demonstrate that reference data availability can be expanded through efficient acquisition methods, automated data fusion, and simulations. Such approaches are not without uncertainties, but they open pathways for improving the scalability of tree-level remote sensing enabling information supply to precision forestry.

References

Aguiar, A.S., Neves, F., Cunha, J.B., Sobreira, H. & Sousa, A.J. (2020). Localization and Mapping for Robots in Agriculture and Forestry: A Survey. *Robotics*, 9 (4), 97. https://doi.org/10.3390/robotics9040097

Almeida, D.R.A., Broadbent, E.N., Zambrano, A.M.A., Wilkinson, B.E., Ferreira, M.E., Chazdon, R., Meli, P., Gorgens, E.B., Silva, C.A., Stark, S.C., Valbuena, R., Papa, D.A. & Brancalion, P.H.S. (2019). Monitoring the structure of forest restoration plantations with a drone-lidar system. *International Journal of Applied Earth Observation and Geoinformation*, 79, 192–198. https://doi.org/10.1016/j.jag.2019.03.014

Appiah Mensah, A., Jonzén, J., Nyström, K., Wallerman, J. & Nilsson, M. (2023). Mapping site index in coniferous forests using bi-temporal airborne laser scanning data and field data from the Swedish national forest inventory. *Forest Ecology and Management*, 547, 121395. https://doi.org/10.1016/j.foreco.2023.121395

Arrizza, S., Marras, S., Ferrara, R. & Pellizzaro, G. (2024). Terrestrial Laser Scanning (TLS) for tree structure studies: a review of methods for wood-leaf classifications from 3D point clouds. *Remote Sensing Applications: Society and Environment*, 36, 101364. https://doi.org/10.1016/j.rsase.2024.101364

Astrup, R., Ducey, M.J., Granhus, A., Ritter, T. & von Lüpke, N. (2014). Approaches for estimating stand-level volume using terrestrial laser scanning in a single-scan mode. *Canadian Journal of Forest Research*, 44 (6), 666–676. https://doi.org/10.1139/cjfr-2013-0535

Bester, M.S., Maxwell, A.E., Nealey, I., Gallagher, M.R., Skowronski, N.S. & McNeil, B.E. (2023). Synthetic Forest Stands and Point Clouds for Model Selection and Feature Space Comparison. *Remote Sensing*, 15, 4077. https://doi.org/10.3390/rs15184407

Bienert, A., Georgi, L., Kunz, M., Maas, H.-G. & von Oheimb, G. (2018). Comparison and combination of mobile and terrestrial laser scanning for natural forest inventories. *Forests*, 9 (7), 395. https://doi.org/10.3390/f9070395

Biometria (2025). Kvalitetsbestämning av sågtimmer av tall och gran - Nationella bestämmelser för virkesmätning [Quality determination of pine and spruce sawn timber National regulations for timber measurement] Version 2025-04-01. Uppsala: Biometria. https://www.biometria.se/publikationer/maetningsinstruktioner/maetningsbestaemmelser/nationella-

maetningsbestaemmelser/downloadfile?itemId=1884&contentType=docx&fileName=Kvalitetsbestämning av sågtimmer.docx

Bornand, A., Rehush, N., Morsdorf, F., Thürig, E. & Abegg, M. (2023). Individual tree volume estimation with terrestrial laser scanning: Evaluating reconstructive and allometric approaches. *Agricultural and Forest Meteorology*, 341, 109654. https://doi.org/10.1016/j.agrformet.2023.109654

Brede, B., Calders, K., Lau, A., Raumonen, P., Bartholomeus, H.M., Herold, M. & Kooistra, L. (2019). Non-destructive tree volume estimation through quantitative structure modelling: Comparing UAV laser scanning with terrestrial LIDAR. *Remote Sensing of Environment*, 233, 111355. https://doi.org/10.1016/j.rse.2019.111355

Brede, B., Terryn, L., Barbier, N., Bartholomeus, H.M., Bartolo, R., Calders, K., Derroire, G., Moorthy, S.M.K., Lau, A., Levick, S.R., Raumonen, P., Verbeeck, H., Wang, D., Whiteside, T., van der Zee, J. & Herold, M. (2022). Non-destructive estimation of individual tree biomass: Allometric models, terrestrial and UAV laser scanning. *Remote Sensing of Environment*, 280, 113180. https://doi.org/10.1016/j.rse.2022.113180

Bryson, M., Wang, F. & Allworth, J. (2023). Using Synthetic Tree Data in Deep Learning-Based Tree Segmentation Using LiDAR Point Clouds. *Remote Sensing*, 15 (9), 2380. https://doi.org/10.3390/rs15092380

Calders, K., Adams, J., Armston, J., Bartholomeus, H., Bauwens, S., Bentley, L.P., Chave, J., Danson, F.M., Demol, M., Disney, M., Gaulton, R., Moorthy, S.M.K., Levick, S.R., Saarinen, N., Schaaf, C., Stovall, A., Terryn, L., Wilkes, P. & Verbeeck, H. (2020). Terrestrial laser scanning in forest ecology: Expanding the horizon. *Remote Sensing of Environment*, 251, 112101. https://doi.org/10.1016/j.rse.2020.112102

Campos, M.B., Litkey, P., Wang, Y., Chen, Y., Hyyti, H., Hyyppä, J. & Puttonen, E. (2021). A Long-Term Terrestrial Laser Scanning Measurement Station to Continuously Monitor Structural and Phenological Dynamics of Boreal Forest Canopy. *Frontiers in Plant Science*, 11, 1–15. https://doi.org/10.3389/fpls.2020.606752

Cattaneo, N., Astrup, R. & Antón-Fernández, C. (2024). PixSim: Enhancing high-resolution large-scale forest simulations. *Software Impacts*, 21, 100695. https://doi.org/10.1016/j.simpa.2024.100695

Disney, M. (2019). Terrestrial LiDAR: a three-dimensional revolution in how we look at trees. *New Phytologist*, 222, 1736–1741. https://doi.org/10.1111/nph.15517

Dungey, H.S., Dash, J.P., Pont, D., Clinton, P.W., Watt, M.S. & Telfer, E.J. (2018). Phenotyping Whole Forests Will Help to Track Genetic Performance. *Trends in Plant Science*, 23 (10), 854–864. https://doi.org/10.1016/j.tplants.2018.08.005

Durrant-Whyte, H. & Bailey, T. (2006). Simultaneous Localization and Mapping: Part I. *IEEE Robotics & Automation Magazine*, 13 (2), 99–110. https://doi.org/10.1109/MRA.2006.1638022

Ecke, S., Dempewolf, J., Frey, J., Schwaller, A., Endres, E., Klemmt, H.-J., Tiede, D. & Seifert, T. (2022). UAV-Based Forest Health Monitoring: A Systematic Review. *Remote Sensing*, 14 (13), 3205. https://doi.org/10.3390/rs14133205

Ehbrecht, M., Seidel, D., Annighöfer, P., Kreft, H., Köhler, M., Zemp, D.C., Puettmann, K., Nilus, R., Babweteera, F., Willim, K., Stiers, M., Soto, D., Boehmer, H.J., Fisichelli, N., Burnett, M., Juday, G., Stephens, S.L. & Ammer, C. (2021). Global patterns and climatic controls of forest structural complexity. *Nature Communications*, 12, 519. https://doi.org/10.1038/s41467-020-20767-z

Faitli, T., Hyyppä, E., Hyyti, H., Hakala, T., Kaartinen, H., Kukko, A., Muhojoki, J. & Hyyppä, J. (2024). Integration of a Mobile Laser Scanning System with a Forest Harvester for Accurate Localization and Tree Stem Measurements. *Remote Sensing*, 16 (17), 3292. https://doi.org/10.3390/rs16173292

Fang, Y., Guo, X., Chen, K., Zhou, Z. & Qing, Y. (2021). Accurate and Automated Detection of Surface Knots on Sawn Timbers Using YOLO-V5 Model. *BioResources*, 16 (3), 5390–5406. https://doi.org/10.15376/biores.16.3.5390-5406

Fassnacht, F.E., Hartig, F., Latifi, H., Berger, C., Hernández, J., Corvalán, P. & Koch, B. (2014). Importance of sample size, data type and prediction method for remote sensing-based estimations of aboveground forest biomass. *Remote Sensing of Environment*, 154 , 102–114. https://doi.org/10.1016/j.rse.2014.07.028

Fassnacht, F.E., Latifi, H. & Hartig, F. (2018). Using synthetic data to evaluate the benefits of large field plots for forest biomass estimation with LiDAR. *Remote Sensing of Environment*, 213, 115–128. https://doi.org/10.1016/j.rse.2018.05.007

Fassnacht, F.E., Latifi, H., Stereńczak, K., Modzelewska, A., Lefsky, M., Waser, L.T., Straub, C. & Ghosh, A. (2016). Review of studies on tree species classification from remotely sensed data. *Remote Sensing of Environment*, 186, 64–87. https://doi.org/10.1016/j.rse.2016.08.013

Fassnacht, F.E., White, J.C., Wulder, M.A. & Næsset, E. (2024). Remote sensing in forestry: current challenges, considerations and directions. *Forestry: An International Journal of Forest Research*, 97, 11–37. https://doi.org/10.1093/forestry/cpad024

Forsman, M., Börlin, N., Olofsson, K., Reese, H. & Holmgren, J. (2018). Bias of cylinder diameter estimation from ground-based laser scanners with different beam widths: A simulation study. *ISPRS Journal of*

Photogrammetry and Remote Sensing, 135, 84–92. https://doi.org/10.1016/j.isprsjprs.2017.11.013

Gollob, C., Krassnitzer, R., Ritter, T., Tockner, A., Erber, G., Kühmaier, M., Hönigsberger, F., Varch, T., Holzinger, A., Stampfer, K. & Nothdurft, A. (2023). Measurement of Individual Tree Parameters with Carriage-Based Laser Scanning in Cable Yarding Operations. *Croatian Journal of Forest Engineering*, 44, 1–17. https://doi.org/10.5552/crojfe.2023.2252

Gollob, C., Ritter, T., Wassermann, C. & Nothdurft, A. (2019). Influence of scanner position and plot size on the accuracy of tree detection and diameter estimation using terrestrial laser scanning on forest inventory plots. *Remote Sensing*, 11 (13), 1602. https://doi.org/10.3390/rs11131602

Görgens, E.B., Mund, J.P., Cremer, T., de Conto, T., Krause, S., Valbuena, R. & Rodriguez, L.C.E. (2020). Automated operational logging plan considering multi-criteria optimization. *Computers and Electronics in Agriculture*, 170, 105253. https://doi.org/10.1016/j.compag.2020.105253

Goulden, T. & Hopkinson, C. (2010). The forward propagation of integrated system component errors within airborne lidar data. *Photogrammetric Engineering and Remote Sensing*, 76 (5), 589–601. https://doi.org/10.14358/PERS.76.5.589

Guimarães, N., Pádua, L., Marques, P., Silva, N., Peres, E. & Sousa, J.J. (2020). Forestry remote sensing from unmanned aerial vehicles: A review focusing on the data, processing and potentialities. *Remote Sensing*, 12 (6), 1046. https://doi.org/10.3390/rs12061046

Hakula, A., Ruoppa, L., Lehtomäki, M., Yu, X., Kukko, A., Kaartinen, H., Taher, J., Matikainen, L., Hyyppä, E., Luoma, V., Holopainen, M., Kankare, V. & Hyyppä, J. (2023). Individual tree segmentation and species classification using high-density close-range multispectral laser scanning data. *ISPRS Open Journal of Photogrammetry and Remote Sensing*, 9, 100039. https://doi.org/10.1016/j.ophoto.2023.100039

Hamedianfar, A., Mohamedou, C., Kangas, A. & Vauhkonen, J. (2022). Deep learning for forest inventory and planning: a critical review on the remote sensing approaches so far and prospects for further applications. *Forestry: An International Journal of Forest Research*, 1–15. https://doi.org/10.1093/forestry/cpac002

Hillman, S., Wallace, L., Reinke, K. & Jones, S. (2021). A comparison between TLS and UAS LiDAR to represent eucalypt crown fuel characteristics. *ISPRS Journal of Photogrammetry and Remote Sensing*, 181, 295–307. https://doi.org/10.1016/j.isprsjprs.2021.09.008

Hoffrén, R., Lamelas, M.T. & de la Riva, J. (2024). Evaluation of Handheld Mobile Laser Scanner Systems for the Definition of Fuel Types in Structurally Complex Mediterranean Forest Stands. *Fire*, 7 (2), 59. https://doi.org/10.3390/fire7020059

Holm, S. (1977). Transformationer av en eller flera beroende variableri regressionsanalys [Transformations of one or several dependent variables in regression analysis]. *HUGIN Report 7. Umeå: Forestry Faculty, Swedish University of Agricultural Sciences. (In Swedish.)*,

Holmgren, J., Barth, A., Larsson, H. & Olsson, H. (2012). Prediction of stem attributes by combining airborne laser scanning and measurements from harvesters. *Silva Fennica*, 46 (2), 227–239. https://doi.org/10.14214/sf.56

Holmgren, J., Lindberg, E., Olofsson, K. & Persson, H.J. (2022). Tree crown segmentation in three dimensions using density models derived from airborne laser scanning. *International Journal of Remote Sensing*, 43 (1), 299–329. https://doi.org/10.1080/01431161.2021.2018149

Holmgren, J., Tulldahl, H.M., Nordlöf, J., Nyström, M., Olofsson, K., Rydell, J. & Willen, E. (2017). Estimation of tree position and stem diameter using simultaneous localization and mapping with data from a backpack-mounted laser scanner., 2017. 59–63. https://doi.org/10.5194/isprs-archives-XLII-3-W3-59-2017

Holmgren, J., Tulldahl, M., Nordlöf, J., Willén, E. & Olsson, H. (2019). Mobile laser scanning for estimating tree stem diameter using segmentation and tree spine calibration. *Remote Sensing*, 11 (23), 1–18. https://doi.org/10.3390/rs11232781

Holvoet, J., Eichhorn, M.P., Giannetti, F., Kükenbrink, D., Liang, X., Mokroš, M., Novotný, J., Pitkänen, T.P., Puliti, S., Skudnik, M., Stereńczak, K., Terryn, L., Vega, C. & Torresan, C. (2025). Terrestrial and mobile laser scanning for national forest inventories: From theory to implementation. *Remote Sensing of Environment*, 329, 114947. https://doi.org/10.1016/j.rse.2025.114947

Hopkinson, C. (2007). The influence of flying altitude, beam divergence, and pulse repetition frequency on laser pulse return intensity and canopy frequency distribution. *Canadian Journal of Remote Sensing*, 33 (4), 312–324. https://doi.org/10.5589/m07-029

Hopkinson, C., Chasmer, L., Young-Pow, C. & Treitz, P. (2004). Assessing forest metrics with a ground-based scanning lidar. *Canadian Journal of Forest Research*, 34 (3), 573–583. https://doi.org/10.1139/x03-225

Hunčaga, M., Chudá, J., Tomaštík, J., Slámová, M., Koreň, M. & Chudý, F. (2020). The comparison of stem curve accuracy determined from point clouds acquired by different terrestrial remote sensing methods. *Remote Sensing*, 12 (17), 2739. https://doi.org/10.3390/RS12172739

Hyyppä, E., Hyyppä, J., Hakala, T., Kukko, A., Wulder, M.A., White, J.C., Pyörälä, J., Yu, X., Wang, Y., Virtanen, J.P., Pohjavirta, O., Liang, X., Holopainen, M. & Kaartinen, H. (2020a). Under-canopy UAV laser scanning for accurate forest field measurements. *ISPRS Journal of Photogrammetry and*

Remote Sensing, 164, 41–60. https://doi.org/10.1016/j.isprsjprs.2020.03.021

Hyyppä, E., Kukko, A., Kaartinen, H., Yu, X., Muhojoki, J., Hakala, T. & Hyyppä, J. (2022). Direct and automatic measurements of stem curve and volume using a high-resolution airborne laser scanning system. *Science of Remote Sensing*, 5, 100050. https://doi.org/10.1016/j.srs.2022.100050

Hyyppä, E., Kukko, A., Kaijaluoto, R., White, J.C., Wulder, M.A., Pyörälä, J., Liang, X., Yu, X., Wang, Y., Kaartinen, H., Virtanen, J.P. & Hyyppä, J. (2020b). Accurate derivation of stem curve and volume using backpack mobile laser scanning. *ISPRS Journal of Photogrammetry and Remote Sensing*, 161, 246–262. https://doi.org/10.1016/j.isprsjprs.2020.01.018

Hyyppä, E., Yu, X., Kaartinen, H., Hakala, T., Kukko, A., Vastaranta, M. & Hyyppä, J. (2020c). Comparison of backpack, handheld, under-canopy UAV, and above-canopy UAV laser scanning for field reference data collection in boreal forests. *Remote Sensing*, 12 (20), 3327. https://doi.org/10.3390/rs12203327

Jaakkola, A., Hyyppä, J., Yu, X., Kukko, A., Kaartinen, H., Liang, X., Hyyppä, H. & Wang, Y. (2017). Autonomous collection of forest field reference—The outlook and a first step with UAV laser scanning. *Remote Sensing*, 9 (8), 785. https://doi.org/10.3390/rs9080785

Jafarbiglu, H. & Pourreza, A. (2022). A comprehensive review of remote sensing platforms, sensors, and applications in nut crops. *Computers and Electronics in Agriculture*, 197, 106844. https://doi.org/10.1016/j.compag.2022.106844

Jin, S., Sun, X., Wu, F., Su, Y., Li, Y., Song, S., Xu, K., Ma, Q., Baret, F., Jiang, D., Ding, Y. & Guo, Q. (2021). Lidar sheds new light on plant phenomics for plant breeding and management: Recent advances and future prospects. *ISPRS Journal of Photogrammetry and Remote Sensing*, 171 (20), 202–223. https://doi.org/10.1016/j.isprsjprs.2020.11.006

Jocher, G., Chaurasia, A. & Qiu, J. (2023). Ultralytics YOLO (Version 8.0.0). https://github.com/ultralytics/ultralytics

Junttila, S., Holopainen, M., Vastaranta, M., Lyytikäinen-Saarenmaa, P., Kaartinen, H., Hyyppä, J. & Hyyppä, H. (2019). The potential of dual-wavelength terrestrial lidar in early detection of Ips typographus (L.) infestation – Leaf water content as a proxy. *Remote Sensing of Environment*, 231, 111264. https://doi.org/10.1016/j.rse.2019.111264

Junttila, V., Finley, A.O., Bradford, J.B. & Kauranne, T. (2013). Strategies for minimizing sample size for use in airborne LiDAR-based forest inventory. *Forest Ecology and Management*, 292, 75–85. https://doi.org/10.1016/j.foreco.2012.12.019

Kattenborn, T., Leitloff, J., Schiefer, F. & Hinz, S. (2021). Review on Convolutional Neural Networks (CNN) in vegetation remote sensing. *ISPRS Journal of*

Photogrammetry and Remote Sensing, 173, 24–49. https://doi.org/10.1016/j.isprsjprs.2020.12.010

Kattenborn, T., Lopatin, J., Förster, M., Braun, A.C. & Fassnacht, F.E. (2019). UAV data as alternative to field sampling to map woody invasive species based on combined Sentinel-1 and Sentinel-2 data. *Remote Sensing of Environment*, 227, 61–73. https://doi.org/10.1016/j.rse.2019.03.025

Kim, T.K., Hong, J., Ryu, D., Kim, S., Byeon, S.Y., Huh, W., Kim, K., Baek, G.H. & Kim, H.S. (2022). Identifying and extracting bark key features of 42 tree species using convolutional neural networks and class activation mapping. *Scientific Reports*, 12, 4772. https://doi.org/10.1038/s41598-022-08571-9

Kukko, A., Kaijaluoto, R., Kaartinen, H., Lehtola, V. V., Jaakkola, A. & Hyyppä, J. (2017). Graph SLAM correction for single scanner MLS forest data under boreal forest canopy. *ISPRS Journal of Photogrammetry and Remote Sensing*, 132, 199–209. https://doi.org/10.1016/j.isprsjprs.2017.09.006

Kulicki, M., Cabo, C., Trzciński, T., Będkowski, J. & Stereńczak, K. (2025). Artificial Intelligence and Terrestrial Point Clouds for Forest Monitoring. *Current Forestry Reports*, 11, 5. https://doi.org/10.1007/s40725-024-00234-4

Kuželka, K., Slavík, M. & Surový, P. (2020). Very high density point clouds from UAV laser scanning for automatic tree stem detection and direct diameter measurement. *Remote Sensing*, 12 (8), 1236. https://doi.org/10.3390/RS12081236

Laino, D., Cabo, C., Prendes, C., Janvier, R., Ordonez, C., Nikonovas, T., Doerr, S. & Santin, C. (2024). 3DFin: a software for automated 3D forest inventories from terrestrial point clouds. *Forestry: An International Journal of Forest Research*, 97, 479–496. https://doi.org/10.1093/forestry/cpae020

Lechner, A.M., Foody, G.M. & Boyd, D.S. (2020). Applications in Remote Sensing to Forest Ecology and Management. *One Earth*, 2, 405–412. https://doi.org/10.1016/j.oneear.2020.05.001

Li, C., Yu, Z., Dai, H., Zhou, X. & Zhou, M. (2023). Effect of sample size on the estimation of forest inventory attributes using airborne LiDAR data in large-scale subtropical areas. *Annals of Forest Science*, 80, 40. https://doi.org/10.1186/s13595-023-01209-4

Li, X., Wang, L., Guan, H., Chen, K., Zang, Y. & Yu, Y. (2024). Urban Tree Species Classification Using UAV-Based Multispectral Images and LiDAR Point Clouds. *Journal of Geovisualization and Spatial Analysis*, 8, 5. https://doi.org/10.1007/s41651-023-00167-9

Li, Y., Su, Y., Hu, T., Xu, G. & Guo, Q. (2018). Retrieving 2-D Leaf Angle Distributions for Deciduous Trees from Terrestrial Laser Scanner Data. *IEEE Transactions on Geoscience and Remote Sensing*, 56 (8), 4945–4955. https://doi.org/10.1109/TGRS.2018.2843382

Liang, X., Hyyppä, J., Kaartinen, H., Lehtomäki, M., Pyörälä, J., Pfeifer, N., Holopainen, M., Brolly, G., Francesco, P., Hackenberg, J., Huang, H., Jo, H.W., Katoh, M., Liu, L., Mokroš, M., Morel, J., Olofsson, K., Poveda-Lopez, J., Trochta, J., Wang, D., Wang, J., Xi, Z., Yang, B., Zheng, G., Kankare, V., Luoma, V., Yu, X., Chen, L., Vastaranta, M., Saarinen, N. & Wang, Y. (2018a). International benchmarking of terrestrial laser scanning approaches for forest inventories. *ISPRS Journal of Photogrammetry and Remote Sensing*, 144, 137–179. https://doi.org/10.1016/j.isprsjprs.2018.06.021

Liang, X., Kukko, A., Balenovic, I., Saarinen, N., Junttila, S., Kankare, V., Holopainen, M., Mokros, M., Surovy, P., Kaartinen, H., Jurjevic, L., Honkavaara, E., Nasi, R., Liu, J., Hollaus, M., Tian, J., Yu, X., Pan, J., Cai, S., Virtanen, J.P., Wang, Y. & Hyyppa, J. (2022). Close-Range Remote Sensing of Forests: The state of the art, challenges, and opportunities for systems and data acquisitions. *IEEE Geoscience and Remote Sensing Magazine*, 10 (3), 32–71. https://doi.org/10.1109/MGRS.2022.3168135

Liang, X., Kukko, A., Hyyppä, J., Lehtomäki, M., Pyörälä, J., Yu, X., Kaartinen, H., Jaakkola, A. & Wang, Y. (2018b). In-situ measurements from mobile platforms: An emerging approach to address the old challenges associated with forest inventories. *ISPRS Journal of Photogrammetry and Remote Sensing*, 143, 97–107. https://doi.org/10.1016/j.isprsjprs.2018.04.019

Liang, X., Yao, H., Qi, H. & Wang, X. (2024). Forest in situ observations through a fully automated under-canopy unmanned aerial vehicle. *Geo-Spatial Information Science*, 27 (4), 983–999. https://doi.org/10.1080/10095020.2024.2322765

Lillesand, T.M., Kiefer, R.W. & Chipman, J.W. (2015). *Remote Sensing and Image Interpretation*. Seventh Ed. Wiley.

Lines, E.R., Allen, M., Cabo, C., Calders, K., Debus, A., Grieve, S.W.D., Miltiadou, M., Noach, A., Owen, H.J.F. & Puliti, S. (2022). AI applications in forest monitoring need remote sensing benchmark datasets. *arXiv: 2212.09937*,

Lisańczuk, M., Mitelsztedt, K., Parkitna, K., Krok, G., Stereńczak, K., Wysocka-Fijorek, E. & Miścicki, S. (2020). Influence of sampling intensity on performance of two-phase forest inventory using airborne laser scanning. *Forest Ecosystems*, 7, 65. https://doi.org/10.1186/s40663-020-00277-6

Liu, B., Chen, S., Huang, H. & Tian, X. (2022). Tree Species Classification of Backpack Laser Scanning Data Using the PointNet++ Point Cloud Deep Learning Method. *Remote Sensing*, 14 (15), 3809. https://doi.org/10.3390/rs14153809

Liu, K., Shen, X., Cao, L., Wang, G. & Cao, F. (2018). Estimating forest structural attributes using UAV-LiDAR data in Ginkgo plantations. *ISPRS Journal of Photogrammetry and Remote Sensing*, 146, 465–482. https://doi.org/10.1016/j.isprsjprs.2018.11.001

Lovell, J.L., Jupp, D.L.B., Culvenor, D.S. & Coops, N.C. (2003). Using airborne and ground-based ranging lidar to measure canopy structure in Australian forests. *Canadian Journal of Remote Sensing*, 29 (5), 607–622. https://doi.org/10.5589/m03-026

Ma, Y., Zhao, Y., Im, J., Zhao, Y. & Zhen, Z. (2024). A deep-learning-based tree species classification for natural secondary forests using unmanned aerial vehicle hyperspectral images and LiDAR. *Ecological Indicators*, 159, 111608. https://doi.org/10.1016/j.ecolind.2024.111608

Maleki, K., Astrup, R., Cattaneo, N., Lara Henao, W. & Antón-Fernández, C. (2024). The effects of data aggregation on long-term projections of forest stands development. *Forest Ecosystems*, 11, 100199. https://doi.org/10.1016/j.fecs.2024.100199

Molina-Valero, J.A., Martins-Neto, R.P., Martínez-Calvo, A., Rodríguez-Ruiz, J., Surový, P., Seppelt, A. & Pérez-Cruzado, C. (2025). Use of close-range LiDAR devices and statistical inference approaches in operational stand-level forest inventories. *Remote Sensing of Environment*, 325, 114773. https://doi.org/10.1016/j.rse.2025.114773

Moriguchi, K. (2023). Estimation of fractal dimension of trees using LiDAR point data with sequential data decimation. *Remote Sensing of Environment*, 295, 113722. https://doi.org/10.1016/j.rse.2023.113722

Muhojoki, J., Tavi, D., Hyyppä, E., Lehtomäki, M., Faitli, T., Kaartinen, H., Kukko, A., Hakala, T. & Hyyppä, J. (2024). Benchmarking Under- and Above-Canopy Laser Scanning Solutions for Deriving Stem Curve and Volume in Easy and Difficult Boreal Forest Conditions. *Remote Sensing*, 16 (10), 1721. https://doi.org/10.3390/rs16101721

Murtiyoso, A., Cabo, C., Singh, A., Obaya, D.P., Cherlet, W., Stoddart, J., Fol, C.R., Beloiu Schwenke, M., Rehush, N., Stereńczak, K., Calders, K., Griess, V.C. & Mokroš, M. (2024). A Review of Software Solutions to Process Ground-based Point Clouds in Forest Applications. *Current Forestry Reports*, 10, 401–419. https://doi.org/10.1007/s40725-024-00228-2

Noordermeer, L., Ørka, H.O. & Gobakken, T. (2023). Imputing stem frequency distributions using harvester and airborne laser scanner data: a comparison of inventory approaches. *Silva Fennica*, 57 (3), 23023. https://doi.org/10.14214/sf.23023

de Oliveira, B.R., da Silva, A.A.P., Teodoro, L.P.R., de Azevedo, G.B., Azevedo, G.T. de O.S., Baio, F.H.R., Sobrinho, R.L., da Silva Junior, C.A. & Teodoro, P.E. (2021). Eucalyptus growth recognition using machine learning methods and spectral variables. *Forest Ecology and Management*, 497, 119496. https://doi.org/10.1016/j.foreco.2021.119496

Olofsson, K. & Holmgren, J. (2016). Single tree stem profile detection using terrestrial laser scanner data, flatness saliency features and curvature properties. *Forests*, 7 (9), 207. https://doi.org/10.3390/f7090207

Olofsson, K. & Holmgren, J. (2023). Stem Quality Estimates Using Terrestrial Laser Scanning Voxelized Data and a Voting-Based Branch Detection Algorithm. *Remote Sensing*, 15 (8), 2082. https://doi.org/10.3390/rs15082082

Olofsson, K., Holmgren, J. & Olsson, H. (2014). Tree stem and height measurements using terrestrial laser scanning and the RANSAC algorithm. *Remote Sensing*, 6 (5), 4323–4344. https://doi.org/10.3390/rs6054323

Pascual, A., Pukkala, T., Rodríguez, F. & De-Miguel, S. (2016). Using spatial optimization to create dynamic harvest blocks from LiDAR-based small interpretation units. *Forests*, 7 (10), 220. https://doi.org/10.3390/f7100220

Pehkonen, M., Vastaranta, M., Holopainen, M., Hyyppä, J., Kukko, A. & Pyörälä, J. (2025). Identification and segmentation of branch whorls and sawlogs in standing timber using terrestrial laser scanning and deep learning. *Forestry: An International Journal of Forest Research*, 1–14. https://doi.org/10.1093/forestry/cpaf006

Persson, H.J., Ekström, M. & Ståhl, G. (2022). Quantify and account for field reference errors in forest remote sensing studies. *Remote Sensing of Environment*, 283, 113302. https://doi.org/10.1016/j.rse.2022.113302

Pierzchała, M., Giguère, P. & Astrup, R. (2018). Mapping forests using an unmanned ground vehicle with 3D LiDAR and graph-SLAM. *Computers and Electronics in Agriculture*, 145, 217–225. https://doi.org/10.1016/j.compag.2017.12.034

Pires, R. de P., Lindberg, E., Persson, H.J., Olofsson, K. & Holmgren, J. (2024). Mobile laser scanning as reference for estimation of stem attributes from airborne laser scanning. *Remote Sensing of Environment*, 315, 114414. https://doi.org/10.1016/j.rse.2024.114414

Pires, R. de P., Olofsson, K., Persson, H.J., Lindberg, E. & Holmgren, J. (2022). Individual tree detection and estimation of stem attributes with mobile laser scanning along boreal forest roads. *ISPRS Journal of Photogrammetry and Remote Sensing*, 187, 211–224. https://doi.org/10.1016/j.isprsjprs.2022.03.004

Pohjala, J., Kankare, V., Hyyppä, J. & Kärhä, K. (2025). Effects of a mobile LiDAR-based thinning density assistant (TDA) system on harvester operator performance. *European Journal of Forest Research*,. https://doi.org/10.1007/s10342-025-01808-y

Puliti, S., Breidenbach, J. & Astrup, R. (2020). Estimation of forest growing stock volume with UAV laser scanning data: Can it be done without field data? *Remote Sensing*, 12 (8), 1245. https://doi.org/10.3390/RS12081245

Puliti, S., Mclean, J.P., Cattaneo, N., Fischer, C. & Astrup, R. (2023). Tree height-growth trajectory estimation using uni-temporal UAV laser scanning data and deep learning. *Forestry: An International Journal of Forest Research*, 96, 37–48. https://doi.org/https://doi.org/10.1093/forestry/cpac026

Pyorala, J., Liang, X., Vastaranta, M., Saarinen, N., Kankare, V., Wang, Y., Holopainen, M. & Hyyppa, J. (2018). Quantitative assessment of scots pine (Pinus Sylvestris L.) whorl structure in a forest environment using terrestrial laser scanning. *IEEE Journal of Selected Topics in Applied Earth Observations and Remote Sensing*, 11 (10), 3598–3607. https://doi.org/10.1109/JSTARS.2018.2819598

Qian, C., Liu, H., Tang, J., Chen, Y., Kaartinen, H., Kukko, A., Zhu, L., Liang, X., Chen, L. & Hyyppä, J. (2017). An integrated GNSS/INS/LiDAR-SLAM positioning method for highly accurate forest stem mapping. *Remote Sensing*, 9 (1), 3. https://doi.org/10.3390/rs9010003

Raigosa-García, I., Rathbun, L.C., Cook, R.L., Baker, J.S., Corrao, M. V. & Sumnall, M.J. (2024). Rethinking Productivity Evaluation in Precision Forestry through Dominant Height and Site Index Measurements Using Aerial Laser Scanning LiDAR Data. *Forests*, 15 (6), 1002. https://doi.org/10.3390/f15061002

Raumonen, P., Casella, E., Calders, K., Murphy, S., Åkerblom, M. & Kaasalainen, M. (2015). Massive-scale tree modelling from TLS data., 2015. 189–196. https://doi.org/10.5194/isprsannals-II-3-W4-189-2015

Sagar, A., Kärhä, K., Einola, K. & Koivusalo, A. (2024). Assessing the Potential of Onboard LiDAR-Based Application to Detect the Quality of Tree Stems in Cut-to-Length (CTL) Harvesting Operations. *Forests*, 15 (5), 818. https://doi.org/10.3390/f15050818

Salmivaara, A., Launiainen, S., Perttunen, J., Nevalainen, P., Pohjankukka, J., Ala-Ilomäki, J., Sirén, M., Laurén, A., Tuominen, S., Uusitalo, J., Pahikkala, T., Heikkonen, J. & Finér, L. (2020). Towards dynamic forest trafficability prediction using open spatial data, hydrological modelling and sensor technology. *Forestry: An International Journal of Forest Research*, 93 (5), 662–674. https://doi.org/10.1093/FORESTRY/CPAA010

Saukkola, A., Melkas, T., Riekki, K., Sirparanta, S., Peuhkurinen, J., Holopainen, M., Hyyppä, J. & Vastaranta, M. (2019). Predicting forest inventory attributes using airborne laser scanning, aerial imagery, and harvester data. *Remote Sensing*, 11 (7), 797. https://doi.org/10.3390/rs11070797

Schäfer, J., Weiser, H., Winiwarter, L., Höfle, B., Schmidtlein, S. & Fassnacht, F.E. (2023). Generating synthetic laser scanning data of forests by combining forest inventory information, a tree point cloud database and an open-source laser scanning simulator. *Forestry: An International Journal of Forest Research*, 96 (5), 653–671. https://doi.org/10.1093/forestry/cpad006

Schäfer, J., Winiwarter, L., Weiser, H., Höfle, B., Schmidtlein, S., Novotný, J., Krok, G., Stereńczak, K., Hollaus, M. & Fassnacht, F.E. (2024). CNN-based transfer learning for forest aboveground biomass prediction from ALS point cloud tomography. *European Journal of Remote Sensing*, 57 (1), 2396932. https://doi.org/10.1080/22797254.2024.2396932

Sheng, Y., Zhao, Q., Wang, X., Liu, Y. & Yin, X. (2024). Tree Diameter at Breast Height Extraction Based on Mobile Laser Scanning Point Cloud. *Forests*, 15 (4), 590. https://doi.org/10.3390/f15040590

Söderberg, J., Wallerman, J., Almäng, A., Möller, J.J. & Willén, E. (2021). Operational prediction of forest attributes using standardised harvester data and airborne laser scanning data in Sweden. *Scandinavian Journal of Forest Research*, 36 (4), 306–314. https://doi.org/10.1080/02827581.2021.1919751

Straker, A., Puliti, S., Breidenbach, J., Kleinn, C., Pearse, G., Astrup, R. & Magdon, P. (2023). Instance segmentation of individual tree crowns with YOLOv5: A comparison of approaches using the ForInstance benchmark LiDAR dataset. *ISPRS Open Journal of Photogrammetry and Remote Sensing*, 9, 100045. https://doi.org/10.1016/j.ophoto.2023.100045

Sun, H., Yan, H., Hassanalian, M., Zhang, J. & Abdelkefi, A. (2023). UAV Platforms for Data Acquisition and Intervention Practices in Forestry: Towards More Intelligent Applications. *Aerospace*, 10 (3), 317. https://doi.org/10.3390/aerospace10030317

Suvanto, S., Heikkinen, J., Holmström, E., Honkaniemi, J., Piri, T., Hantula, J., Räsänen, T., Riekki, K., Sorsa, J.-A., Hytönen, H., Höglund, H., Rajala, T., Lehtonen, A. & Peltoniemi, M. (2025). Rot or not? Uncovering the spatial patterns and drivers of Norway spruce root rot with harvester data. *bioRxiv preprint*,. https://doi.org/10.1101/2025.02.07.637055

Terryn, L., Calders, K., Bartholomeus, H., Bartolo, R.E., Brede, B., D'hont, B., Disney, M., Herold, M., Lau, A., Shenkin, A., Whiteside, T.G., Wilkes, P. & Verbeeck, H. (2022). Quantifying tropical forest structure through terrestrial and UAV laser scanning fusion in Australian rainforests. *Remote Sensing of Environment*, 271, 112912. https://doi.org/10.1016/j.rse.2022.112912

Terryn, L., Calders, K., Disney, M., Origo, N., Malhi, Y., Newnham, G., Raumonen, P., Å kerblom, M. & Verbeeck, H. (2020). Tree species classification using structural features derived from terrestrial laser scanning. *ISPRS Journal of Photogrammetry and Remote Sensing*, 168, 170–181. https://doi.org/10.1016/j.isprsjprs.2020.08.009

Torralba, J., Carbonell-Rivera, J.P., Ruiz, L.Á. & Crespo-Peremarch, P. (2022). Analyzing TLS Scan Distribution and Point Density for the Estimation of Forest Stand Structural Parameters. *Forests*, 13 (12), 2115. https://doi.org/10.3390/f13122115

Vaaja, M.T., Virtanen, J.-P., Kurkela, M., Lehtola, V., Hyyppä, J. & Hyyppä, H. (2016). THE EFFECT OF WIND ON TREE STEM PARAMETER ESTIMATION USING TERRESTRIAL LASER SCANNING., 2016. 117–122. https://doi.org/10.5194/isprsannals-iii-8-117-2016

Valbuena, R., O'Connor, B., Zellweger, F., Simonson, W., Vihervaara, P., Maltamo, M., Silva, C.A., Almeida, D.R.A., Danks, F., Morsdorf, F., Chirici, G., Lucas, R., Coomes, D.A. & Coops, N.C. (2020). Standardizing Ecosystem Morphological Traits from 3D Information Sources. *Trends in Ecology and Evolution*, 35 (8), 656–667. https://doi.org/10.1016/j.tree.2020.03.006

Venanzi, R., Latterini, F., Civitarese, V. & Picchio, R. (2023). Recent Applications of Smart Technologies for Monitoring the Sustainability of Forest Operations. *Forests*, 14 (7), 1503. https://doi.org/10.3390/f14071503

Walker, M. & Dahle, G.A. (2023). Literature Review of Unmanned Aerial Systems and LIDAR with Application to Distribution Utility Vegetation Management. *Arboriculture and Urban Forestry*, 49 (3), 144–156. https://doi.org/10.48044/jauf.2023.011

Wallace, L., Hillman, S., Hally, B., Taneja, R., White, A. & McGlade, J. (2022). Terrestrial Laser Scanning: An Operational Tool for Fuel Hazard Mapping? *Fire*, 5 (4), 1–20. https://doi.org/10.3390/fire5040085

Westling, F., Bryson, M. & Underwood, J. (2021). SimTreeLS: Simulating aerial and terrestrial laser scans of trees. *Computers and Electronics in Agriculture*, 187, 106277. https://doi.org/10.1016/j.compag.2021.106277

Wielgosz, M., Puliti, S., Xiang, B., Schindler, K. & Astrup, R. (2024). SegmentAnyTree: A sensor and platform agnostic deep learning model for tree segmentation using laser scanning data. *Remote Sensing of Environment*, 313, 114367. https://doi.org/10.1016/j.rse.2024.114367

Wilhelmsson, P., Sjödin, E., Wästlund, A., Wallerman, J., Lämås, T. & Öhman, K. (2021). Dynamic treatment units in forest planning using cell proximity. *Canadian Journal of Forest Research*, 51 (7), 1065–1071. https://doi.org/10.1139/cjfr-2020-0210

Winiwarter, L., Esmorís Pena, A.M., Weiser, H., Anders, K., Martínez Sánchez, J., Searle, M. & Höfle, B. (2022). Virtual laser scanning with HELIOS++: A novel take on ray tracing-based simulation of topographic full-waveform 3D laser scanning. *Remote Sensing of Environment*, 269, 112772. https://doi.org/10.1016/j.rse.2021.112772

Wu, Y., Zhong, S., Ma, Y., Zhang, Y. & Liu, M. (2025). Application of SLAM-Based Mobile Laser Scanning in Forest Inventory: Methods, Progress, Challenges, and Perspectives. *Forests*, 16 (6), 920. https://doi.org/10.3390/f16060920

Xiang, B., Wielgosz, M., Kontogianni, T., Peters, T., Puliti, S., Astrup, R. & Schindler, K. (2024). Automated forest inventory: Analysis of high-density airborne LiDAR point clouds with 3D deep learning. *Remote Sensing of Environment*, 305, 114078. https://doi.org/10.1016/j.rse.2024.114078

Yang, X., Li, R., Jablonski, A., Stovall, A., Kim, J., Yi, K., Ma, Y., Beverly, D., Phillips, R., Novick, K., Xu, X. & Lerdau, M. (2023). Leaf angle as a leaf

and canopy trait: Rejuvenating its role in ecology with new technology. *Ecology Letters*, 26 (6), 1005–1020. https://doi.org/10.1111/ele.14215

Popular science summary

Forests are managed to meet many different goals, including timber production, biodiversity conservation, climate change mitigation, and recreation. These objectives are often in conflict, which makes management increasingly complex and dependent on reliable information. Precision forestry has emerged as a framework to address this challenge. It aims to optimize management by using site-specific information at fine spatial scales, often at the level of individual trees, supported by measurements, modelling, and automation. To make precision forestry possible, large amounts of detailed data are required. Traditionally, this information has been obtained from field surveys, where a limited number of trees are carefully measured in sample plots. These methods are accurate and remain essential, but they are expensive and time-consuming, and often not scalable to the level of detail demanded by precision forestry. This thesis investigates how complementary data sources can help bridge this gap. Close-range laser scanning from vehicles, digital records generated during forest harvesting, and synthetic datasets that replicate real conditions all provide new opportunities to expand the availability of tree-level information. These approaches can supply data in the quality and quantity needed to support a range of applications, from modelling forest growth and species composition to identifying irregularities in tree stems relevant for timber quality. Taken together, the findings show how emerging data sources can complement traditional surveys and strengthen the basis for forest assessments. By doing so, they contribute to making precision forestry more operational, enabling management decisions that are better adapted to the diverse and often competing demands placed on today's forests.

Populärvetenskaplig sammanfattning

Skogshushållning har många olika mål, t.ex. virkesproduktion, bevarande av biodiversitet, motverka klimatförändringar och främja rekreation. Dessa mål är ofta i konflikt med varandra vilket medför allt oftare komplexa beslutsprocesser där pålitlig information behövs. Precisionsskogsbruk har växt fram som ett koncept där dessa utmaningar kan adresseras. I detta skogsbruk strävar man efter att optimera genom att använda geografisk information med hög upplösning, ofta på trädnivå, baserat på mätningar, modelleringar och automation. För att möjliggöra precisionsskogsbruk behövs stora mängder detaljerade data. Traditionellt kommer denna information från fältinventeringar där ett begränsat antal träd mäts noggrant på provytor. Dessa metoder är noggranna och är fortfarande mycket viktiga, men de är kostsamma och långsamma. Det är därför inte möjligt att skala upp dessa metoder med en bibehållen upplösning som är tillräcklig hög för kraven på information i skogsbruket. I denna avhandling undersökts hur kompletterande datakällor kan användas för att skapa relevant information. Laserskanning på korta avstånd från fordon, digital registrering med hjälp av moderna skördare, och syntetiska data som speglar verkliga förhållanden skapar alla nya möjligheter att utöka tillgången av information på trädnivå. Dessa tillvägagångsätt kan användas för att skapa data i den kvantitet och med sådan kvalitet som behövs för att stödja många olika tillämpningar, från modellering av skogstillväxt och trädslagsfördelning till att identifiera oregelbundenheter på trädstammar kopplade till virkeskvalitet. Sammanfattningsvis visar resultaten hur framväxande datakällor kan komplettera traditionella inventeringar och stärka grunden för skogsuppskattning. De nya datakällorna kan bidra till att göra precisionsskogsbruk mer operationellt, vilket möjliggör beslutsprocesser som är bättre anpassade till de många olika och ofta konkurrerande krav som finns på dagens skogsbruk.

Acknowledgements

Many people have been part of this journey. First of all, I had the privilege of counting on an amazing supervision group: Eva, Henrik, Kenneth, and Johan. They made the process not only productive but also genuinely pleasant, always supported my ideas, gave feedback that lifted me up, and were ready to teach, explain, or discuss whenever I needed. With them, I learned not only about remote sensing and doing research but also had a live demonstration of what great mentorship looks like. This is something I will carry with me, and I can only hope to pass it forward in the future.

I would also like to thank my colleagues at Remote Sensing division and at the Department more broadly. This is a truly special place to work, with a light and friendly atmosphere that supports PhD students in many ways: from introducing us to *fika* to the constant willingness of all research staff, administrators, and engineers to offer help and guidance whenever needed. I can honestly say that I enjoyed coming to work, and I am very grateful for the sense of community we share.

To my colleagues at Stora Enso AB, in special to Daniel Forsberg, Peder Wikström, Anna Karlberg, and Erik Willén, thanks for getting me familiar with Swedish forestry. Our collaboration showed me how research connects with forestry and made the whole experience more rewarding.

To my fellow (present and past) PhD students and postdocs, thank you for all the laughs we shared and for always being ready for the next adventure. The everyday moments with you, filled with the most incredible non-sense, have turned into stories that I will retell many times. Special thanks to Emanuele Pappucci, for creating the beautiful artwork on the cover.

Um agradecimento mais que especial aos meus amigos brasileiros aqui em Umeå, que me ajudaram a matar a saudade de casa e riram dos efeitos sonoros do Ratinho. A presença de vocês tornou essa jornada mais leve.

Por último mas não menos importante, meu muito obrigado à minha familia e minha esposa. Eu sempre senti o apoio e o carinho de vocês. Quando eu achava que algo não ia dar certo, vocês sempre diziam: 'lógico que vai dar, Raul, sempre dá certo'. Esse voto de confiança me acompanhou durante toda a jornada e faz mais sentido a cada conquista. Esse trabalho também é de vocês.

I

ISPRS Journal of Photogrammetry and Remote Sensing 187 (2022) 211–224

Contents lists available at ScienceDirect

ISPRS Journal of Photogrammetry and Remote Sensing

journal homepage: www.elsevier.com/locate/isprsjprs

Individual tree detection and estimation of stem attributes with mobile laser scanning along boreal forest roads

Raul de Paula Pires *, Kenneth Olofsson, Henrik Jan Persson, Eva Lindberg, Johan Holmgren

Dept. of Forest Resource Management, Swedish University of Agricultural Sciences, Umeå, Sweden

ARTICLE INFO

Keywords:
Stem diameter
Stem volume
Car-mounted
Automatic stem detection
MLS

ABSTRACT

The collection of field-reference data is a key task in remote sensing-based forest inventories. However, traditional methods of collection demand extensive personnel resources. Thus, field-reference data collection would benefit from more automated methods. In this study, we proposed a method for individual tree detection (ITD) and stem attribute estimation based on a car-mounted mobile laser scanner (MLS) operating along forest roads. We assessed its performance in six ranges with increasing mean distance from the roadside. We used a Riegl VUX-1LR sensor operating with high repetition rate, thus providing detailed cross sections of the stems. The algorithm we propose was designed for this sensor configuration, identifying the cross sections (or arcs) in the point cloud and aggregating those into single trees. Furthermore, we estimated diameter at breast height (DBH), stem profiles, and stem volume for each detected tree. The accuracy of ITD, DBH, and stem volume estimates varied with the trees' distance from the road. In general, the proximity to the sensor of branches 0–10 m from the road caused commission errors in ITD and over estimation of stem attributes in this zone. At 50–60 m from roadside, stems were often occluded by branches, causing omissions and underestimation of stem attributes in this area. ITD's precision and sensitivity varied from 82.8% to 100% and 62.7% to 96.7%, respectively. The RMSE of DBH estimates ranged from 1.81 cm (6.38%) to 4.84 cm (16.9%). Stem volume estimates had RMSEs ranging from 0.0800 m^3 (10.1%) to 0.190 m^3 (25.7%), depending on the distance to the sensor. The average proportion of detected reference volume was highly affected by the performance of ITD in the different zones. This proportion was highest from 0 to 10 m (113%), a zone that concentrated most ITD commission errors, and lowest from 50 to 60 m (66.6%), mostly due to the omission errors in this area. In the other zones, the RMSE ranged from 87.5% to 98.5%. These accuracies are in line with those obtained by other state-of-the-art MLS and terrestrial laser scanner (TLS) methods. The car-mounted MLS system used has the potential to collect data efficiently in large-scale inventories, being able to scan approximately 80 ha of forests per day depending on the survey setup. This data collection method could be used to increase the amount of field-reference data available in remote sensing-based forest inventories, improve models for area-based estimations, and support precision forestry development.

1. Introduction

The first studies that used ground-based LiDAR (Light Detection and Ranging) to measure forests date from the early 2000 s (Hopkinson et al., 2004; Lovell et al., 2003). Since then, different authors have explored and reported on the accuracy of stationary (Terrestrial Laser Scanner – TLS) and mobile (Mobile Laser Scanner – MLS) ground-based LiDAR to measure forest parameters and stem attributes. These systems can provide accurate measurements of stem profiles and diameter at breast height (DBH) at tree-level in a relatively short time and with centimeter-level accuracy (Balenović et al., 2020; Hyyppä et al., 2020c; Olofsson and Holmgren, 2016; Pierzchała et al., 2018; Puliti et al., 2020). In addition, some ground-based laser systems can go beyond estimation of traditional plot-level attributes (Newnham et al., 2015) and provide, for instance, information on trees' branch structure (Lau et al., 2018; Zhang et al., 2020) and sawmill timber quality (Pyörälä et al., 2019b, 2019a) with good accuracy and a high level of detail.

However, ground-based LiDAR systems are not operationally used in forest inventory despite their proven suitability for retrieving field data due to different reasons, for instance, the high prices of the equipment

* Corresponding author.
E-mail addresses: raul.de.paula.pires@slu.se (R.P. Pires), kenneth.olofsson@slu.se (K. Olofsson), henrik.persson@slu.se (H.J. Persson), eva.lindberg@slu.se (E. Lindberg), johan.holmgren@slu.se (J. Holmgren).

https://doi.org/10.1016/j.isprsjprs.2022.03.004
Received 20 October 2021; Received in revised form 28 February 2022; Accepted 8 March 2022
Available online 18 March 2022

and the availability of data processing tools. In addition, the intensive manual work required for collection of TLS and MLS data (Calders et al., 2020), with field campaigns comparable to those of traditional forest inventory, make these technologies less competitive with traditional methods.

Area-based approaches (ABA, Næsset 2002) have been used in many operational remote sensing-based forest inventories, providing estimates for a given region or pixel that can vary in size from a few square meters to hectares (Holopainen et al., 2014). In this approach, field-reference data are used as a response variable in the calibration of remote sensing-based models. Such models can be used to estimate forest attributes, such as timber volume per hectare, over the entire inventoried area. To develop a good model, the reference data should be representative of the whole study area, covering as much of the forest variability as possible. However, drawing a sample that sufficiently represents the whole inventoried area is time- and resource-consuming, which causes surveys to be a trade-off between cost efficiency and accuracy gain. The ABA has been used in simple homogenous forest conditions such as Scandinavian forests to provide rather accurate stand-level estimates. However, such estimates usually lack the details necessary for optimal planning of forest usage for different goals, such as tree-level information (Holopainen et al., 2014). Hence, the term Precision Forestry has been introduced and is often used to describe the stage at which individual tree maps are generated (Hyyppä et al., 2020c), including both qualitative (e.g., species) and quantitative (e.g., diameter and volume) information about each tree. This stage requires efficient methods for collecting reference data in an amount sufficient to train models at the individual tree level.

Recently, MLS systems appeared as efficient alternatives to conduct forest measurements (Holmgren et al., 2019; Hyyppä et al., 2020b; Liu et al., 2021; Puliti et al., 2020). They can be grouped according to their platform, namely handheld, on a backpack, or vehicle- or UAV-mounted (also called ULS). One important challenge of using MLS is the positioning signal under the forest canopy, which makes the co-registration of the point clouds a challenge to be solved by different methods (Bakula et al., 2015; Kukko et al., 2017; Qian et al., 2017). Improvements in the accuracy of positioning under forest canopy, and in the LiDAR sensor technology, have made it possible to acquire MLS point clouds comparable with those obtained with TLS in terms of accuracy and precision. For instance, Hyyppä et al. (2020c) obtained point clouds with point registration accuracies ranging from $\pm$ 1 cm in a backpack MLS to $\pm$ 3 cm in a handheld MLS and under canopy ULS.

Amongst the different MLS systems, the ones mounted on all-terrain vehicles (ATVs) or cars are used in the assessment of some types of urban infrastructure and by the automotive industry (Puente et al., 2013), but less often in forestry compared to TLS or other MLS systems. This system has a great potential to be used in automatic large-scale forest assessments and to provide an alternative to traditional reference data collection. Nevertheless, only a few promising studies have assessed its suitability to measure forest structure at individual tree-level. For instance, Forsman et al. (2016) proposed an algorithm to detect stem points in a point cloud acquired from a car-mounted MLS, yielding an RMSE (Root Mean Squared Error) of 3.7 cm on DBH estimations. Later, Čerňava et al. (2019) tested the performance of a highly accurate MLS mounted on a tractor under heavy canopy conditions, reporting an RMSE of 3.1 cm on DBH estimations in these areas. Both studies suggest that vehicle-mounted MLS could be used to conduct forest measurements.

A car-mounted MLS can provide reference data in the quantity and quality required to calibrate models at individual tree level and reduce the need of labor-intensive field campaigns, thus supporting efficient Precision Forestry. This system can take advantage of forest road networks in regions like Sweden, where there are approximately 210,000 km of forest roads accounting for about one-third of the total road network in the country (Axelsson et al., 2018), making measurements on the go during field visits or operations. However, areas with dense forest cover and sparse road network could not be suitable for using of a vehicle-mounted MLS with inventory purposes, once the sampling would be restricted to only a few areas. In terms of autonomy, cars or ATVs are capable of operating for longer during field campaigns when compared to other MLS systems (e.g., under-canopy ULS). Moreover, it would be possible to train models with local reference data in remote sensing-based forest inventory, instead of using samples at the regional or national level. Finally, the smooth trajectory on forest roads together with a clear positioning signal can yield high accuracy point clouds, making it possible to derive accurate estimates of forest variables at individual tree level.

A method able to estimate stem attributes using MLS from forest roads could change the current opportunities of using remote sensing-based methods that require large amounts of reference data for calibration and parametrization. For instance, Kolendo et al. (2021) used a large-scale reference dataset to parameterize ITD algorithms in coniferous forests, reaching tree count RMSEs varying from approximately 6 to 13%, depending on the forest type. Skudnik and Jevšenak (2022) found that, in the presence of sufficient reference data for calibration, artificial neural network-derived tree height predictions can outperform predictions derived from mixed effect models. Generally, deep learning methods require large datasets for calibration to be used at their full potential (Hamraz et al., 2019; Xi et al., 2020).

In addition, the type of reference data is a constraint while working with remote sensing-based environmental assessments, because some forest attributes are not easily measurable with manual methods. For instance, Zhen et al. (2016) pointed out the difficulty to acquire precise tree locations in field reference data as a disadvantage of individual tree detection approaches in forest inventories. Another example is the estimation of stem profiles, which requires either destructive methods or heavy machinery to be measured. In this sense, the car-mounted MLS has the potential to provide data of the type and amount required by different applications and pose as a suitable reference data collection component in remote sensing-based forest inventories.

A possible drawback of such a solution is that at the roadside, where there is usually less competition among individual trees, the trees are under edge effect and may show different growth rates and patterns compared to trees further into the stand (Delgado et al., 2007; Harper et al., 2015). Consequently, a car-mounted MLS solution that limits data collection to the roadside might sample mostly trees that are not representative of the whole forest and may not be suitable for calibrating remote sensing-based models.

The main objective of this study is to assess the suitability of a car-mounted MLS sensor to retrieve field reference data along forest roads. We assess the potential of such technology in providing reference data for remote sensing-based forest inventories. The specific objectives are: (1) to propose algorithms for ITD (Individual Tree Detection), DBH, stem profiles, and total volume estimation with MLS data, and (2) to assess the influence of distance from the roadside on the estimations.

2. Material and methods

2.1. Study area and reference data

The proposed algorithms were validated on the Remningstorp test site, in Southern Sweden (lat. 58.5 degreesN, long. 13.6 degreesE), where the dominant tree species were Norway spruce (*Picea abies*) – 85.7%, Scots pine (*Pinus sylvestris*) – 9.1%, and Birch (*Betula* spp.) – 3.4%, with density of 580 trees/ha. Altogether, 18 circular plots with a radius of 10 m were measured in the field during summer 2017. In each field plot, all living trees with a DBH greater than 4 cm had their DBH and position recorded. The mean DBH of the measured trees was 26.7 cm, with approximately 95% of all measured trees having DBH >= 15 cm. The plots were organized in six groups, with the plot centers aligned perpendicularly to the road (Fig. 1).

To evaluate the effect of the distance from the road on the proposed

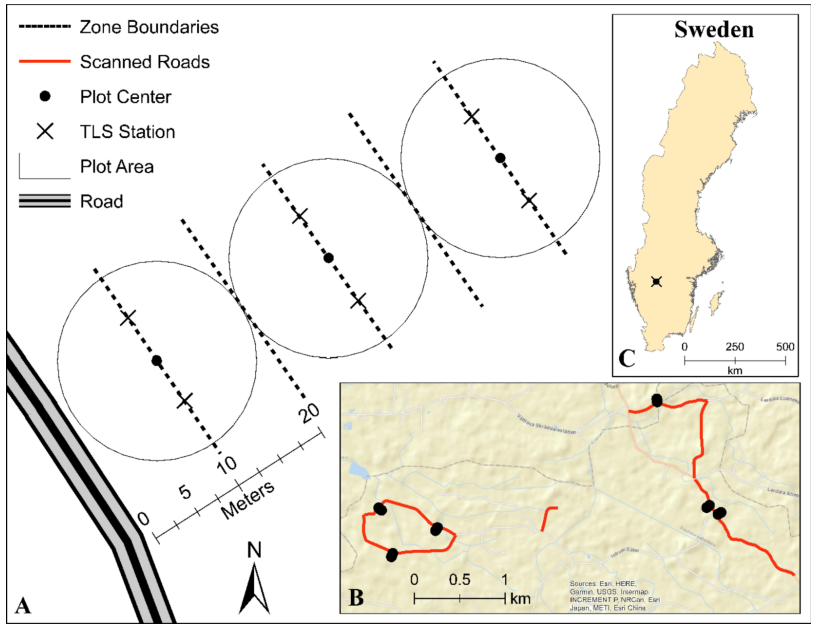

Fig. 1. Schematic representation of spatial disposition of a group of plots in relation to the roadside and TLS survey setup (A), with details of the position of the plots in the study area (B), and position of the field plots in Sweden (C).

method's accuracy, we divided the trees into 6 range zones, according to their distances from the roadside: 0–10 m, 10–20 m, 20–30 m, 30–40 m, 40–50 m, and 50–60 m (Fig. 1).

In November 2019, TLS surveys were conducted in each group using a multi-scan setup, with 2 scans per plot (Fig. 1). The TLS sensor used was a Trimble TX8. The wavelength was near-infrared (1500 nm) and repetition rate was 1 million points per second. The field of view was 360 degrees in the horizontal and 317 degrees in the vertical direction, and the point spacing of 0.4 cm at 10 m from the scanner. The footprint diameter was 3.4 cm at 100 m from the sensor. The system records up to three returns from the same pulse with a range accuracy less than 0.2 cm.

The TLS point cloud was processed according to Olofsson and Holmgren (2016). The stem volume was estimated for the TLS data using the stem curve procedure described in section 2.3.7. In comparison with field-measured DBHs, the TLS measurements had an overall Root Mean Squared Error (RMSE) and bias of 1.54 cm and 0.93 cm, respectively. Table 1 shows the RMSE of TLS-derived DBH estimates for each distance range from the road. These values are higher than the reported by Olofsson & Holmgren (2016) of 1 cm RMSE. This difference may be partly explained by the two years elapsed between the field and TLS surveys, which might also have caused the systematic overestimation evidenced by the positive bias. In addition, zones as 0–10 m and 50–60 m were scanned by the TLS from only one direction, whereas the zones from 10 to 50 m had TLS positioned in both sides of the trees. This scanning set up might have caused lower accuracy in the closest and furthest distance ranges.

Table 1
RMSE and bias of TLS-derived DBH estimates according to the distance range from the road.

Zone	RMSE	Bias
0–10 m	2.57 cm (10.7%)	2.35 cm (9.87%)
10–20 m	1.53 cm (5.60%)	1.04 cm (3.81%)
20–30 m	1.40 cm (5.06%)	1.11 cm (4.02%)
30–40 m	1.55 cm (5.62%)	0.85 cm (3.11%)
40–50 m	1.32 cm (5.15%)	1.01 cm (3.94%)
50–60 m	1.62 cm (6.36%)	0.82 cm (3.22%)

2.2. Mobile and Airborne laser scanning systems and Pre-processing

The MLS data survey was carried out using a car-mounted Riegl VUX-1LR sensor in November 2019. In total, approximately 7 km of forest roads were scanned in the both sides, yielding 84 ha of scanned forests considering the 0–60 m range. The car had a speed of 8 km/h and the sensor was leaning 30 degrees from the horizontal plane, with the side of the sensor pointing up and turned toward the front part of the car. The sensor shot near-infrared (1550 nm) pulses at a repetition rate of 820 Hz, which together with a field of view of 330 degrees yielded the angular step width (ASW) of 0.0066 degrees. The footprint diameter was 5 cm at 100 m from the sensor. The system records up to three returns from the same pulse with point registration accuracy of 1.5 cm.

The Airborne laser scanning (ALS) data was collected in October 2019 with a Leica TerrainMapper-LN system from approximately 1450 m above ground. The airplane had an average speed of 115 knots. The laser beam footprint was 0.35 m, the pulse frequency equal to 1600 Hz, and the scanner field of view equal to 30 degrees. The average point density was approximately 22 points/m^2.

Before ITD, the point clouds were classified into ground and non-ground points using the ground classification algorithm by Zhang et al. (2016) implemented in the lidR R package (Roussel et al., 2020). Once classified, we divided the MLS point clouds in two. The first point cloud excluded the ground points, and this was used for ITD, diameter, and stem profile estimation. The second point cloud was formed by only

the ground points and used to find the aboveground height of the trees.

2.3. Individual tree Detection, stem Profiling, and stem curve estimation

The scanner's setup was chosen to facilitate tree detection and stem diameter estimation. The sensor's high repetition rate, combined with a scanning frequency lower than that normally used in surveys, yielded point clouds with high density within scan lines, but two consecutive scan lines are more separated in space. For instance, at 40 m from the sensor, two consecutive points were approximately 0.5 cm apart, whereas two consecutive scan lines were approximately 17 cm apart. The scanning frequency was chosen to yield very high density in stem cross sections, facilitating branch filtering and circle fits. However, it caused a significant loss of information in the vertical direction along the stem. Thus, this setup provided a better representation of the the targets in the scanline direction than in three dimensions, since solid targets—like stems—do not become represented in the point cloud as continuous surfaces, but rather as a collection of cross sections (Fig. 2). For this reason, the proposed ITD algorithm assumed that points belonging to the same stem appear in the point cloud as arcs, and it finds point clusters with circular shape within each scan line. After that, the identified arcs were segmented into single stems. Next, to estimate the stem profile, we divided the detected stems into sections, corrected their inclination (to point straight up), and estimated their diameter.

One characteristic of the car-mounted MLS data is the uneven point density of the point cloud (Fig. 3), which varied according to the distance from the sensor: while areas closer to the road (and thus closer to the sensor) had trees with both the stem and canopy scanned, trees further into the stand might have lacked several portions of the stem and did not have returns from the upper canopy part, which prevented the retrieval of total heights from the MLS point cloud for many trees in these areas. To contour this issue, each tree's total height was retrieved from ALS instead of MLS point clouds. Total heights can also be modelled based on other tree attributes, however, in this study we used ALS-retrieved values in order to better understand the effects of the distance from the road in the estimates.

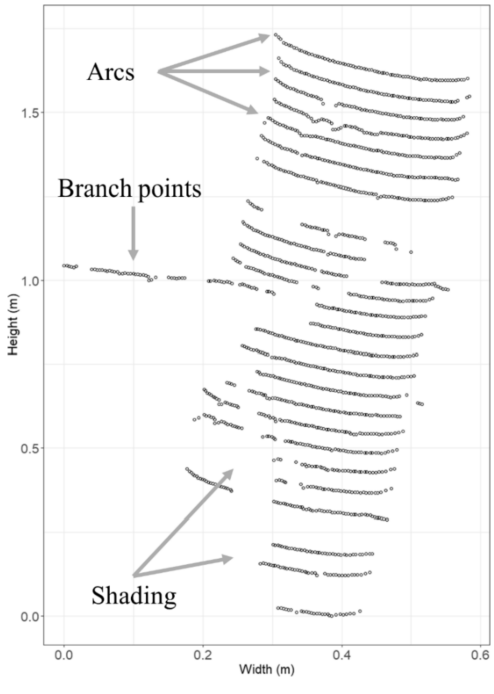

Fig. 2. Representation of a stem section in the car-mounted MLS point cloud. The stem is represented as a collection of arcs. It is possible to notice branches and shaded areas.

Finally, once the stem profiles of each tree were estimated, a stem curve model was fit to each detected tree. With such model, we could estimate diameters at any height of the tree even though it might not have been scanned. A flow chart of the method is presented in Fig. 4, and the details of each step are described in the following sections.

2.3.1. Intensity-based point clustering per scanline

The trees were independently detected in each scanline by finding arcs in the point cloud, as in Forsman et al. (2016). In this step, we assumed that points close enough to each other could be considered as returns from the same target, e.g., the same stem.

The algorithm operates in each scanline in two steps. First, it clusters points together and secondly, it uses intensity thresholds to select only reliable laser returns in each cluster. This avoided inaccurate echoes at the edge of the stem due to, for instance, the laser beam's footprint (Forsman et al., 2018, 2016). This process works as follows:.

- For each scan line, cluster together points that are at a maximum distance d_t cm from each other. In other words, inside a cluster a point should be maximum dt cm from its nearest neighbor in the same cluster. The cluster should have at least 15 points;
- For each cluster, save the 95th intensity percentile as the intensity peak (*Ip*). Then filter out points with intensity value less than 70% of *Ip*.

The threshold distance d_t used to cluster points together was based on the laser survey's angular step width (*ASW*) and accuracy (*A*). It denotes the maximum distance a point in a given cluster should be from its closest point in the same cluster. It is given by equation (1),

$$d_t = \sin(ASW/2)*D*2 + 2*A, \quad (1)$$

where the first part of the equation denotes the minimum distance between two consecutive points at a given distance *D* from the sensor, assuming the points have reflected from a perfectly flat target. The ASW represents the angular separation between two consecutive laser pulses. Finally, different factors, such as the stem shape and point positioning errors, could cause the distance between two consecutive points to be bigger than the theoretical one. For this reason, we added two times *A* to d_{min} to form d_t, accounting thus for both the circular shape of the stem and inaccuracies in the point's position.

2.3.2. Circle fitting

The first circle fitting was done for two reasons: first, to eliminate point clusters that do not have the arc shape we assume stems to have, and second, to obtain coordinates for each circular cluster, which will be subsequently used to segment the arcs into tree stems.

To fit the circle, we used the modified version of the Random Sample Consensus (RANSAC) algorithm described by Olofsson et al. (2014). This algorithm iteratively fits circles to a given set of points and chooses the best fit (Fig. 5). The circles were fit to the projection of the points on the horizontal plane, i.e., only the X and Y coordinates were used in the fitting process. The number of iterations for each cluster was set to 140, based on the probability of finding a good circle model, as in the paper by Olofsson et al. (2014). In each iteration for a given cluster, three points were randomly selected and a circle was fit to them. For each iteration, we recorded the number of inliers as being the number of points within a given tolerance distance from the circle. The points outside this tolerance distance were considered outliers. Each iteration determines unique sets of inliers and outliers, which are not dependent

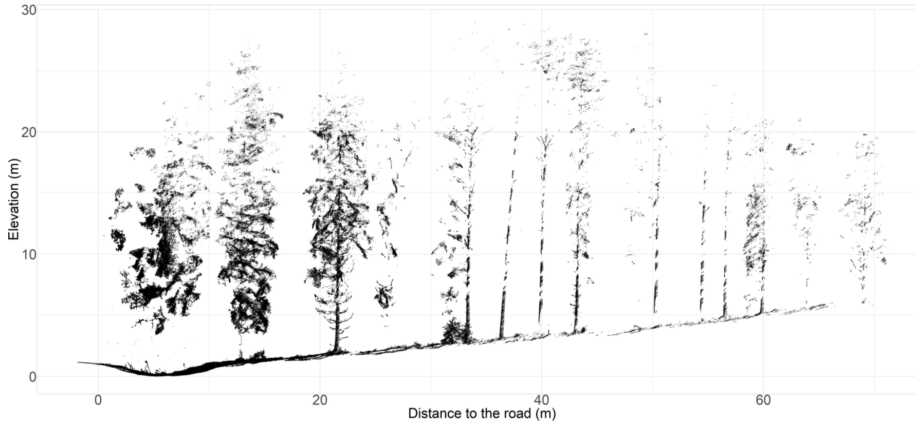

Fig. 3. Representation of 3D point cloud, where the point density varies according to the distance from the sensor. The left side is closer to the sensor than the right side and has more points in the canopy and on the stem compared to the trees in the right side of the figure.

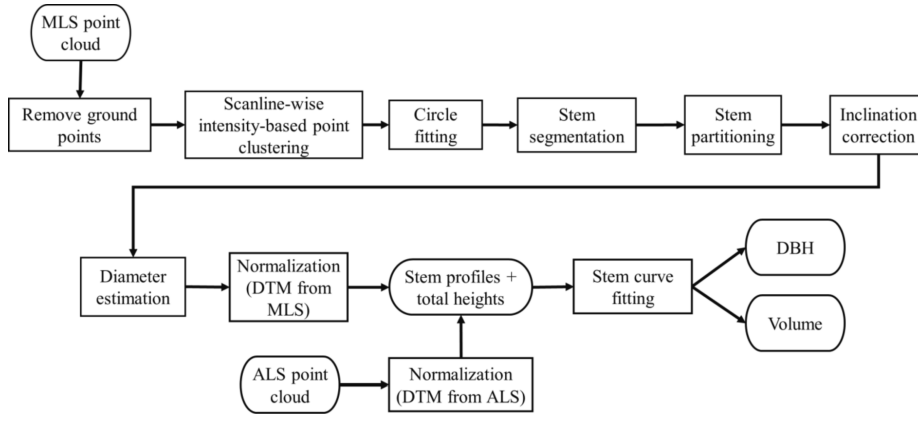

Fig. 4. Flowchart showing the processing of MLS point cloud.

on the other iterations. In this study, we decided to set this tolerance distance equal to the accuracy of the laser survey, which was 1.5 cm.

We assumed that the laser beam cannot go through the stem, so if the randomly chosen circle in a given iteration had more than 1% of the outliers inside the trunk, the iteration was considered invalid. Then, we selected the fit with the highest number of inliers amongst the valid iterations as the best fit. After the best fit is selected, the outcomes of all the other iterations are ignored. The inliers of the best fit were used in a final adjustment by iteratively looking for the circle with smallest mean squared distance between its inliers and its edge. The center coordinates (X, Y), its radius and height (median height of the points), were recorded for the next step.

2.3.3. Stem segmentation

Since the trees were detected independently in each scan line, it was necessary to vertically aggregate the arcs to build consecutive tree stems. Thus, in the stem segmentation, we associated several arcs to a single stem using the circle center locations obtained in the previous step, according to the tree stem segmentation proposed by Holmgren et al. (2019):

- For each arc's circle, estimate a direction vector (Vd_i) using other circles within a 50 cm radius of the target circle with Principal Component Analysis (PCA). Use the center coordinates (X, Y and height) of the circles as input;
- For each Vd_i, calculate the root-mean-square-deviation (RMSD) of the 3D linear distance of the circles' centers to Vd_i;
- Sort all the *Vds* from the smallest to the largest RMSD;
- For each Vd_i, starting from that with smallest RMSD, segment to the same stem all the arcs whose circular areas – generated in section 2.3.2 – are crossed by Vd_i. In other words, segment to the same stem all circles crossed by the direction vector calculated in the first step. Repeat this step until no more arcs are available (i.e., no more arcs without a stem associated).

Once the arcs were segmented into stems, we recorded the position of the lowest arc as the position of the stem.

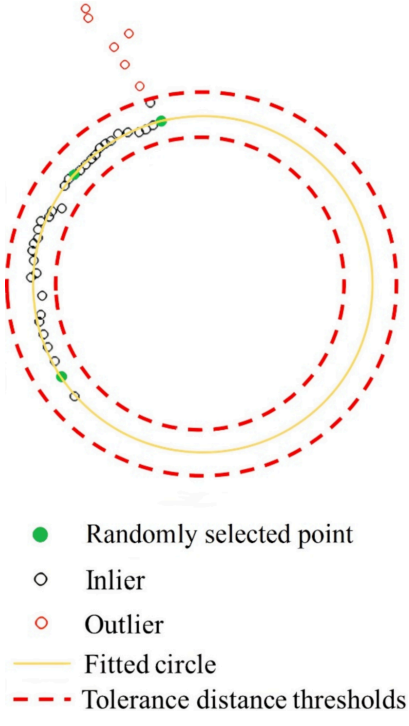

Fig. 5. Schematic representation of the point selection done by the modified RANSAC (Olofsson et al., 2014).

2.3.4. Stem partitioning

Neighboring arcs from the same stem were grouped to provide better input data for the circle fitting than would be possible using a single arc (Fig. 6 A and B). This process, which we called stem partitioning, was necessary for two reasons. First, branch points are often classified as stems, especially in transition areas where both connect. Second, the identified arcs might have imperfections, such as gaps or noise around them (Fig. 2).

The grouping was done by partitioning the segmented stem into small sections of 30 to 50 cm. The size of the section was dependent on how many arcs could be found in each height interval. In this study, the minimum number of arcs in each section was defined according to the laser survey's setup, which gives that two consecutive scan lines would be 17.1 cm apart from each other in height. Thus, on a 30 cm long section of a given stem, we expect to find two arcs. However, this distance between scan lines can vary according to the car's speed during the survey. Hence, when fewer than two arcs were found in a 30 cm section, the section size was increased by 10 cm until it reached 50 cm, or until the minimum of two arcs were found. If at least two arcs were not found in a 50 cm interval, this interval was considered empty and not used in the stem profiling. In the first two zones, from 0 to 10 m and 10–20 m, we recorded stems with at least 10 sections, to avoid classifying bushes or branches as trees. When stems in those zones had fewer than 10 sections, they were considered noise.

2.3.5. Inclination correction

Hyyppä et al. (2020b) demonstrated that the horizontal projection of points from inclined stems can lead to biased diameter estimations when trees lean more than 3–4 degrees. To avoid such errors, stem direction should always be perpendicular to the plane on which the points are projected.

In this study, diameters were always estimated in the horizontal plane. Therefore, the stem's inclination was corrected before projecting its sections. It is also important to note that a stem's inclination is not constant along the tree. For this reason, we corrected the inclination at each 2 m of stem, respecting the sections defined in the previous step: we found the direction vector of each 2-meter log simply by getting the centroids of the log's upper- and lowermost sections. Then, we rotated

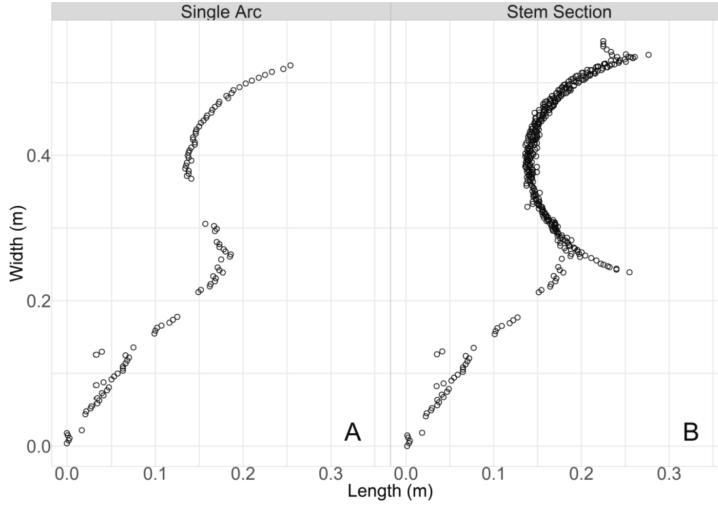

Fig. 6. Representation of a stem section from a Norway spruce tree where all points were classified as stem points. A: Single arc seen from above; B: group of arcs (stem section) seen from above.

the log to match a vector of the same size with its upper- and lowermost sections vertically aligned.

2.3.6. Diameter estimation

After defining the sections and correcting their inclination, we estimated the sections' diameters by fitting circles to the projection of each section's points on the horizontal plane. The main difference between the two circle fit steps in this study is that in section 2.3.2 the process was done at arc level (i.e., only one scan line), whereas in the current step the fit was done at section level (i.e., group of arcs).

In addition, the circle fit for diameter estimation was done in two stages as proposed by Lindberg et al. (2012), making the estimation less sensitive to the local influence of branches. In the first stage, we fitted circles as described by Olofsson et al. (2014). In the second stage, the center positions (X_c, Y_c) and diameters (D) from the circles in the first stage were used to select a new set of points. If we let (x_i, y_i) be a point coordinate from the stem section we are analyzing, we select the points that meet the criteria in equation (3) in the second stage.

$$(X_c - x_i)^2 + (Y_c - y_i)^2 \leq (p^*D/2)^2 \quad (2)$$

where p is a constant that expresses the maximum distance from the circle center (X_c, Y_c) a point (x_i, y_i) should be so it would be included in the second stage, expressed as a proportion of the radius value found in the first stage. In this study, we use $p = 1.1$.

At last, a final circle fitting was done using the points selected in the second stage, and the diameter value and section height found were recorded as the stem profile of the tree.

2.3.7. Stem curve

We used the stem curve model by Hyyppä et al. (2020b) to describe the diameter variation along a tree's stem, estimating diameter values for regions of the tree that have not been scanned, e.g., the treetop and DBH height. The model combines equations (4) and (5).

$$R_a(z) = a_1{}^*(H - z) + a_2{}^*(H - z)^2, \quad (3)$$

$$R_b(z) = b^*\sqrt{(H - z)}, \quad (4)$$

where H is the total height of the tree retrieved from ALS, and $R(z)$ is the radius at the height z. Both a_1, a_2, and b are coefficients to be determined with least square regression. With the coefficients, equation (5) gives the stem volume (V).

$$V = \pi \Big/ 2^*\left(\int_0^H R_a(z)^2 dz + \int_0^H R_b(z)^2 dz\right). \quad (5)$$

The system composed by equations (3) and (4) was chosen for several reasons, as pointed by Hyyppä et al. (2020b). First, the small number of coefficients used in the equations make the model robust to deal with outliers along the stem profile. Second, the average of both equations (effective fit) fits well to the stem profile, performing similarly in trees with several diameter values measures along the stem (Fig. 7 – Tree A), and trees with less measurements (Fig. 7 – Tree B).

To obtain accurate total heights for all the trees we use ALS data over the same area. The retrieval of total heights from the ALS point cloud was done with a 30 cm radius search around the MLS-retrieved tree positions. Inside this radius, the highest height value was considered the tree's total height.

2.4. Accuracy assessment

Different reference data sources were used to assess the accuracy of the variables retrieved with the car-mounted MLS. The accuracy of the ITD was assessed in each zone by matching the MLS-detected trees with the field-recorded tree positions. This was done by conducting a radius search around 30 cm of each MLS-detected tree. If an MLS-detected tree corresponded to a field-recorded one, the tree was considered a true positive. If it did not correspond to any field-recorded tree, it was considered a commission error. Finally, we considered omission when a field-recorded tree position did not have any correspondence with the MLS-detected individuals. Then, we computed the precision (equation (6)) and sensitivity (equation (7)) to quantify the accuracy of the ITD:

$$Precision = TP/DT, \quad (6)$$

$$Sensitivity = TP/(DT + OT), \quad (7)$$

where TP is the number of trees correctly detected (true positives), DT is the total number of trees found by the proposed ITD algorithm, and OT is the number of trees present in the reference data which were not found by the proposed method (omissions).

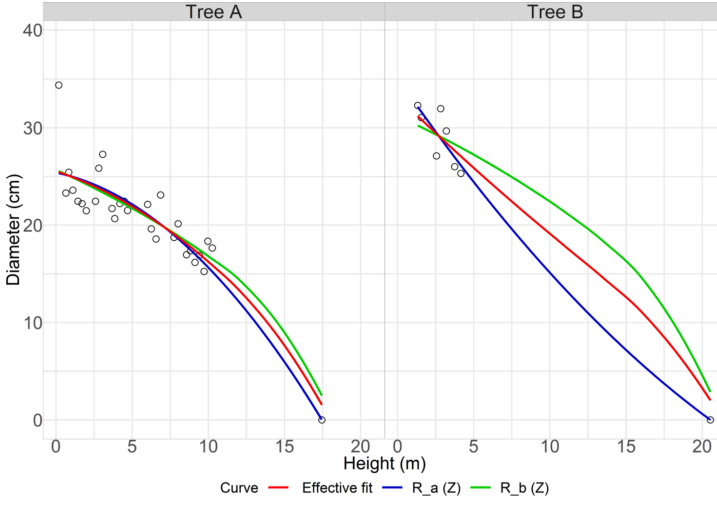

Fig. 7. Parabolic function R_a (z) in blue (equation (3)), square root function R_b (z) in green (equation (4)) that compose the stem curve model fit to the stem profiles of two different trees (Tree A and B). The average (effective fit) of R_a (z) and R_b (z), which is used to estimate the effective diameter values and stem volume, is shown in red. Trees A and B have different number of diameter measurements along the stem. (For interpretation of the references to colour in this figure legend, the reader is referred to the web version of this article.)

TLS-derived DBHs, stem profiles and total volumes were used as reference to assess the accuracy of MLS-derived estimates of these three forest attributes. In this study, TLS-derived values were preferred over other methods of reference data collection once the measurement of stem profiles and volume though destructive methods was not feasible. Thus, in each zone, the performance of the proposed method was evaluated by comparing the MLS-derived and TLS-derived DBHs, stem profiles and total volumes of each detected tree by computing the RMSE - equation (8) - and bias - equation (9). The relative RMSE and bias were calculated in relation to the reference mean values of each variable.

$$RMSE = \sqrt{\sum_{i=1}^{N} (\hat{y}_i - y_i)^2} \Big/ n, \tag{8}$$

$$bias = \sum_{i=1}^{N} (\hat{y}_i - y_i) \Big/ n, \tag{9}$$

where y_i and $\hat{y}_i$ are the target's variable reference and estimated values, respectively, for unit i and n is the total number of units.

To compare the stem profiles obtained with the two methods, we defined a comparison range that comprehends the height interval of the stem where both MLS and TLS measurements are available. Inside the comparison range, we calculated the average diameter for each 1-meter interval, thus reducing the local influence of outliers in both the MLS and reference datasets.

Finally, we evaluated the difference of the diameter distributions obtained with the different sensors in each detection zone (5 cm classes). For that, we used the error index e (Reynolds et al., 1988) proposed by Packalén and Maltamo (2008), as in equation (10),

$$e = \sum_{i=1}^{N} 0.5 \times |f_i/N - \hat{f}_i/\hat{N}|, \tag{10}$$

where f_i and $\hat{f}_i$ are the number reference and MLS-detected trees in diameter class i, respectively. N and $\hat{N}$ are the total number of reference and MLS-detected trees, respectively.

3. Results

3.1. Individual tree detection

Table 2 shows a summary of ITD's precision and sensitivity in different zones. The ITD performance varied according to the tree's distance from the road. From 0 to 10 m, we noticed the lowest precision and sensitivity in the study. This is mostly due to the high number of large branches and the proximity to the sensor. From 0 to 10 m from the road, we observed bigger branches compared to areas further into the stand. This factor, combined with the proximity to the sensor, meant that such branches were heavily scanned, causing some of them to be classified as separate trees (commission errors). At the same time, omission errors were caused by the high proportion of branches in the trees in this zone, which made discriminating between branches and stems not always possible. For instance, some stems might have been visible but could not be considered circular due to the amount of noise around them. In these cases, the stems were filtered out of the point cloud.

Table 2
Individual tree detection (ITD) precision and sensitivity according to the distance range from the road.

Zone	Precision	Sensitivity
0–10 m	82.8%	85.7%
10–20 m	96.5%	96.7%
20–30 m	98.8%	94.2%
30–40 m	92.5%	92.5%
40–50 m	98.0%	86.1%
50–60 m	100.0%	62.7%

The ITD had the best performance in the intermediate zones. Similar figures were observed from 10 to 20 m, 20–30 m, and 30–40 m, with both precision and sensitivity exceeding 90%. In these zones, the branches are smaller compared to the first zone, which made discriminating between branches and stems easier. Besides, in the intermediate zones, the point density is not as high as at 0–10 m from the road, causing fewer commission errors.

Beyond 40 m from the roadside, as distance to the sensor increases, we observe high precision and decreasing sensitivity. In these zones, few or no commission errors were observed, which justified the high precision values. However, as trees get more distant, the chances of occlusion increase and point density decreases, making it more likely that fewer points would hit the stems, and thus more difficult to discriminate between stem and crown.

3.2. DBH, stem profile, and DBH distributions

The prediction accuracy of DBH varied through the different zones (Fig. 8), with the RMSE and bias ranging from 1.81 cm (6.38%) to 4.84 cm (16.9%), and −0.41 cm (-1.35%) to 0.82 cm (2.86%), respectively. In some zones, e.g., from 0 to 10 m, the presence of outliers and the lower accuracy of the reference data in this zone influenced the accuracy of the predictions more. However, most errors were between ± 10%. In addition, the variation of RMSE in the different zones is a consequence of the presence or absence of scan arcs around the DBH height (1.3 m). Some trees do not have arcs near 1.3 m, which causes their DBH values to be a result of the stem curve built from diameter values at higher parts of the tree and creates the observed outliers.

The stem profile estimates (Fig. 9) had slightly lower RMSE than the DBH estimates, ranging from 1.58 cm (6.26 %) to 2.18 cm (8.76%). The bias ranged from −0.44 cm (-1.58%) to 0.22 cm (0.84%). We assessed the accuracy only in the scanned regions of the stem (comparison range), so these error values concern only the stem regions with both MLS and TLS data. On the other hand, DBH estimates were retrieved from a stem curve model, since not all the trees were scanned at 1.3 m height. For this reason, the DBH-related accuracy contains not only errors from the stem profiling, but also errors from stem curve fitting.

The error index of diameter distributions ranged from 0.11 to 0.33 (Fig. 10), with no trees below 10 cm DBH being correctly estimated, regardless of the zone. However, our study area had a few small trees (DBH < 10 cm), which does not allow a proper evaluation of the estimations in this stratum. The largest e was observed from 0 to 10 m. The smallest e values were found from 30 to 60 m, where e was equal to 0.11.

3.3. Volume

The stem volume estimates had the highest relative RMSEs in this study, ranging from 0.08 m^3 (10.1%) to 0.19 m^3 (25.7%) and bias from −0.03 m^3 (-4.07%) to 0.19 m^3 (8.25%) (Fig. 11). The highest RMSE and bias are in the first zone (0–10 m). The stem volumes are more likely to be overestimated in the zones closer to the road, whereas values further into the stand tend to be systematically underestimated.

We also compared the total reference and estimated total volumes of each zone (Table 3). For these estimates, the accuracy was highly correlated with the ITD performance in each zone, with the volume of omitted or commissioned trees being the main error source. For instance, both commission errors and the systematic overestimation of stem volumes observed from 0 to 10 m caused the total volume for the zone to be overestimated by 13% in average. On the other hand, omissions might have caused the underestimation observed from 50 to 60 m, where 66.6% of the total reference volume was detected. The area-level estimates performed better in the intermediate zones, where the ITD had the best overall performance. In the intermediate zones, the mostly small trees are omitted, which did not seem to influence the total volume

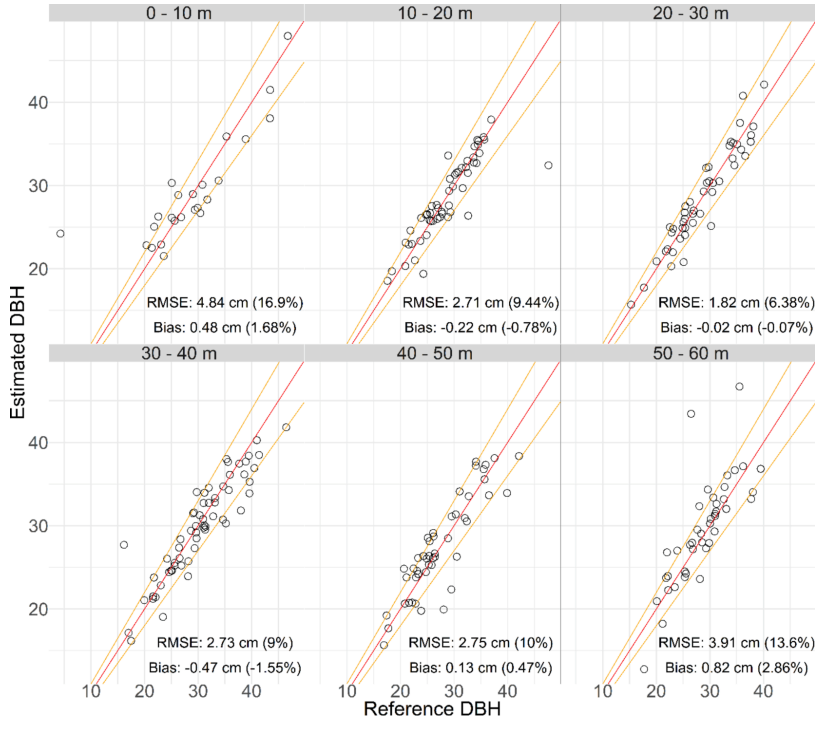

Fig. 8. Reference vs. estimated DBH. The red line is the 1:1 line, where reference and estimated values are equal. The orange lines represent a 10% deviation from the 1:1 line. RMSE = Root Mean Square Error. (For interpretation of the references to colour in this figure legend, the reader is referred to the web version of this article.)

estimates.

4. Discussion

4.1. Algorithm performance

The sensor configuration was tailored to detect tree stems along forest roads. Its high repetition rate combined with the sensor's inclination provided detailed cross sections of stems and enabled collection of data from both the ground and upper canopy. In this study, we proposed an algorithm for individual tree detection designed for such a sensor configuration, identifying the cross sections (or arcs) in the point cloud and aggregating those into single trees.

ITD is the key task in many MLS applications and is often the first result reported in several studies. The ITD method we proposed had a performance in the zones from 10 to 40 m (Table 2) comparable with that of other state-of-the-art methods: Liu et al. (2021) reported 96.7% precision and 93.5% sensitivity in a natural forest site with approximately 411 trees per hectare. Different precisions and sensitivities were found in the benchmark study by Hyyppä et al. (2020c), depending on the type of forest and MLS sensor. In obstructed forest (approximately 420 stems/hectare), the authors reported precisions and sensitivities of 100% and 79% respectively with backpack MLS, 100% and 76.7% with hand-held MLS, and 100% and 81.4% with under-canopy ULS. In sparse forest plots, with around 410 stems/hectare, the ITD performed better. Under these conditions, precisions and sensitivities of 100% and 92.9% respectively were found with all three systems, the backpack and hand-held MLSs and the under-canopy ULS. In these studies, the sensors were moving inside the forest plot, with a maximum distance from tree to the closest sensor of 20 m. In our study, depending on the zone, trees could be up to 60 m from the closest sensor location, which explains the lower ITD accuracy in zones far from the road.

The accuracy of DBH estimates (Fig. 8) achieved with our method ranged from 1.82 cm (6.38%) to 4.84 cm (16.9%) in the different zones. These estimates were less sensitive to the distance from the road, which made it possible to obtain accurate DBH estimates in all six zones. Our results are in-line with accuracies reported by other authors with different vehicle-mounted MLS systems. For instance, Bienert et al. (2018) used a highly accurate car-mounted MLS to estimate DBH with 3.7 cm RMSE, using field-measured DBHs as references. In addition, Liang et al. (2018b) reported an RMSE of 11.2% in DBH predictions with ATV-mounted MLS in boreal forests with approximately 600 stems/ha. Finally, Pierzchała et al. (2018) used a ATV-mounted MLS system composed by a Velodyne VLP-16 sensor, a stereo camera, an IMU, and a GPS to measure DBHs with RMSE equal to 2.4 cm.

The lowest RMSE in DBH estimation was found at 20–30 m from the road, a zone where we did not observe any outliers, which implies that the accuracies in the other zones could potentially be improved by using refined methods of outlier correction and different sensor set-up. For instance, a more efficient branch filtering method could improve not only the accuracy of DBH estimates but also tree detection, e.g. in zones where the large amount of unfiltered branches prevent the stems from being detected due to the algorithm's inability to identify circles in such cases. In addition, a reduced gap between two consecutive scan lines

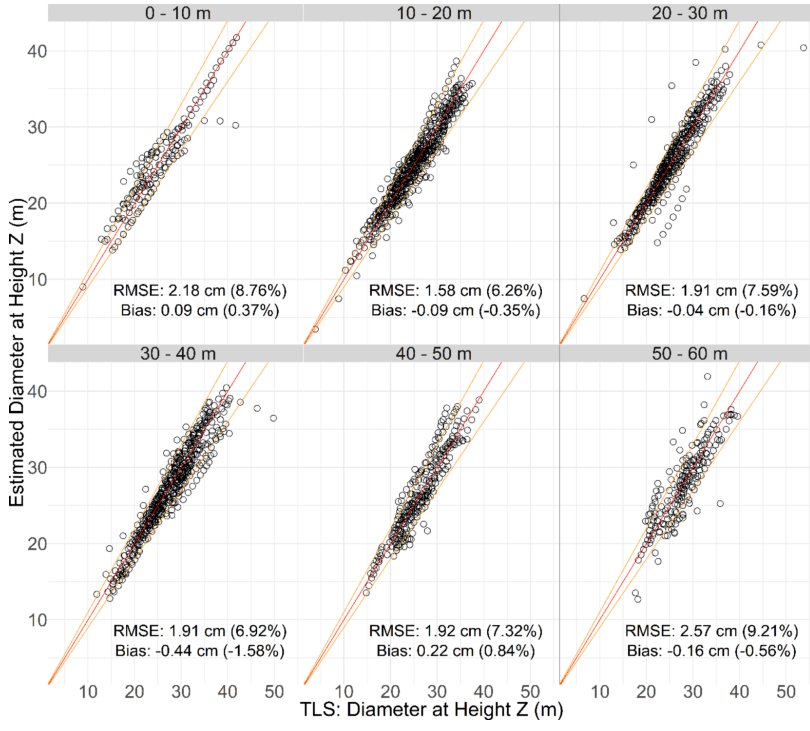

Fig. 9. Reference (TLS) vs. estimated (MLS) stem profile. The red line is the 1:1 line, where reference and estimated values are equal. The orange lines represent a 10% deviation from the 1:1 line. (For interpretation of the references to colour in this figure legend, the reader is referred to the web version of this article.)

could increase the amount of diameter measurements along the stem and the chances of having a measurement around 1.3 m, which would make both DBH and stem volume estimates more accurate regardless of the zone.

e is a measure of disparity between two distributions generated with different methods. In our study, the variation in *e* could be partially explained by the DBH estimates' error: tree-level errors caused stems to be allocated in the wrong diameter classes, thus increasing *e* when comparing the estimated and reference DBH distributions. For instance, in our study the highest *e* (0.33) was found in the 0–10 m zone, with one of the highest RMSEs (4.84 cm) and biases in DBH estimation (0.48 cm).

Stem profiles describe stems' shape and can be used to calculate stem volume. However, a manual diameter measurement of the higher part of the stem is impractical in operational forest inventory, since the trees would need to be felled before the measurements are conducted. Therefore, different TLS and MLS solutions have been proposed as non-destructive and efficient alternatives to stem profile measurement, and the method we describe in this study provided stem profiles with comparable accuracies (Fig. 9). For instance, a benchmark study by Liang et al. (2018a) found RMSEs of stem curve estimation ranging from 0.9 cm to 5.0 cm when comparing 13 multi-scan TLS-based algorithms under different forest conditions. Hunčaga et al. (2020) compared the accuracies of stem profiles obtained with different sensors, finding RMSEs equal to 1 cm, 1.3 cm and 1.9 cm in stem profiles obtained with TLS, hand-held MLS and close-rage photogrammetric point clouds, respectively. In addition, Hyyppä et al. (2020a) assessed the accuracy of stem curves obtained with under-canopy ULS, reaching RMSEs equal to 1.2 cm and 1.4 cm in sparse and obstructed forest plots, respectively. Finally, MLS-derived stem profiles can also be obtained with RMSEs ranging from 5.0% to 18.7% (Hyyppä et al., 2020b; Liang et al., 2018b) depending on, among other things, the type of MLS system and forest.

A drawback of the proposed method is that the stem profiles it provided were limited to the detectable portion of a tree's stem. In other words, even though we could obtain accurate estimates of the stem diameters at different heights regardless of the tree's distance from the road, the number of detected stem sections varied amongst trees, in our study ranging from a few units to tens. A challenge of working with largely varying stem profiles is finding a model capable of describing the stem curve accurately regardless of the number of available sections. To overcome this challenge, we used stem curve equations by Hyyppä et al. (2020b) (equations (3) and (4)), which were robust with both numerous and few stem profile measurements due to the low number of parameters to be calculated, thus preventing overfitting in stem profiles with only a few sections.

The accuracy of the stem volume estimates in our study varied from 0.08 m^3 (10.6%) to 0.12 m^3 (15.9%) in most of the zones, except at 0–10 m, where the RMSE was 0.20 m^3 (32.0%). The higher RMSE at 0–10 m can be at least partially explained by the lower accuracy of the reference in the same zone (Table 1). The bias of stem volume was mostly related to the distance from the road, varying from −0.03 m^3 (-3.25%), at 30–40 m, to 0.06 m^3 (10.2%), at 0–10 m. Closer to the road (e.g. 0–10 m), branches were often classified as stem points, which caused them to be included in the circle fitting and diameter estimation procedures. For this reason, the stem volumes closer to the road were systematically over estimated (Fig. 11). Further from the road (e.g., at 50–60 m) the systematic underestimation was often due to the few sections used to

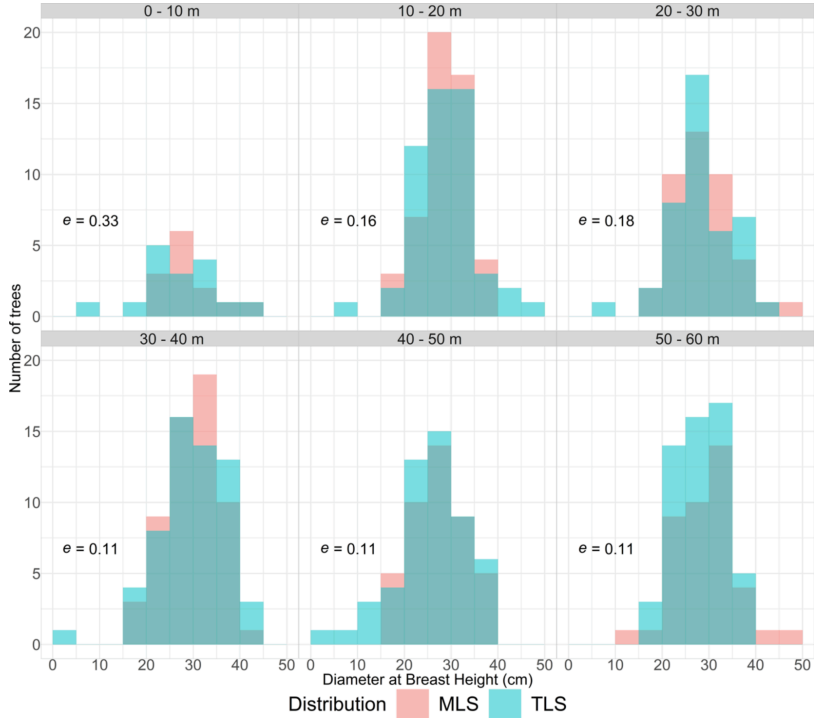

Fig. 10. DBH distributions and error index according to the distance from the roadside obtained with MLS (pink) and TLS (cyan), with overlaps in dark cyan. (For interpretation of the references to colour in this figure legend, the reader is referred to the web version of this article.)

estimate the stem curves in these areas. In other words, further from the sensor, the stem profiles may not represent the whole stem accurately and therefore lead to the observed underestimation.

Despite higher error at 0–10 m, our method performed in-line with other state-of-the-art methods for stem volume estimation. For instance, Hyyppä et al. (2020c) estimated stem volumes with relative RMSE ranging from 10% to 15% while benchmarking backpack and handheld MLS and depending on the MLS system used. Second, Liang et al. (2018a) reported relative RMSEs of volume estimates varying from 16.7% to 60.4% with different TLS-based algorithms in multi-scan setups. Third, Bienert et al. (2018) used car-mounted MLS to estimate, among other variables, merchantable and total stem volumes, reporting RMSEs equal to 0.4 m^3 and 0.6 m^3, respectively. Finally, the benchmark study by Liang et al. (2018a) compared different TLS systems and presented average RMSEs of 0.12 m^3, 0.21 m^3 and 0.18 m^3, in the easy, medium and difficult plots, respectively,.

Regarding total volume estimates, the RMSE (Table 3) ranged from 7.97% to 10.5% in most zones, except for the first and last zones, where commission and omission errors caused over and under estimations, respectively. These values are comparable with the accuracy of different LiDAR-based methods at the area level. For instance, Puliti et al. (2020) found a deviance of 32.2% at the plot level, 28.9% at the stand level, and 3.5% at the forest level when comparing under-canopy ULS- and field-based volume estimates. Maltamo et al. (2019) used accurate tree position data from harvester and ALS-based metrics to train k-NN (k nearest neighbor) estimators of total volume, reaching 9% RMSE in stand-level validations. Finally, Liang et al. (2018a) reported an average of 94% of total volume being detected with different TLS-based algorithms.

4.2. Applicability

One advantage of using car-mounted MLS instead of other ground-based LiDAR systems is the data collection efficiency provided by the car-mounted platform and the forest roads. The MLS survey used in this study took 2 h, scanning approximately 7 km of forests on both sides of the road. Therefore, at least 20 km of forest roads could be scanned in one day. When using the estimates from two zones (e.g., from 20 to 30 m and 30–40 m), the survey yields two sections, 20 m × 20 km, totaling 80 ha of scanned forest per day. In comparison, using traditional forest inventory methods, the same crew would measure approximately 10 circular plots, with a radius of 10 m, per day, yielding approximately 0.31 ha of inventoried area.

The choice of zones to use as reference data depends mostly on the edge effect and accuracy loss due to the distance from the sensor. First, it is important to make sure that the trees used as reference to train models are not under edge influence. Harper et al. (2015) suggested that boreal forests are less affected by both natural and human-caused edges, with the edge effect influence rarely exceeding 20 m in parameters such as basal area and canopy cover. Second, the low accuracy of the predictions in the zones from 40 to 60 m indicates that these areas are less suitable as reference for, e.g., remote sensing-based models. With the proposed sensor configuration, the data acquired at 20–40 m from the road or stand's edge had the highest overall accuracy, being the most recommended for use as reference for model calibration.

The algorithm we describe is easy to implement. The parameters

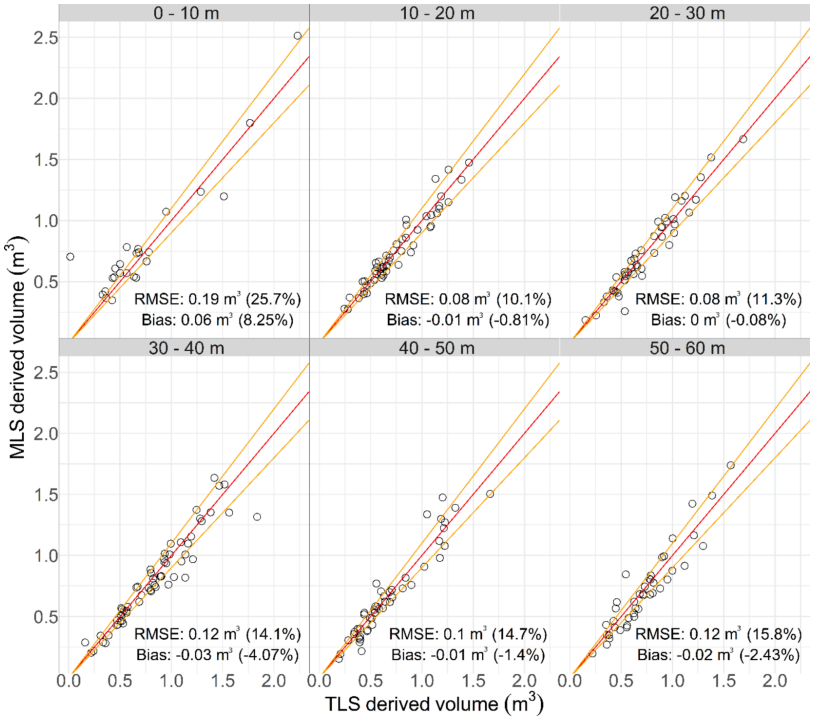

Fig. 11. Reference (TLS) vs. estimated (MLS) stem volume, in m^3. The red line is the 1:1 line, where reference and estimated values are equal. The orange lines represent a 10% deviation from the 1:1 line. RMSE = Root Mean Square Error. (For interpretation of the references to colour in this figure legend, the reader is referred to the web version of this article.)

Table 3
RMSE and bias of total volume estimates together with the average proportion of reference volume detected in each zone. The relative values were calculated using the reference total volume.

Zone	RMSE	Bias	Average Proportion ofReference Volume Detected (±SD)
0–10 m	1.00 m^3 ~ 27.2%	0.48 m^3 ~ 13.1%	113% (±22.7%)
10–20 m	0.64 m^3 ~ 8.33%	−0.42 m^3 ~ -5.47%	94.2% (±6.69%)
20–30 m	0.50 m^3 ~ 7.97%	0.07 m^3 ~ 1.20%	98.5% (±8.98%)
30–40 m	0.86 m^3 ~ 8.96%	−0.50 m^3 ~ -5.21%	94.0% (±9.52%)
40–50 m	0.65 m^3 ~ 10.5%	−0.54 m^3 ~ -8.82%	87.5% (±12.3%)
50–60 m	2.6 m^3 ~ 39.5%	−2.24 m^3 ~ -30.9%	66.6 % (±14.8%)

used, including angular step width and average distance between scan lines, were mostly derived from the survey's setup, enabling implementation in different forest conditions without the need of further parametrization. However, the difference in the accuracy of the analyzed variables in the different zones suggests that the algorithm's performance could be enhanced by using zone specific parameters.

5. Conclusions

In this study, we propose an algorithm to extract stem attributes from a car-mounted MLS circulating on forest roads, with focus on quantitative forest attributes such as DBH and stem volume in boreal forest conditions. Furthermore, we analyzed its performance at different distance ranges from the roadside. The results indicate that the proposed method can be an alternative for efficient reference data collection in forest inventories. With the presented sensor set up and algorithm, we were able to reduce the bias despite the proximity to the road by reaching beyond the forest area under edge effect. In addition, the accuracy of DBH and stem profile estimates remained stable from 10 to 60 m from the road, with the presence of few outliers. However, the accuracy of individual tree detection and stem volume estimates decreases as the distance from the road increases. Finally, future work might focus on improving branch filtering and explore how the predictions can be used to train remote sensing-based models in large-scale forest inventories.

CRediT authorship contribution statement

Raul de Paula Pires: Methodology, Software, Validation, Formal analysis, Writing – original draft, Visualization. **Kenneth Olofsson:** Methodology, Software, Validation, Resources, Writing – review & editing, Supervision. **Henrik Persson:** Methodology, Resources, Writing – review & editing, Supervision. **Eva Lindberg:** Methodology, Resources, Writing – review & editing, Supervision. **Johan Holmgren:**

Conceptualization, Methodology, Software, Resources, Writing – review & editing, Supervision, Funding acquisition.

Declaration of Competing Interest

The authors declare that they have no known competing financial interests or personal relationships that could have appeared to influence the work reported in this paper.

Acknowledgements

This research was jointly financed by Stora Enso AB and the Swedish University of Agriculture Sciences as part of a long-term research collaboration. The research was also financed by KSLA and the Kempe foundations though the project "Estimating Forest Resources and Quality-related Attributes Using Automated Methods andTechnologies", Grant Number TF 2019-0064 (Tandem Forest values research program). The MLS and field data collection were financed by Hildur and Sven Wingquist foundation for forest science research, Grant number 17/18-2 / 107-5 SOJOH. Finally, Visimind AB is acknowledged for the support with MLS data collection.

References

Axelsson, T., Bengtsson, P., Blomqvist, G., Landström, A., Melin, A., Fries, C., Möller, L., Holmström, A., 2018. Infrastruktur i skogsbruket med betydelse för skogsproduktionen : Nuläge och åtgärdsförslag. Delrapport inom Samverkan för ökad skogsproduktion. Skogsstyrelsen Rapp. 3, 42.

Bakula, M., Przestrzelski, P., Kazmierczak, R., 2015. Reliable technology of centimeter GPS/GLONASS surveying in forest environments. IEEE Trans. Geosci. Remote Sens. 53 (2), 1029–1038. https://doi.org/10.1109/TGRS.2014.2332372.

Balenović, I., Liang, X., Jurjević, L., Hyyppä, J., Seletković, A., Kukko, A., 2020. Hand-held personal laser scanning – current status and perspectives for forest inventory application. Croat. J. For. Eng. 42, 165–183. https://doi.org/10.5552/crojfe.2021.858.

Bienert, A., Georgi, L., Kunz, M., Maas, H.G., von Oheimb, G., 2018. Comparison and combination of mobile and terrestrial laser scanning for natural forest inventories. Forests 8, 1–25. https://doi.org/10.3390/f9070395.

Calders, K., Adams, J., Armston, J., Bartholomeus, H., Bauwens, S., Bentley, L.P., Chave, J., Danson, F.M., Demol, M., Disney, M., Gaulton, R., Krishna Moorthy, S.M., Levick, S.R., Saarinen, N., Schaaf, C., Stovall, A., Terryn, L., Wilkes, P., Verbeeck, H., 2020. Terrestrial laser scanning in forest ecology: Expanding the horizon. Remote Sens. Environ. 251, 112102. https://doi.org/10.1016/j.rse.2020.112102.

Černava, J., Mokroš, M., Tuček, J., Antal, M., Slatkovská, Z., 2019. Processing Chain for Estimation of Tree Diameter from GNSS-IMU-Based Mobile Laser Scanning Data. Remote Sens. 11, 615. https://doi.org/10.3390/rs11060615.

Delgado, J.D., Arroyo, N.L., Arévalo, J.R., Fernández-Palacios, J.M., 2007. Edge effects of roads on temperature, light, canopy cover, and canopy height in laurel and pine forests (Tenerife, Canary Islands). Landsc. Urban Plan. 81 (4), 328–340. https://doi.org/10.1016/j.landurbplan.2007.01.005.

Forsman, M., Börlin, N., Olofsson, K., Reese, H., Holmgren, J., 2018. Bias of cylinder diameter estimation from ground-based laser scanners with different beam widths: A simulation study. ISPRS J. Photogramm. Remote Sens. 135, 84–92. https://doi.org/10.1016/j.isprsjprs.2017.11.013.

Forsman, M., Holmgren, J., Olofsson, K., 2016. Tree stem diameter estimation from mobile laser scanning using line-wise intensity-based clustering. Forests 7, 206. https://doi.org/10.3390/f7090206.

Hamraz, H., Jacobs, N.B., Contreras, M.A., Clark, C.H., 2019. Deep learning for conifer/deciduous classification of airborne LiDAR 3D point clouds representing individual trees. ISPRS J. Photogramm. Remote Sens. 158, 219–230. https://doi.org/10.1016/j.isprsjprs.2019.10.011.

Harper, K.A., Macdonald, S.E., Mayerhofer, M.S., Biswas, S.R., Esseen, P.A., Hylander, K., Stewart, K.J., Mallik, A.U., Drapeau, P., Jonsson, B.G., Lesieur, D., Kouki, J., Bergeron, Y., 2015. Edge influence on vegetation at natural and anthropogenic edges of boreal forests in Canada and Fennoscandia. J. Ecol. 103, 550–562. https://doi.org/10.1111/1365-2745.12398.

Holmgren, J., Tulldahl, M., Nordlöf, J., Willén, E., Olsson, H., 2019. Mobile laser scanning for estimating tree stem diameter using segmentation and tree spine calibration. Remote Sens. 11, 1–18. https://doi.org/10.3390/rs11232781.

Holopainen, M., Vastaranta, M., Hyyppä, J., 2014. Outlook for the next generation's precision forestry in Finland. Forests 5, 1682–1694. https://doi.org/10.3390/f5071682.

Hopkinson, C., Chasmer, L., Young-Pow, C., Treitz, P., 2004. Assessing forest metrics with a ground-based scanning lidar. Can. J. For. Res. 34 (3), 573–583. https://doi.org/10.1139/x03-225.

Hunčaga, M., Chudá, J., Tomaštík, J., Slámová, M., Koreň, M., Chudý, F., 2020. The comparison of stem curve accuracy determined from point clouds acquired by different terrestrial remote sensing methods. Remote Sens. 12 (17), 2739. https://doi.org/10.3390/rs12172739.

Hyyppä, E., Hyyppä, J., Hakala, T., Kukko, A., Wulder, M.A., White, J.C., Pyörälä, J., Yu, X., Wang, Y., Virtanen, J.P., Pohjavirta, O., Liang, X., Holopainen, M., Kaartinen, H., 2020a. Under-canopy UAV laser scanning for accurate forest field measurements. ISPRS J. Photogramm. Remote Sens. 164, 41–60. https://doi.org/10.1016/j.isprsjprs.2020.03.021.

Hyyppä, E., Kukko, A., Kaijaluoto, R., White, J.C., Wulder, M.A., Pyörälä, J., Liang, X., Yu, X., Wang, Y., Kaartinen, H., Virtanen, J.P., Hyyppä, J., 2020b. Accurate derivation of stem curve and volume using backpack mobile laser scanning. ISPRS J. Photogramm. Remote Sens. 161, 246–262. https://doi.org/10.1016/j.isprsjprs.2020.01.018.

Hyyppä, E., Yu, X., Kaartinen, H., Hakala, T., Kukko, A., Vastaranta, M., Hyyppä, J., 2020c. Comparison of backpack, handheld, under-canopy UAV, and above-canopy UAV laser scanning for field reference data collection in boreal forests. Remote Sens. 12, 1–31. https://doi.org/10.3390/rs12203327.

Kolendo, Ł., Kozniewski, M., Ksepko, M., Chmur, S., Neroj, B., 2021. Parameterization of the individual tree detection method using large dataset from ground sample plots and airborne laser scanning for stands inventory in coniferous forest. Remote Sens. 13 (14), 2753. https://doi.org/10.3390/rs13142753.

Kukko, A., Kaijaluoto, R., Kaartinen, H., Lehtola, V.V., Jaakkola, A., Hyyppä, J., 2017. Graph SLAM correction for single scanner MLS forest data under boreal forest canopy. ISPRS J. Photogramm. Remote Sens. 132, 199–209. https://doi.org/10.1016/j.isprsjprs.2017.09.006.

Lau, A., Bentley, L.P., Martius, C., Shenkin, A., Bartholomeus, H., Raumonen, P., Malhi, Y., Jackson, T., Herold, M., 2018. Quantifying branch architecture of tropical trees using terrestrial LiDAR and 3D modelling. Trees - Struct. Funct. 32 (5), 1219–1231. https://doi.org/10.1007/s00468-018-1704-1.

Liang, X., Hyyppä, J., Kaartinen, H., Lehtomäki, M., Pyörälä, J., Pfeifer, N., Holopainen, M., Brolly, G., Francesco, P., Hackenberg, J., Huang, H., Jo, H.W., Katoh, M., Liu, L., Mokroš, M., Morel, J., Olofsson, K., Poveda-Lopez, J., Trochta, J., Wang, D., Wang, J., Xi, Z., Yang, B., Zheng, G., Kankare, V., Luoma, V., Yu, X., Chen, L., Vastaranta, M., Saarinen, N., Wang, Y., 2018a. International benchmarking of terrestrial laser scanning approaches for forest inventories. ISPRS J. Photogramm. Remote Sens. 144, 137–179. https://doi.org/10.1016/j.isprsjprs.2018.06.021.

Liang, X., Kukko, A., Hyyppä, J., Lehtomäki, M., Pyörälä, J., Yu, X., Kaartinen, H., Jaakkola, A., Wang, Y., 2018b. In-situ measurements from mobile platforms: An emerging approach to address the old challenges associated with forest inventories. ISPRS J. Photogramm. Remote Sens. 143, 97–107. https://doi.org/10.1016/j.isprsjprs.2018.04.019.

Lindberg, E., Holmgren, J., Olofsson, K., Olsson, H., 2012. Estimation of stem attributes using a combination of terrestrial and airborne laser scanning. Eur. J. For. Res. 131 (6), 1917–1931. https://doi.org/10.1007/s10342-012-0642-5.

Liu, L., Zhang, A., Xiao, S., Hu, S., He, N., Pang, H., Zhang, X., Yang, S., 2021. Single Tree Segmentation and Diameter at Breast Height Estimation with Mobile LiDAR. IEEE Access 9, 24314–24325. https://doi.org/10.1109/ACCESS.2021.3056877.

Lovell, J.L., Jupp, D.L.B., Culvenor, D.S., Coops, N.C., 2003. Using airborne and ground-based ranging lidar to measure canopy structure in Australian forests. Can. J. Remote Sens. 29 (5), 607–622. https://doi.org/10.5589/m03-026.

Maltamo, M., Hauglin, M., Næsset, E., Gobakken, T., 2019. Estimating stand level stem diameter distribution utilizing harvester data and airborne laser scanning. Silva Fenn. 53, 1–19. https://doi.org/https://doi.org/10.14214/sf.10075.

Næsset, E., 2002. Predicting forest stand characteristics with airborne scanning laser using a practical two-stage procedure and field data. Remote Sens. Environ. 80 (1), 88–99. https://doi.org/10.1016/S0034-4257(01)00290-5.

Newnham, G.J., Armston, J.D., Calders, K., Disney, M.I., Lovell, J.L., Schaaf, C.B., Strahler, A.H., Danson, F.M., 2015. Terrestrial laser scanning for plot-scale forest measurement. Curr. For. Rep. 1 (4), 239–251. https://doi.org/10.1007/s40725-015-0025-5.

Olofsson, K., Holmgren, J., 2016. Single tree stem profile detection using terrestrial laser scanner data, flatness saliency features and curvature properties. Forests 7, 207. https://doi.org/10.3390/f7090207.

Olofsson, K., Holmgren, J., Olsson, H., 2014. Tree stem and height measurements using terrestrial laser scanning and the RANSAC algorithm. Remote Sens. 6, 4323–4344. https://doi.org/10.3390/rs6054323.

Packalén, P., Maltamo, M., 2008. Estimation of species-specific diameter distributions using airborne laser scanning and aerial photographs. Can. J. For. Res. 38 (7), 1750–1760. https://doi.org/10.1139/X08-037.

Pierzchała, M., Giguère, P., Astrup, R., 2018. Mapping forests using an unmanned ground vehicle with 3D LiDAR and graph-SLAM. Comput. Electron. Agric. 145, 217–225. https://doi.org/10.1016/j.compag.2017.12.034.

Puente, I., González-Jorge, H., Martínez-Sánchez, J., Arias, P., 2013. Review of mobile mapping and surveying technologies. Meas. J. Int. Meas. Confed. 46 (7), 2127–2145. https://doi.org/10.1016/j.measurement.2013.03.006.

Puliti, S., Breidenbach, J., Astrup, R., 2020. Estimation of forest growing stock volume with UAV laser scanning data: Can it be done without field data? Remote Sens. 12, 1245. https://doi.org/10.3390/RS12081245.

Pyörälä, J., Kankare, V., Liang, X., Saarinen, N., Rikala, J., Kivinen, V.P., Sipi, M., Holopainen, M., Hyyppä, J., Vastaranta, M., 2019a. Assessing log geometry and wood quality in standing timber using terrestrial laser-scanning point clouds. Forestry 92, 177–187. https://doi.org/10.1093/forestry/cpy044.

Pyörälä, J., Saarinen, N., Kankare, V., Coops, N.C., Liang, X., Wang, Y., Holopainen, M., Hyyppä, J., Vastaranta, M., 2019b. Variability of wood properties using airborne and terrestrial laser scanning. Remote Sens. Environ. 235, 111474. https://doi.org/10.1016/j.rse.2019.111474.

Qian, C., Liu, H., Tang, J., Chen, Y., Kaartinen, H., Kukko, A., Zhu, L., Liang, X., Chen, L., Hyyppä, J., 2017. An integrated GNSS/INS/LiDAR-SLAM positioning method for

highly accurate forest stem mapping. Remote Sens. 9, 1–16. https://doi.org/10.3390/rs9010003.

Reynolds, M.R., Burk, T.E., Huang, W.-C., 1988. Goodness-of-fit tests and model selection procedures for diameter distribution models. For. Sci. 34 (2), 373–399. https://doi.org/10.1093/forestscience/34.2.373.

Roussel, J.-R., Auty, D., Coops, N.C., Tompalski, P., Goodbody, T.R.H., Meador, A.S., Bourdon, J.-F., de Boissieu, F., Achim, A., 2020. lidR: An R package for analysis of Airborne Laser Scanning (ALS) data. Remote Sens. Environ. 251, 112061. https://doi.org/10.1016/j.rse.2020.112061.

Skudnik, M., Jevšenak, J., 2022. Artificial neural networks as an alternative method to nonlinear mixed-effects models for tree height predictions. For. Ecol. Manage. 507, 120017. https://doi.org/10.1016/j.foreco.2022.120017.

Xi, Z., Hopkinson, C., Rood, S.B., Peddle, D.R., 2020. See the forest and the trees: Effective machine and deep learning algorithms for wood filtering and tree species classification from terrestrial laser scanning. ISPRS J. Photogramm. Remote Sens. 168, 1–16. https://doi.org/10.1016/j.isprsjprs.2020.08.001.

Zhang, C., Jiang, Y., Xu, B., Li, X., Zhu, Y., Lei, L., Chen, R., Dong, Z., Yang, H., Yang, G., 2020. Apple tree branch information extraction from terrestrial laser scanning and backpack-LiDAR. Remote Sens. 12, 1–17. https://doi.org/10.3390/rs12213592.

Zhang, W., Qi, J., Wan, P., Wang, H., Xie, D., Wang, X., Yan, G., 2016. An easy-to-use airborne LiDAR data filtering method based on cloth simulation. Remote Sens. 8, 1–22. https://doi.org/10.3390/rs8060501.

Zhen, Z., Quackenbush, L.J., Zhang, L., 2016. Trends in automatic individual tree crown detection and delineation-evolution of LiDAR data. Remote Sens. 8, 1–26. https://doi.org/10.3390/rs8040333.

II

Remote Sensing of Environment 315 (2024) 114414

Contents lists available at ScienceDirect

Remote Sensing of Environment

journal homepage: www.elsevier.com/locate/rse

Mobile laser scanning as reference for estimation of stem attributes from airborne laser scanning

Raul de Paula Pires *, Eva Lindberg, Henrik Jan Persson, Kenneth Olofsson, Johan Holmgren

Department of Forest Resource Management, Swedish University of Agricultural Sciences, Umeå, Sweden

ARTICLE INFO

Edited by Marie Weiss

Keywords:
Mobile laser scanning
Forest inventory
Stem diameter
Stem volume
Training data

ABSTRACT

The acquisition of high-quality reference data is essential for effectively modelling forest attributes. Incorporating close-range Light Detection and Ranging (LiDAR) systems into the reference data collection stage of remote sensing-based forest inventories can not only increase data collection efficiency but also increase the number of attributes measured with high quality. Therefore, we propose a model-based forest inventory method that uses reference data collected by a car-mounted mobile laser scanning (MLS) system along boreal forest roads. This approach is used for the estimation of diameter at breast height (DBH) and stem volume at the individual tree-level from airborne laser scanning (ALS) data. In addition, we compare the estimates obtained using the proposed method with the ones derived from reference data collected by traditional field inventory of 265 field plots systematically distributed over the study area. The accuracy of the estimates remained comparable regardless of the reference dataset used for estimation of DBH and stem volume. When using the field inventory dataset for model training, the root mean square error (RMSE) of DBH estimates were 4.06 cm (18.8 %) for Norway spruce trees, 6.3 cm (29.6 %) for Scots pine and 8.61 cm (55.9 %) for deciduous trees. Similarly, when evaluating predictions based on the MLS dataset as reference, RMSEs were equal to 3.97 cm (18.4 %) for Norway spruce, 6.12 cm (28.8 %) for Scots pine, and 8.98 cm (58.3 %) for deciduous trees. In general, biases were below 1 cm for most species classes, with the exception of deciduous trees. The accuracy of stem volume also had RMSEs varying across different tree species. For the estimates based on traditional field inventory, the RMSEs were 0.176 m^3 (38.8 %) for Norway spruce, 0.228 m^3 (52.4 %) for Scots pine and 0.246 m^3 (158 %) for deciduous trees. When using the MLS dataset as a reference, the RMSEs were equal to 0.176 m^3 (38.8 %), 0.228 m^3 (52.4 %), and 0.246 m^3 (158 %) for Norway spruce, Scots pine, and deciduous trees, respectively. Car-mounted MLS demonstrated its potential as an efficient alternative for collecting reference data in remote sensing-based forest inventories, which could complement traditional methods.

1. Introduction

Forests are crucial ecosystems that sustain a diverse range of plant and animal species, while also providing essential services as carbon sequestration, water conservation, and soil stabilization. Moreover, they play a key role in transitioning towards a carbon-neutral economy and mitigating climate change impacts (European Commission, 2021). However, the demand for timber as a renewable material puts pressure on forest resources worldwide, making the establishment of management practices that account for the complexity of forest ecosystems increasingly necessary. Hence, accurate assessments of forest structure and growth are necessary in order to plan interventions that balance the maintenance of biodiversity and sustainable timber production. In response to this need, LiDAR (Light Detection and Ranging) technology is used to obtain auxiliary information in the production of spatially explicit estimations of forest attributes such as growing stock, site index, and biodiversity mapping (Appiah Mensah et al., 2023; Lefsky et al., 2002; Maltamo et al., 2014).

LiDAR-based variables are frequently combined with field reference data to construct predictive models for key forest attributes, such as Diameter at Breast Height (DBH) and stem volume, at individual tree- or area-level (Maltamo et al., 2014). These models are subsequently used to generate wall-to-wall maps of such attributes over large areas, varying from single forest estates to entire countries (Nilsson et al., 2017).

* Corresponding author.
E-mail addresses: raul.de.paula.pires@slu.se (R.P. Pires), eva.lindberg@slu.se (E. Lindberg), henrik.persson@slu.se (H.J. Persson), kenneth.olofsson@slu.se (K. Olofsson), johan.holmgren@slu.se (J. Holmgren).

https://doi.org/10.1016/j.rse.2024.114414
Received 16 May 2024; Received in revised form 16 August 2024; Accepted 5 September 2024
Available online 10 September 2024

In most operational remote sensing-based forest inventories, LiDAR-derived metrics are used to predict forest attributes at area-level, named area-based approach (ABA - Næsset, 2004, Næsset, 2002), with field plot data serving as the reference values in the modelling process (da Bispo et al., 2020; Kotivuori et al., 2016; Leite et al., 2020; Nilsson et al., 2017; Novo-Fernández et al., 2019). Such training data is usually collected using manual methods, which require low start-up cost but can be logistically challenging, since extensive field campaigns are usually necessary in order to sample the complete range of a given forest attribute over large areas (Hyyppä et al., 2020a; Persson et al., 2022; Wang et al., 2016). In addition, the inclusion of variables such as stem profiles and above ground biomass (AGB) in reference data collection can be impractical, requiring destructive techniques or laboratory infrastructure and increase the total cost and time required for sampling (Hauglin et al., 2014; Hunčaga et al., 2020; Stovall et al., 2018). As an alternative, some attributes might not be measured during the surveys but estimated using mathematical models or approximations, which may cause the derived data to be non-representative of the actual forest conditions. For instance, using globally calibrated models on local scale to predict attributes such as AGB can result in biased estimates as demonstrated by Brede et al. (2022) and Calders et al., 2022

Therefore, at the same pace as different LiDAR sensors and platforms become available, authors have explored the suitability of such technologies not only for producing wall-to-wall maps of forest attributes, but also for reference data collection. Different close-range LiDAR sensors such as Terrestrial, Mobile and UAV-borne laser scanners (TLS, MLS and UAVLS, respectively) can collect high-resolution point clouds, proving three-dimensional data with unprecedented level of detail on forest structure and tree architecture (Hyyppä et al., 2020c; Olofsson et al., 2014). With such sensors, it is possible to extract tree attributes such as DBH directly from the point clouds with relatively high accuracy (Brede et al., 2022; Brede et al., 2017; Holmgren et al., 2019; Hyyppä et al., 2020c; Hyyppä et al., 2020b; Kuželka et al., 2020; Olofsson and Holmgren, 2016). For instance, Hyyppä et al. (2020c) found RMSEs of DBH estimates ranging from 2 to 8 % while comparing the performance of different MLSs and UAVLS. In addition, transitioning to LiDAR-based reference data collection could reduce uncertainties related with field measurements (Persson et al., 2022) and enable the sampling of attributes that are difficult to measure by traditional means in large-scale surveys, as stem profiles and branch structure.

Nevertheless, the implementation of LiDAR-based reference data collection in operational scale remains a challenge. Apart from the high acquisition costs, some ground-based LiDAR systems such as TLSs and backpack-mounted or hand-held MLSs have limited scalability, since they are restricted to specific areas or plots, and require labor-intensive surveying campaigns (Calders et al., 2020). Such limitations hinder the operational use, particularly in cases where broad spatial coverage is required. In order to overcome these limitations, researchers have been investigating various combinations of sensors and platforms as potential tools for efficient data collection. As an example, Pires et al. (2022) presented a solution for measuring DBH and stem curves in boreal forests along roads using car-mounted MLS. The study reported DBH measurement accuracies ranging from 1.8 cm to 4.8 cm, which varied depending on the distance of the trees from the roadside. Similarly, Hyyppä et al. (2022) used a high-resolution airborne laser scanning (ALS) system mounted on a helicopter flying at low altitude to measure stem curves and DBH over boreal forest areas, yielding accuracies ranging from 2.2 cm to 2.9 cm in DBH estimation, depending on the test sites. In another study, Hyyppä et al. (2020a) extracted stem curves from below-canopy UAVLS, reaching RMSEs equal to 1.2 cm and 1.4 cm in sparse and obstructed forest plots, respectively (Hyyppä et al., 2020a).

Such combinations of sensors and platforms could enable automatic and detailed forest inventories of large areas and provide researchers and forest managers with a wider range of information, supporting better-informed decision-making. Furthermore, the automation of data collection and analysis can reduce the time and costs associated with traditional field surveys, while also providing more frequent updates on the forest conditions.

Understanding the effect of using innovative data collection methods in large-scale forest inventories is important for ensuring precise and effective forest management. Integrating an additional data collection method, such as car-mounted MLS, into forest inventory could introduce new uncertainties, which depend on the choice of the sensor and platform used for surveying. As an example, the accessibility to certain parts of a forest stand by different platforms, such as all-terrain vehicles, cars, and below-canopy UAVs, may be restricted by terrain and vegetation conditions, resulting in the inability to collect reference data in those areas. Such limitation could result in the systematic inclusion of trees growing under certain condition (e.g. edge effects) in the reference dataset, and these trees might not be representative of the forest as a whole (Delgado et al., 2007; Harper et al., 2015). Moreover, problems with tree detection may lead to certain strata, such as trees with small DBH values, being underrepresented in the reference dataset (Brede et al., 2017; Holmgren et al., 2019; Hyyppä et al., 2020a, 2020b, 2020c; Liu et al., 2021).

With that in mind, this study proposes a model-based forest inventory approach that uses a car-mounted MLS for reference data collection, and compares the estimates obtained using the novel method with those derived from reference data collected by traditional field inventory. With this analysis, we want to contribute to the advancement of remote sensing-based forest inventory methods and elucidate possible implications of using remote sensing-based tools in forest inventory. Specifically, we compare estimates of DBH and stem volume at the individual tree-level by using models trained with different reference datasets. Specific objectives are (i) to train ALS-based models for DBH and stem volume prediction using car-mounted MLS as reference for model training, (ii) to train ALS-based models using field inventory data as reference for model training, and (iii) to compare the estimates generated by both models.

2. Material and methods

2.1. Study area

The study area Remningstorp has approximately 1039 ha (ha) of forest area and is located in Southern Sweden (lat. 58.5 degrees N, long. 13.6 degrees E), in a boreal forest region (Fig. 1). The dominant tree species are Norway spruce (*Picea abies* (L.) H. Karst.) – 85.7 %, Scots pine (*Pinus sylvestris* L.) – 9.1 %, and Birch (*Betula* spp.) – 3.4 %. The average stem density in the area is 580 trees/ha.

2.2. Aerial laser scanning

In October 2019, ALS data was acquired over the study area (Fig. 1) using a Leica Terrain Mapper-LN system mounted on an aircraft. The sensor operated at an altitude of approximately 1450 m and with an average speed of 115 knots, with a pulse frequency of 1600 Hz. The laser beam footprint was 35 cm and the field of view was 30 degrees. The resulting point density in the cloud is 22 points/m^2, on average. Following the acquisition, the ALS point clouds were classified into ground and non-ground using the classification algorithm by Zhang et al. (2016), as implemented in the lidR package (Roussel et al., 2020) in R (R Core Team, 2020).

After the classification, the point cloud was segmented into individual trees using the three-dimensional tree segmentation procedure by Holmgren et al. (2022). In this study, it was assumed that each segment corresponded to one tree crown. Finally, a set of ALS-derived metrics were calculated for each tree segment obtained in the previous step (Table 1). In this study, every 10th height and intensity percentiles, the 95th and 99th height and intensity percentiles, along with descriptive statistics of intensity values, were used as predictors. In addition, a set of tree crown-related attributes, such as crown radius, area, and extent,

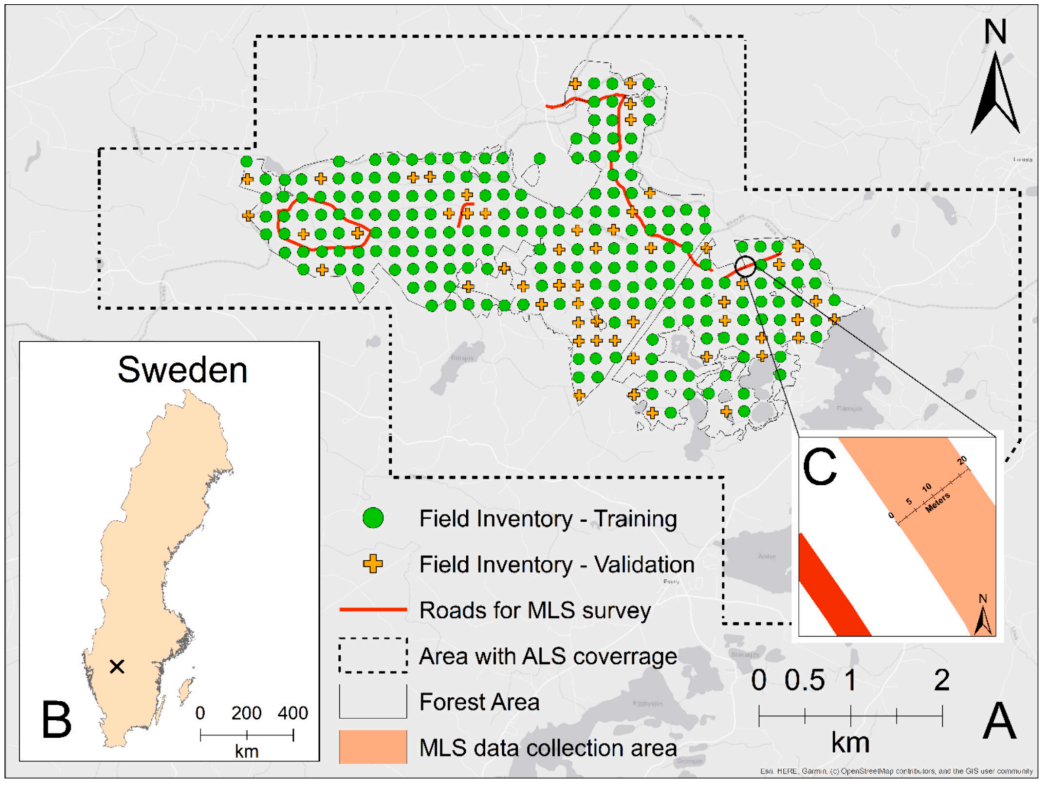

Fig. 1. (A) Overview of the study area, with field plots used for training showed as green circles, the field inventory plots used for validation shown as orange crosses and the roads scanned by the MLS survey in red. (B) Position of the study area in Sweden. (C) Close-up on the area from which MLS data was collected, considering the 20-40 m distance range to the roadside. (For interpretation of the references to colour in this figure legend, the reader is referred to the web version of this article.)

Table 1
Description of the ALS-based metrics used as independent variables in this study.

Metric	Description
$h_{10} - h_{99}$	10th to the 99th height percentiles
$i_{10} - i_{99}$	10th to the 99th intensity percentiles
$mean_i$	Mean of intensity values
std_i	Standard deviation of intensity values
$skew_i$	Skewness of intensity values
kur_i	Kurtosis of intensity values
CR	Crown radius
CA	Crown area
CE	Extent of crown polygon
CRh95	$CR \times h_{95}$
CR^2h95_{sqrt}	$\sqrt{CR^2 \times h_{95}}$

were included in the ALS-based metrics pool for their influence on a tree's DBH (Hemery et al., 2005; Iizuka et al., 2022; Iizuka et al., 2018). These attributes were derived from the delineated tree crown produced by the tree segmentation algorithm. Crown area (CA) was defined as the area of the delineated tree crown and, given that crowns are not perfectly circular, the crown radius (CR) of a tree was defined as the radius of a perfect circle with an area equal to its crown area. Later, the crown extent (CE) was defined as diagonal length of the smallest rectangle containing each crown polygon. Finally, combinations of CR and the 95th height percentile were identified for their significant linear correlation with either DBH or stem volume.

2.3. Reference data collection

We use the terms "reference data" or "training data" to refer to the data used for estimating the model parameters in the model-based inference. In this study, two reference datasets were collected in the study area using different data collection methods. Therefore, we denote the reference dataset obtained through conventional field inventory as the "field inventory dataset", or simply "FI dataset". Similarly, we refer to the reference dataset collected through car-mounted MLS as the "MLS dataset".

2.3.1. Field inventory dataset

The survey using standard field-based forest inventory consisted of a set of 265 circular plots with 10 m radius systematically distributed over the study area (Fig. 1). The plot centers were placed at 200 m distance from each other and, inside each plot, all living trees with DBH $\geq$ 4 cm had the DBH and tree position recorded using a DP POSTEX system (http://www.haglofsweden.com). In each plot, the heights of 1 to 5

sample trees were measured with a hypsometer and the remaining trees had their heights estimated using the model in Eq. (1). The model was adjusted using the ordinary least squares with the height from the sample trees as reference and 95th height percentile from ALS predictor. The model's goodness of fit is shown in the appendix A.

$$\widehat{H} = \beta_0 + \beta_1 \bullet h95 \quad (1)$$

where $\widehat{H}$ is the estimated tree height, $h95$ is the ALS-derived 95th height percentile and β_0 and β_1 are the model parameters. The stem volumes were calculated by using the species-specific volume functions by Brandel (1990).

The tree positions acquired in the field were co-registered with the ones derived from ALS data using the co-registration algorithm by Olofsson et al. (2008). This algorithm aligns the positions of the field-measured trees to the ALS-derived positions using cross-correlation of the position images within a search radius from the field-measured positions. In this step, we used a search radius of 20 m and the ALS-derived positions considered the location of highest point within each ALS-derived tree segment. This step was necessary in order to ensure the correspondence between each field-measured tree and its respective ALS-derived segment. If a segment contained more than one field-recorded tree position, the tree with highest DBH was considered to be the ALS-detected tree (i.e. the one tree represented by the segment) and the other field-recorded trees within that segment were considered omission errors. Segments that did not contain any field-recorded tree positions were considered commission errors.

Altogether, 62 plots had no trees with DBH $\geq$ 4 cm and were not used in this study. Additionally, a visual assessment was conducted in order to assure the quality of the co-registration. The co-registration was considered not successful when the corrected tree positions were outside the plot area or when no field-detected tree was matched to an ALS segment. According to these criteria, the matching procedure was not successful in 9 plots. Finally, 13 plots were overlapping MLS data collection areas and were excluded from the analysis, resulting in 181 plots effectively being used in this study. In terms of individual trees, 3023 field-recorded positions were associated with their respective ALS-derived tree segment in the FI dataset (Fig. 2).

2.3.2. MLS dataset

In 2019, a car-mounted MLS survey was conducted in the study area (Fig. 1). The system consisted of a Riegl VUX1LR laser scanner, synchronized with an Inertial Measurement Unit (IMU) and a GPS/GNSS system, resulting in a georeferenced point cloud with a point registration accuracy of 1.5 cm. The sensor was leaning 30 degrees from the horizontal plane and had 330 degrees of field of view. The car kept an average speed of 8 km/h. Approximately 7 km of forests were scanned along both sides of the road during a 2-h survey. The roads were chosen according to their accessibility by car so the system could measure a large part of the test site without having to turn back. Stem attributes were extracted from the resulting point clouds as described by Pires et al. (2022): first, tree stems were identified in the point clouds using an arc detection procedure. Afterwards, a stem curve model was fitted to each detected tree stem. Finally, DBH and stem volume values were derived from the stem curves of each detected individual.

To ensure the best possible tree detection accuracy and prevent the inclusion of trees influenced by edge effects, Pires et al. (2022) suggested limiting the reference data for model calibration to only include detected trees within the distance range of 20–40 m from the roadside. Considering this range from the roadside and the distance traveled by the car as shown in Fig. 1 - C, the MLS data collection area summed approximately 28 ha of forests, which were used in the study. Moreover, the MLS-derived tree positions showed a systematic displacement in relation to the ALS-derived segments of approximately 1.5 m. Thus, the tree positions were manually adjusted to align the MLS-derived positions with the ALS-detected trees, resulting in 6432 MLS-derived tree positions matching their corresponding ALS-derived tree crowns (Fig. 2).

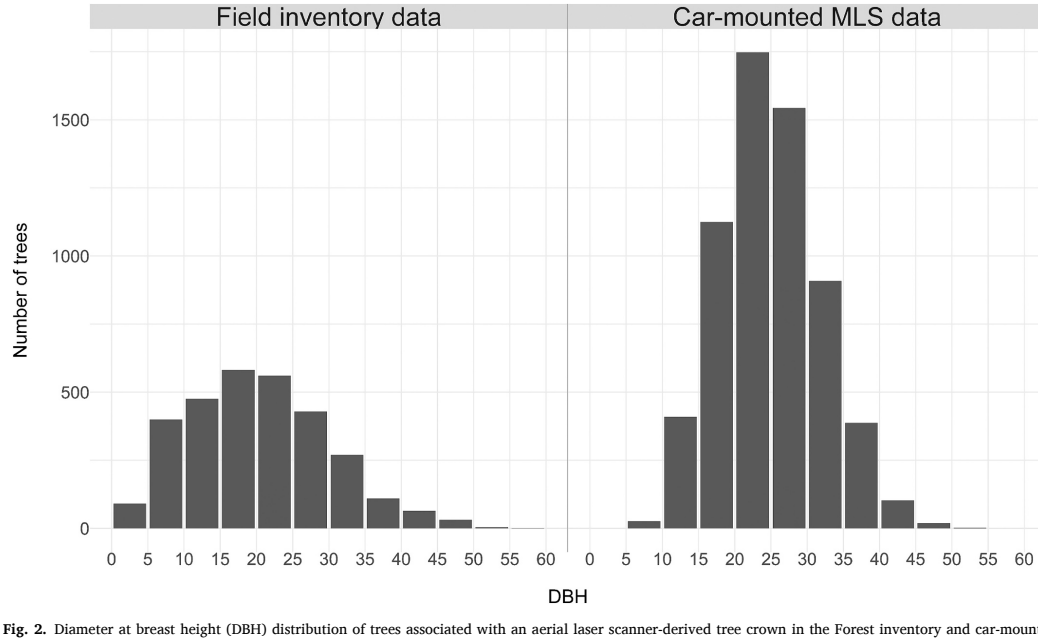

Fig. 2. Diameter at breast height (DBH) distribution of trees associated with an aerial laser scanner-derived tree crown in the Forest inventory and car-mounted mobile laser scanner (MLS) datasets.

2.4. Estimation of forest attributes

Before training the models to estimate stem attributes based on the FI and MLS datasets, the trees in the FI dataset were divided into training and validation groups according to their field plots, creating a benchmark dataset for the MLS- and FI-derived models. Specifically, 70 % of the plots in the FI dataset (2050 trees) were used for model training, while the remaining 30 % (973 trees) were used for validation (Fig. 1 - A). Consequently, the FI-based models were trained on 70 % of the FI dataset, whereas the MLS-based models were trained using the entire MLS dataset. All models were then validated using the validation portion of the FI dataset.

In order to avoid collinearity issues in the models, only the 95th height percentile was considered amongst all height percentiles during variable selection. Ordinary least squares regression was used to estimate the models' coefficients independently for each reference dataset, and the results of the variable selection procedure are presented in the results section. DBH and stem volume estimation models were developed independently for each reference dataset. In this step, the selection of models with different combinations of explanatory variables was carried out using the backwards variable selection method implemented in the caret package (Kuhn, 2020) in R (R Core Team, 2020). Altogether, three models including one to three explanatory variables were evaluated for each reference dataset. The objective was to identify the model that achieved the highest adjusted R^2 value with the fewest number of explanatory variables. To prevent bias in estimating the DBH for trees with small values, the intercept in the DBH prediction model was set to zero. Furthermore, we applied a logarithmic transformation to the stem volume and ALS-derived metrics in order to enhance the linearity in the relationship between explanatory and target variables. To address potential bias introduced by transforming the stem volume before model fitting, we employed the bias correction estimator (b) proposed by Snowdon (1991) - Equation 2). b is estimated separately for each dataset after training the volumetric model (i) and the final volume prediction is calculated by Eq. (3). This approach was adopted to ensure a more accurate and unbiased estimation process.

$$b_i = \sum_{j=1}^{n_i} V_{ij} \Big/ \sum_{j=1}^{n_i} \hat{v}_{ij} \tag{2}$$

$$\hat{V}_{ij} = \hat{v}_{ij} \bullet b_i \tag{3}$$

where n is the number of trees in the dataset i, V_{ij} is the stem volume of tree j from dataset i. $\hat{v}_{ij}$ and $\hat{V}_{ij}$ are the estimated stem volumes of tree j from dataset i before and after bias correction, respectively.

2.5. Accuracy assessment

The accuracy of DBH estimates was assessed by comparing the ALS-derived predictions trained on either the FI or MLS datasets to the field-measured values on the validation portion of the FI dataset at tree-level. Similarly, stem volume estimates were evaluated both at the individual tree- and plot-level by comparing ALS-derived predictions, trained on either the FI or MLS datasets, with the stem volume reference values on the validation subset of the FI dataset. As predictions for both variables were made at the tree level, plot-level estimates of stem volume were obtained by summing up all ALS-derived predictions within the area of each validation plot.

Specifically, the estimates were compared with their respective field-measured values in terms of Root Mean Square Error (RMSE - Eq. (4)) and bias (Eq. (5)). The relative RMSE and bias were calculated in relation to the mean values of the target variables in the FI dataset.

$$RMSE = \sqrt{\sum_{j}^{n} \left(\hat{y}_j - y_j\right)^2 \Big/ n} \tag{4}$$

$$bias = \sum_{j}^{n} \left(\hat{y}_j - y_j\right) \Big/ n \tag{5}$$

where n is the number of trees. $\hat{y}_j$ and y_j are target variable's ALS-derived and field inventory values for tree j.

We used precision (Eq. (6)) and sensitivity (Eq. (7)) to assess the accuracy of the individual tree detection in the validation plots.

$$Precision_p = TP_p \Big/ \left(TP_p + C_p\right) \tag{6}$$

$$Sensitivity_p = TP_p \Big/ \left(TP_p + O_p\right) \tag{7}$$

where TP_p is the number of trees correctly detected trees (true positives), $C_p$and O_p are the number of commission and omission errors in plot p.

3. Results

3.1. Individual tree detection

Table 2 shows the mean precision and sensitivity values in different diameter classes. The results indicate that the ITD method used in this study performs best in larger DBH classes, with precision and sensitivity values reaching nearly 100 % in trees greater than 40 cm in DBH. On the other hand, the method had its worst performance in detecting trees with DBHs ranging from 0 to 10 cm, where the highest commission and omission errors were noticed. In general, the performance of ITD in this DBH class negatively affected the overall accuracy of ITD, with approximately 70 % of all omission errors being trees with DBH $\leq$ 10 cm (Fig. 3).

3.2. Modelling forest attributes

Table 4 show the variables selected for different model sizes in the two reference datasets when modelling DBH and stem volume, respectively. In both cases, models with 2 predictors were preferred over other options due to their fewer explanatory variables, despite achieving similar adjusted R^2 values as the other models. Thus, while using the FI dataset, the selected independent variables for the DBH model were h_{95} and CA. Using the MLS dataset, the combination of CRh95 and h_{95} had the best performance in the variable selection step (Table 3). For the stem volume models, h_{95} and CA were chosen as explanatory variables while using either the FI or the MLS dataset for model training (Table 4).

3.3. Prediction of stem attributes

The RMSE of the DBH estimates differed from 0.09 to 0.37 cm when comparing the models trained on the different datasets (Fig. 4). When using the FI dataset as reference, RMSEs ranged from 4.06 cm (18.8 %) in Norway spruce trees to 8.61 cm (55.9 %) in deciduous trees for predictions made a tree-level. When evaluating the predictions made using the MLS dataset as reference, RMSEs ranged from 3.97 cm (18.4 %) in Norway spruce to 8.98 cm (58.3 %) in deciduous trees also at tree-level, as shown in Fig. 4. Most biases were under 1 cm, with exception of the deciduous trees group, which exhibited bias of 2.77 cm (18 %) and 2.32

Table 2
Precision and sensitivity values of Individual Tree Detection (ITD) in Aerial Laser Scanning (ALS) data.

Diameter Class	Precision	Sensitivity
0–10 cm	51.6 %	22.8 %
10–20 cm	71.7 %	66 %
20–30 cm	83 %	89.6 %
30–40 cm	91.5 %	90.9 %
$\geq$ 40 cm	98.5 %	98.5 %
Overall	**81.3 %**	**70.9 %**

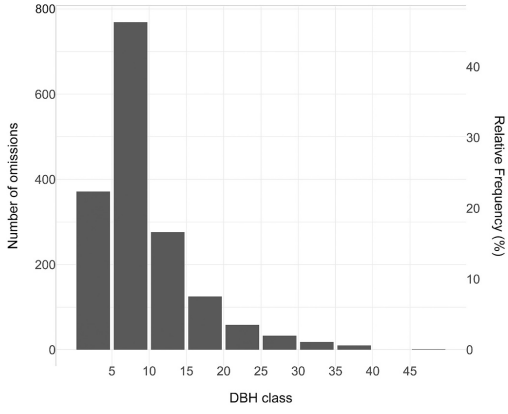

Fig. 3. Histogram of number of omissions and relative frequency in each diameter at breast height (DBH) class. Only trees with DBH ≥ 4 were measured.

Table 3
Models with one, two and three independent variables for DBH (Diameter at Breast Height) estimation using the forest inventory (FI) or car-mounted MLS (MLS). Adj. R^2: adjusted R^2.

N° of predictors	FI dataset		MLS dataset	
	Model	Adj. R^2	Model	Adj. R^2
1	$DBH_{FI} = \alpha_1 \bullet h_{95}$	0.93	$DBH_{MLS} = \alpha_1 \bullet CRh95$	0.96
2	$DBH_{FI} = \alpha_1 \bullet h_{95} + \alpha_2 \bullet CR^2h95_{sqrt}$	0.94	$DBH_{MLS} = \alpha_1 \bullet CRh95 + \alpha_2 \bullet h_{95}$	0.98
3	$DBH_{FI} = \alpha_1 \bullet h_{95} + \alpha_2 \bullet CR^2h95_{sqrt} + \alpha_3 \bullet skew_i$	0.94	$DBH_{MLS} = \alpha_1 \bullet CRh95 + \alpha_2 \bullet h_{95} + \alpha_3 \bullet i_{90}$	0.98

cm (15.1 %) for predictions made using the FI and MLS datasets, respectively.

For stem volume estimates, RMSE values obtained at individual tree-level (Fig. 5) were similar regardless of the dataset used for model training, with RMSEs ranging from 0.176 m^3 (38.8 %) in the Norway spruce group to 0.228 m^3 (52.4 %) in the Scots pine group for the FI-based estimations, as shown in Fig. 5. Meanwhile, the MLS dataset-based estimations per tree species showed RMSEs ranging from 0.176 m^3 (38.8 % - Norway spruce) to 0.246 m^3 (158 % - deciduous). On the other hand, RMSE and bias were lower when comparing the results at plot-level (Fig. 6). In this case, MLS-based predictions had RMSE equal to 46.2 m^3/ha (19.8 %) and bias equal to 2.5 m^3/ha (1.07 %), while FI-based predictions showed RMSE of 43.7 m^3/ha (18.7 %) and bias of −11.5 m^3/ha (−4.92 %), as shown in Fig. 6.

4. Discussion

The purpose of this study was to compare the results from two model-based forest inventory approaches that use on different training datasets. The first training dataset was sampled with traditional field data collection techniques, in other words field plots allocated according to a systematic sampling design and measured using standard equipment such as calipers and hypsometers. In contrast, we assessed the suitability of car-mounted MLS as a method for field data collection. This method uses a purposive sampling design, restricting data collection to a range of 20–40 m from the road network. Overall, both inventory methods resulted in similar models with respect to variable selection and prediction accuracy.

The MLS and FI datasets differed with respect to the sample size and possible measurement errors, which affected the estimated model parameters. With respect to the sample size, while the FI dataset contained 2050 trees for training, the MLS dataset contained 6432 trees. At the same time the training sample size may impact model-based inference (Li et al., 2023), adding reference data does not necessarily enhance estimation accuracy (i.e. RMSE) after a certain threshold (Fassnacht et al., 2014; Lisańczuk et al., 2020). In this context, adequate representation of the modeled trees attribute's variability across the study area may have a more substantial impact on a model's output than the actual size of the training dataset (Junttila et al., 2013). Moreover, both datasets are susceptible to different types of measurement and estimation errors due to limitations from the instruments used during data collection. The DBHs in the FI dataset were measured with calipers, thus being subject to human errors such as challenges associated with measuring at 1.3 m height and incorrect annotation. Additionally, in this dataset the stem volume was estimated by a volumetric model calibrated at landscape-level, potentially introducing bias on the estimates when applied to a local scale as in this study (Brede et al., 2022; Calders et al., 2022).

At the same time, the laser-based measurements of DBH and stem volume on the MLS dataset were subject to different kinds of errors. For instance, Pires et al. (2022) pointed out that the variability in stem detection by the MLS system, influenced by factors such as distance from the sensor to the tree and the presence of branches and understory vegetation around the stem can affect the accuracy of DBH and stem volume values on the MLS dataset. Accurate and precise measurements are crucial when collecting training data as they directly affect the reliability of the resulting models. In this sense, Hyyppä et al. (2022), Hyyppä et al., 2020b, Hyyppä et al., 2020c) suggested that maintaining errors on the training dataset under 10 % would be sufficient to produce accurate models based on close-range laser scanning. Hence, by restricting data collection to a 20–40 m range from the road, we obtained MLS-derived measurements with sufficient quality to produce estimation models with similar prediction accuracy as the ones trained on the FI-dataset. Nevertheless, using data collected closer to the roadside, such as within a 10–20 m range, could potentially improve MLS-based estimates by reducing measurement errors in the MLS dataset. When evaluating the accuracy of estimates in different distance ranges from the roadside, Pires et al. (2022) found that tree detection and estimates of DBH and stem volume within this 10–20 m range had lower errors when compared to estimates from greater distances, such as

Table 4
Models with one, two and three independent variables for stem volume estimation using the forest inventory (FI) or car-mounted MLS (MLS). Adj. R^2: adjusted R^2. $\hat{v}$ is the estimated stem volume before bias correction.

N° of predictors	FI dataset		MLS dataset	
	Model	Adj. R^2	Model	Adj. R^2
1	$\hat{v}_{FI} = e^{\beta_0+\beta_1 \bullet lnh_{95}}$	0.78	$\hat{v}_{MLS} = e^{\beta_0+\beta_1 \bullet lnh_{95}}$	0.74
2	$\hat{v}_{FI} = e^{\beta_0+\beta_1 \bullet lnh_{95}+\beta_2 \bullet lnCA}$	0.80	$\hat{v}_{MLS} = e^{\beta_0+\beta_1 \bullet lnh_{95}+\beta_2 \bullet lnCA}$	0.79
3	$\hat{v}_{FI} = e^{\beta_0+\beta_1 \bullet lnh_{95}+\beta_2 \bullet lnCA+\beta_3 \bullet ln\ h_{10}}$	0.80	$\hat{v}_{MLS} = e^{\beta_0+\beta_1 \bullet lnh_{95}+\beta_2 \bullet lnCA+\beta_3 \bullet lnmean_i}$	0.79

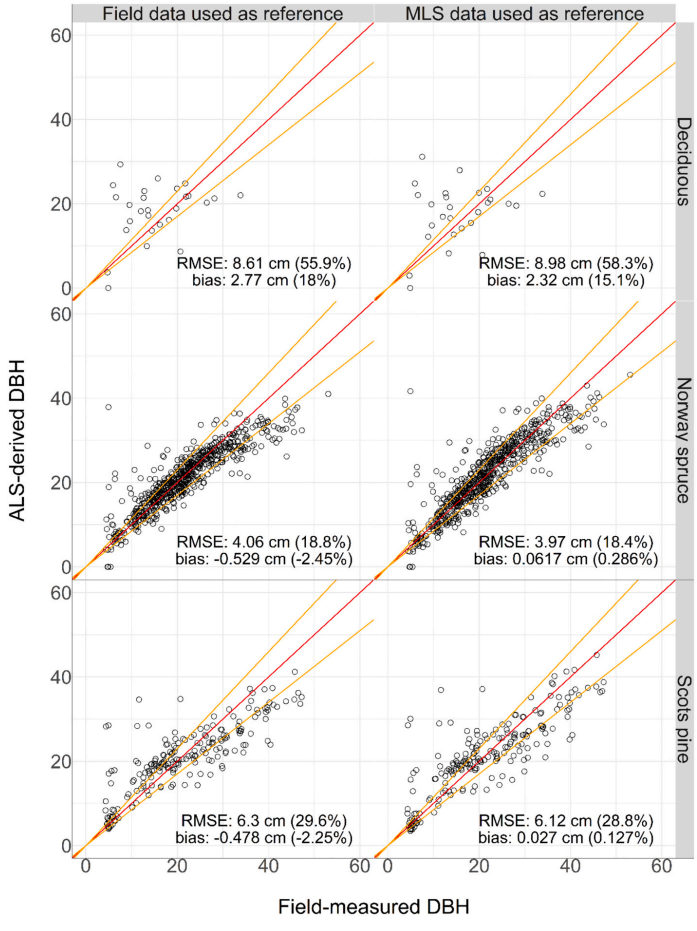

Fig. 4. Field-measured vs. ALS-derived Diameter at Breast Height (DBH), in cm. The columns represent different reference datasets and the rows represent the different species groups. The red line is the 1:1 line, where field-measured and ALS-derived values are equal. The orange lines represent a 15 % deviation from the 1:1 line. RMSE = Root Mean Square Error. (For interpretation of the references to colour in this figure legend, the reader is referred to the web version of this article.)

30–40 m from the roadside. In our analysis, data collected from 0 to 20 m to the roadside was not used for modelling to avoid over-representing trees potentially affected by edge effects in the training data (Harper et al., 2015). However, further analysis is needed to evaluate how including these trees potentially under edge effect in the training data might influence the accuracy and robustness of the prediction models.

Despite the similar model predictions and prediction accuracies evaluated in this study, the DBH errors observed were generally 1–2 cm higher than the ones reported in other studies that aimed at modelling diameter at the individual tree level, when considering the DBH estimation accuracy for the Norway spruce trees. For example, Sun et al. (2022) tested six different modelling methods for DBH prediction at individual tree level of Larch trees (*Larix olgensis* A. Henry), reaching RMSE values ranging from 1.92 cm with artificial neural networks to 2.56 cm with linear regression. However, regardless of the method used, all models tend to underestimate the DBH values of trees with larger diameters. Fu et al. (2020) used a nonlinear mixed-effects model (NLME) for DBH prediction of *Picea crassifolia* (Kom.) trees, reaching RMSE equal to 4.4 cm at individual tree level. Finally, Hao et al. (2021) also used NLME for DBH prediction of Larch trees, yield RMSE of 1.94 cm at individual tree level with the inclusion of site-specific random effects, which significantly improved the model's performance.

The errors in DBH estimation noticed in our study could have been caused different factors, such as the complexity of the target variable being modeled and the robustness of the statistical models used for prediction, which may involve considerations regarding model assumptions, parameter estimation methods, and the incorporation of relevant covariates or predictors. In addition, the different accuracies in the estimation of DBH and stem volume across species groups can be partially explained by the fact that Norway spruce is the main tree species in the study area, accounting for 85.7 % of all trees, which caused the models to be optimized for this specific species. For this target variable, the inclusion of site- and species-specific relationships between DBH and the explanatory variables could potentially improve the accuracy of our predictions (Hao et al., 2021; Raumonen et al., 2015).

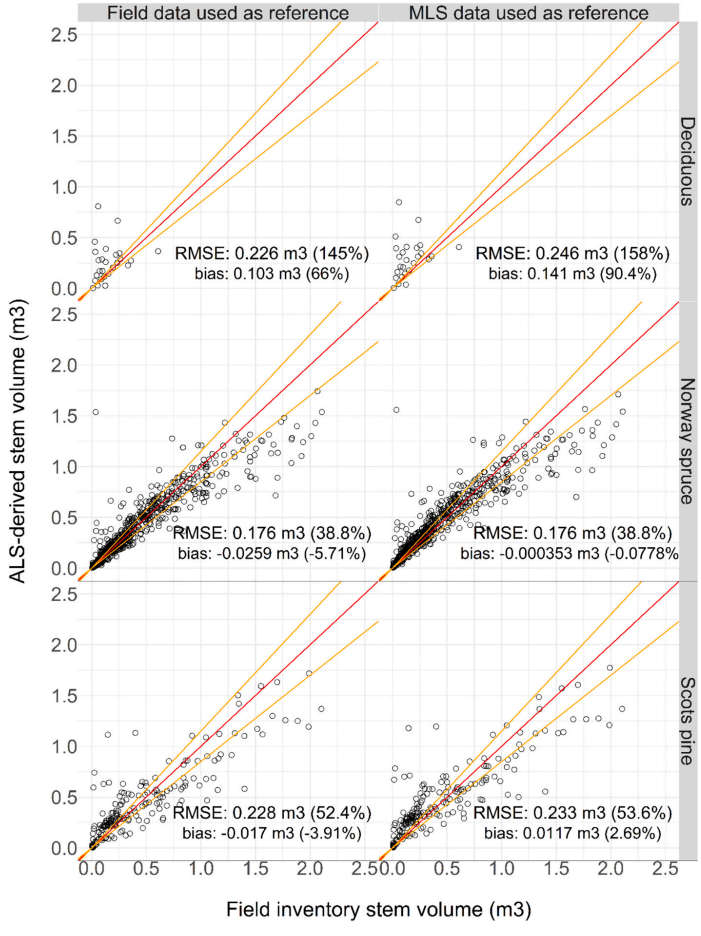

Fig. 5. Individual tree-level field inventory vs. ALS-derived stem volume, in m^3. The columns represent different reference datasets and the rows represent the different species groups. The red line is the 1:1 line, where the field inventory and ALS-derived values are equal. The orange lines represent a 15 % deviation from the 1:1 line. RMSE = Root Mean Square Error. (For interpretation of the references to colour in this figure legend, the reader is referred to the web version of this article.)

Analogously, individual tree-level estimates of stem volume may also be improved by using different modelling techniques, such as generalized linear models and non-parametric estimation methods (Hauglin et al., 2018). For instance, Karjalainen et al. (2019) reached generally lower relative RMSEs for this variable, which varied from 29 % to 41 %, while testing the transferability of a non-parametric stem volume model amongst different sites. When aggregated to plot-level (Fig. 5), the values obtained in this study were in-line with other volume estimation methods, which reported RMSEs ranging from 15.5 % to 56.2 % in boreal and temperate forest conditions (Kandare et al., 2017; Kankare et al., 2011; Kukkonen et al., 2021; Vastaranta et al., 2012; Yu et al., 2010). Similarly, Puliti et al. (2020) observed decreasing errors when comparing volume estimates at coarser levels, reaching relative RMSEs of 32.2 %, 27.1 % and 3.5 % at plot-, stand- and forest-level, respectively, while assessing the potential of UAVLS in estimating growing stock without field data for model calibration. Furthermore, Hauglin et al. (2018) used accurately positioned harvester data as reference for volume models and reported relative RMSEs ranging from 19 % to 60 % at plot-level, depending on the forest strata.

Omission and commission errors in individual tree detection can also influence the accuracy of plot-level volume estimates. In this study, omission errors were also the most pronounced in small DBH classes, resulting in sensitivities equal to 22.8 % in trees from 0 to 10 cm and 66 % in trees from 10 to 20 cm. Although these classes account for a smaller proportion of the total volume, cumulative omissions can result in significant bias in total or mean values. This kind of detection error is a common cause of stem volume underestimation when aggregating tree-level results to an area unit (Kandare et al., 2017; Kukkonen et al., 2021; Sačkov et al., 2019; Vastaranta et al., 2012), as the omission of trees in the suppressed or understory forest layers is common in ITD algorithms. For instance, Wang et al. (2016) found omission rates varying from approximately 40 % to nearly 100 % of suppressed trees when comparing 9 distinct ITD algorithms in boreal forest conditions. Analogously, Sparks et al. (2022) reported higher rates of omissions in

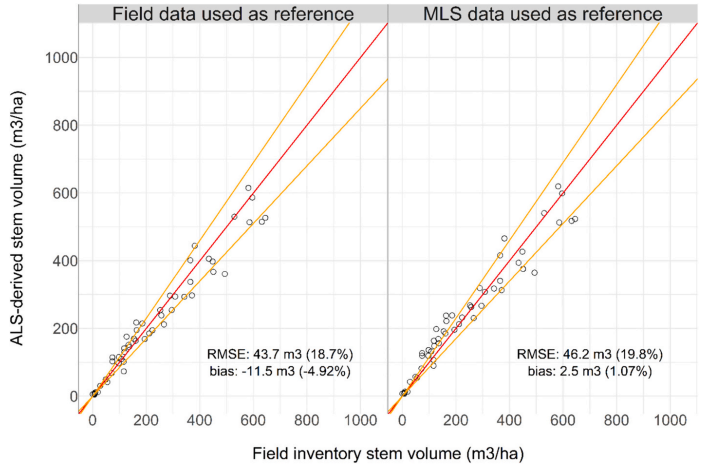

Fig. 6. Plot-level field inventory vs. ALS-derived stem volume, in m^3. The columns represent different reference datasets. The red line is the 1:1 line, where the field inventory and ALS-derived values are equal. The orange lines represent a 15 % deviation from the 1:1 line. RMSE = Root Mean Square Error. (For interpretation of the references to colour in this figure legend, the reader is referred to the web version of this article.)

suppressed trees when benchmarking ITD algorithms in mixed-conifer temperate forests.

Finally, future studies should focus on improving individual tree-level DBH and stem volume models, as well as exploring the estimation of tree species using remote sensing data. Potential improvements in tree attribute estimation and accurate identification of tree species would significantly contribute to more accurate and ecologically informed forest inventory and management practices.

5. Conclusion

In our analysis, we found that the estimation models trained with either the FI or MLS datasets presented similar values for RMSE and bias for estimates of DBH and stem volume at individual tree level. This implies that both methods perform similarly and hence the use of MLS for training data collection instead of conventional field inventory can save time and costs. Nevertheless, the results obtained in this study are limited to a Norway spruce dominated boreal forest ecosystem. Therefore, future analyses, such as the proposed method's performance in different forest conditions and the impact of seasonal environment variations on the data quality, are needed to fully elucidate the capabilities and limitations of car-mounted MLS for training data collection.

CRediT authorship contribution statement

Raul de Paula Pires: Writing – review & editing, Writing – original draft, Visualization, Validation, Methodology, Formal analysis, Conceptualization. **Eva Lindberg:** Writing – review & editing, Supervision, Resources, Methodology, Conceptualization. **Henrik Jan Persson:** Writing – review & editing, Supervision, Methodology, Conceptualization. **Kenneth Olofsson:** Writing – review & editing, Supervision, Methodology, Conceptualization. **Johan Holmgren:** Writing – review & editing, Supervision, Software, Resources, Methodology, Funding acquisition, Conceptualization.

Declaration of competing interest

The authors declare the following financial interests/personal relationships which may be considered as potential competing interests.

Raul de Paula Pires reports financial support was provided by Stora Enso AB.

Data availability

The authors do not have permission to share data.

Acknowledgements

This study was financed by Stora Enso, and the Kempe foundations through the project "Estimating Forest Resources and Quality-related Attributes Using Automated Methods and Technologies" which was part of the Tandem Forest values research program (Grant Number TF 2019-0064). In addition, funding was provided by the Hildur and Sven Wingquist foundation for forest science research though the project "Multi sensor remote sensing for improved information in forest management planning" (Grant number 17/18-2 / 107-5 SOJOH) and the Bo Rydin Foundation for Scientific Research thought the project "F 06/21 Multi-phase inventory of forest using high-resolution laser scanning". Finally, co-financing was provided by the Swedish Foundation for Strategic Environmental Research with the research program Mistra Digital Forest (DIA 2017/14 #6).

Appendix A. Appendix

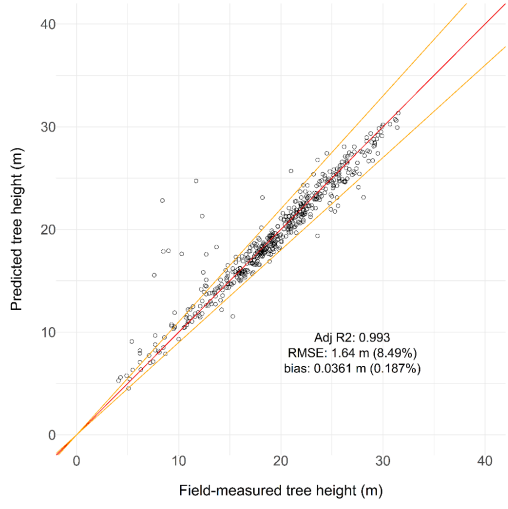

Fig 1. A – Goodness of fit of tree height estimation model based on the 95th height percentile from aerial laser scanning data

References

Appiah Mensah, A., Jonzén, J., Nyström, K., Wallerman, J., Nilsson, M., 2023. Mapping site index in coniferous forests using bi-temporal airborne laser scanning data and field data from the Swedish national forest inventory. For. Ecol. Manag. 547 https://doi.org/10.1016/j.foreco.2023.121395.

Brandel, G., 1990. Volymfunktioner för Enskilda Träd : Tall, Gran Och björk = Volume Functions for Individual Trees : Scots Pine (*Pinus sylvestris*), Norway Spruce (*Picea abies*) and Birch (Betula Pendula & *Betula pubescens*). Swedish Univ. Agric. Sci. Skogsfakta 11, 1-10. Garpenberg.

Brede, B., Lau, A., Bartholomeus, H.M., Kooistra, L., 2017. Comparing RIEGL RiCOPTER UAV LiDAR derived canopy height and DBH with terrestrial LiDAR. Sensors (Switzerland) 17, 1–16. https://doi.org/10.3390/s17102371.

Brede, B., Terryn, L., Barbier, N., Bartholomeus, H.M., Bartolo, R., Calders, K., Derroire, G., Krishna Moorthy, S.M., Lau, A., Levick, S.R., Raumonen, P., Verbeeck, H., Wang, D., Whiteside, T., van der Zee, J., Herold, M., 2022. Non-destructive estimation of individual tree biomass: Allometric models, terrestrial and UAV laser scanning. Remote Sens. Environ. 280 https://doi.org/10.1016/j.rse.2022.113180.

Calders, K., Adams, J., Armston, J., Bartholomeus, H., Bauwens, S., Bentley, L.P., Chave, J., Danson, F.M., Demol, M., Disney, M., Gaulton, R., Krishna Moorthy, S.M., Levick, S.R., Saarinen, N., Schaaf, C., Stovall, A., Terryn, L., Wilkes, P., Verbeeck, H., 2020. Terrestrial laser scanning in forest ecology: expanding the horizon. Remote Sens. Environ. 251, 112102 https://doi.org/10.1016/j.rse.2020.112102.

Calders, K., Verbeeck, H., Burt, A., Origo, N., Nightingale, J., Malhi, Y., Wilkes, P., Raumonen, P., Bunce, R.G.H., Disney, M., 2022. Laser scanning reveals potential underestimation of biomass carbon in temperate forest. Ecol. Solut. Evid. 3, 1–14. https://doi.org/10.1002/2688-8319.12197.

da Bispo, P.C., Rodríguez-Veiga, P., Zimbres, B., de Miranda, S.C., do Cezare, C.H.G., Fleming, S., Baldacchino, F., Louis, V., Rains, D., Garcia, M., Espírito-Santo, F.D.B., Roitman, I., Pacheco-Pascagaza, A.M., Gou, Y., Roberts, J., Barrett, K., Ferreira, L.G., Shimbo, J.Z., Alencar, A., Bustamante, M., Woodhouse, I.H., Sano, E.E., Ometto, J.P., Tansey, K., Balzter, H., 2020. Woody aboveground biomass mapping of the brazilian savanna with a multi-sensor and machine learning approach. Remote Sens. 12 https://doi.org/10.3390/RS12172685.

Delgado, J.D., Arroyo, N.L., Arévalo, J.R., Fernández-Palacios, J.M., 2007. Edge effects of roads on temperature, light, canopy cover, and canopy height in laurel and pine forests (Tenerife, Canary Islands). Landsc. Urban Plan. 81, 328–340. https://doi.org/10.1016/j.landurbplan.2007.01.005.

European Commission, 2021. New EU Forest Strategy for 2030, Communication from the Commission to the European Parliament, the Council, the European Economic and Social Committee of the regions. https://doi.org/10.2307/j.ctv2zp4wq1.5.

Fassnacht, F.E., Hartig, F., Latifi, H., Berger, C., Hernández, J., Corvalán, P., Koch, B., 2014. Importance of sample size, data type and prediction method for remote sensing-based estimations of aboveground forest biomass. Remote Sens. Environ. 154, 102–114. https://doi.org/10.1016/j.rse.2014.07.028.

Fu, L., Duan, G., Ye, Q., Meng, X., Luo, P., Sharma, R.P., Sun, H., Wang, G., Liu, Q., 2020. Prediction of individual tree diameter using a nonlinear mixed-effects modeling approach and airborne LiDAR data. Remote Sens. 12 https://doi.org/10.3390/rs12071066.

Hao, Y., Widagdo, F.R.A., Liu, X., Quan, Y., Dong, L., Li, F., 2021. Individual tree diameter estimation in small-scale forest inventory using uav laser scanning. Remote Sens. 13, 1–21. https://doi.org/10.3390/rs13010024.

Harper, K.A., Macdonald, S.E., Mayerhofer, M.S., Biswas, S.R., Esseen, P.A., Hylander, K., Stewart, K.J., Mallik, A.U., Drapeau, P., Jonsson, B.G., Lesieur, D., Kouki, J., Bergeron, Y., 2015. Edge influence on vegetation at natural and anthropogenic edges of boreal forests in Canada and Fennoscandia. J. Ecol. 103, 550–562. https://doi.org/10.1111/1365-2745.12398.

Hauglin, M., Gobakken, T., Astrup, R., Ene, L., Næsset, E., 2014. Estimating single-tree crown biomass of Norway spruce by airborne laser scanning: a comparison of methods with and without the use of terrestrial laser scanning to obtain the ground reference data. Forests 5, 384–403. https://doi.org/10.3390/f5030384.

Hauglin, M., Hansen, E., Sørngård, E., Næsset, E., Gobakken, T., 2018. Utilizing accurately positioned harvester data: modelling forest volume with airborne laser scanning. Can. J. For. Res. 48, 913–922. https://doi.org/10.1139/cjfr-2017-0467.

Hemery, G.E., Savill, P.S., Pryor, S.N., 2005. Applications of the crown diameter-stem diameter relationship for different species of broadleaved trees. For. Ecol. Manag. 215, 285–294. https://doi.org/10.1016/j.foreco.2005.05.016.

Holmgren, J., Tulldahl, M., Nordlöf, J., Willén, E., Olsson, H., 2019. Mobile laser scanning for estimating tree stem diameter using segmentation and tree spine calibration. Remote Sens. 11, 1–18. https://doi.org/10.3390/rs11232781.

Holmgren, J., Lindberg, E., Olofsson, K., Persson, H.J., 2022. Tree crown segmentation in three dimensions using density models derived from airborne laser scanning. Int. J. Remote Sens. 43, 299–329. https://doi.org/10.1080/01431161.2021.2018149.

Hunčaga, M., Chudá, J., Tomaštík, J., Slámová, M., Koreň, M., Chudý, F., 2020. The comparison of stem curve accuracy determined from point clouds acquired by different terrestrial remote sensing methods. Remote Sens. 12 https://doi.org/10.3390/RS12172739.

Hyyppä, E., Hyyppä, J., Hakala, T., Kukko, A., Wulder, M.A., White, J.C., Pyörälä, J., Yu, X., Wang, Y., Virtanen, J.P., Pohjavirta, O., Liang, X., Holopainen, M., Kaartinen, H., 2020a. Under-canopy UAV laser scanning for accurate forest field measurements. ISPRS J. Photogramm. Remote Sens. 164, 41–60. https://doi.org/10.1016/j.isprsjprs.2020.03.021.

Hyyppä, E., Kukko, A., Kaijaluoto, R., White, J.C., Wulder, M.A., Pyörälä, J., Liang, X., Yu, X., Wang, Y., Kaartinen, H., Virtanen, J.P., Hyyppä, J., 2020b. Accurate derivation of stem curve and volume using backpack mobile laser scanning. ISPRS J. Photogramm. Remote Sens. 161, 246–262. https://doi.org/10.1016/j.isprsjprs.2020.01.018.

Hyyppä, E., Yu, X., Kaartinen, H., Hakala, T., Kukko, A., Vastaranta, M., Hyyppä, J., 2020c. Comparison of backpack, handheld, under-canopy UAV, and above-canopy

UAV laser scanning for field reference data collection in boreal forests. Remote Sens. 12, 1–31. https://doi.org/10.3390/rs12203327.
Hyyppä, E., Kukko, A., Kaartinen, H., Yu, X., Muhojoki, J., Hakala, T., Hyyppä, J., 2022. Direct and automatic measurements of stem curve and volume using a high-resolution airborne laser scanning system. Sci. Remote Sens. 5, 100050 https://doi.org/10.1016/j.srs.2022.100050.
Iizuka, K., Yonehara, T., Itoh, M., Kosugi, Y., 2018. Estimating tree height and diameter at breast height (DBH) from digital surface models and orthophotos obtained with an unmanned aerial system for a Japanese cypress (Chamaecyparis obtusa) Forest. Remote Sens. 10 https://doi.org/10.3390/rs10010013.
Iizuka, K., Kosugi, Y., Noguchi, S., Iwagami, S., 2022. Toward a comprehensive model for estimating diameter at breast height of Japanese cypress (Chamaecyparis obtusa) using crown size derived from unmanned aerial systems. Comput. Electron. Agric. 192, 106579 https://doi.org/10.1016/j.compag.2021.106579.
Junttila, V., Finley, A.O., Bradford, J.B., Kauranne, T., 2013. Strategies for minimizing sample size for use in airborne LiDAR-based forest inventory. For. Ecol. Manag. 292, 75–85. https://doi.org/10.1016/j.foreco.2012.12.019.
Kandare, K., Dalponte, M., Ørka, H.O., Frizzera, L., Næsset, E., 2017. Prediction of species-specific volume using different inventory approaches by fusing airborne laser scanning and hyperspectral data. Remote Sens. 9, 1–19. https://doi.org/10.3390/rs9050400.
Kankare, V., Vastaranta, M., Holopainen, M., Yu, X., Hyyppä, J., Hyyppä, H., 2011. The fusion of individual tree detection and visual interpretation in assessment of Forest variables from laser point clouds. Int. Arch. Photogramm. Remote. Sens. Spat. Inf. Sci. 157–161. https://doi.org/10.5194/isprsarchives-xxxviii-5-w12-157-2011. XXXVIII-5/.
Karjalainen, T., Korhonen, L., Packalen, P., Maltamo, M., 2019. The transferability of airborne laser scanning based tree-level models between different inventory areas. Can. J. For. Res. 49, 228–236. https://doi.org/10.1139/cjfr-2018-0128.
Kotivuori, E., Korhonen, L., Packalen, P., 2016. Nationwide airborne laser scanning based models for volume, biomass and dominant height in Finland. Silva Fenn. 50, 1–28. https://doi.org/10.14214/sf.1567.
Kuhn, M., 2020. Caret: Classification and Regression Training. R Package Version 6.0–86. https://CRAN.R-project.org/package=caret.
Kukkonen, M., Maltamo, M., Korhonen, L., Packalen, P., 2021. Fusion of crown and trunk detections from airborne UAS based laser scanning for small area forest inventories. Int. J. Appl. Earth Obs. Geoinf. 100, 102327 https://doi.org/10.1016/j.jag.2021.102327.
Kuželka, K., Slavík, M., Surový, P., 2020. Very high density point clouds from UAV laser scanning for automatic tree stem detection and direct diameter measurement. Remote Sens. 12 https://doi.org/10.3390/RS12081236.
Lefsky, M.A., Cohen, W.B., Parker, G.G., Harding, D.J., 2002. Lidar Remote Sensing for Ecosystem Studies, 52, 19–30.
Leite, R.V., Silva, C.A., Mohan, M., Cardil, A., de Almeida, D.R.A., de e Carvalho, S.P.C., Jaafar, W.S.W.M., Hernández, J.G., Weiskittel, A., Hudak, A.T., Broadbent, E.N., Prata, G., Valbuena, R., Leite, H.G., Taquetti, M.F., Soares, A.A.V., Scolforo, H.F., Do Amaral, C.H., Corte, A.P.D., Klauberg, C., 2020. Individual tree attribute estimation and uniformity assessment in fast-growing eucalyptus spp. Forest plantations using lidar and linear mixed-effects models. Remote Sens. 12, 1–20. https://doi.org/10.3390/rs12213599.
Li, C., Yu, Z., Dai, H., Zhou, X., Zhou, M., 2023. Effect of sample size on the estimation of forest inventory attributes using airborne LiDAR data in large-scale subtropical areas. Ann. For. Sci. 80 https://doi.org/10.1186/s13595-023-01209-4.
Lisańczuk, M., Mitelsztedt, K., Parkitna, K., Krok, G., Stereńczak, K., Wysocka-Fijorek, E., Miścicki, S., 2020. Influence of sampling intensity on performance of two-phase forest inventory using airborne laser scanning. For. Ecosyst. 7 https://doi.org/10.1186/s40663-020-00277-6.
Liu, L., Zhang, A., Xiao, S., Hu, S., He, N., Pang, H., Zhang, X., Yang, S., 2021. Single tree segmentation and diameter at breast height estimation with mobile LiDAR. IEEE Access 9, 24314–24325. https://doi.org/10.1109/ACCESS.2021.3056877.
Maltamo, M., Næsset, E., Vauhkonen, J., 2014. Forestry applications of airborne laser scanning: concepts and case studies, Springer Netherlands, Dordrecht. https://doi.org/10.1007/978-94-017-8663-8.
Næsset, E., 2002. Predicting forest stand characteristics with airborne scanning laser using a practical two-stage procedure and field data. Remote Sens. Environ. 80, 88–99. https://doi.org/10.1016/S0034-4257(01)00290-5.
Næsset, E., 2004. Practical large-scale forest stand inventory using a small-footprint airborne scanning laser. Scand. J. For. Res. 19, 164–179. https://doi.org/10.1080/02827580310019257.
Nilsson, M., Nordkvist, K., Jonzén, J., Lindgren, N., Axensten, P., Wallerman, J., Egberth, M., Larsson, S., Nilsson, L., Eriksson, J., Olsson, H., 2017. A nationwide forest attribute map of Sweden predicted using airborne laser scanning data and field data from the national forest inventory. Remote Sens. Environ. 194, 447–454. https://doi.org/10.1016/j.rse.2016.10.022.
Novo-Fernández, A., Barrio-Anta, M., Recondo, C., Cámara-Obregón, A., López-Sánchez, C.A., 2019. Integration of national forest inventory and nationwide airborne laser scanning data to improve forest yield predictions in North-Western Spain. Remote Sens. 11, 1–25. https://doi.org/10.3390/rs11141693.
Olofsson, K., Holmgren, J., 2016. Single tree stem profile detection using terrestrial laser scanner data, flatness saliency features and curvature properties. Forests 7, 207. https://doi.org/10.3390/f7090207.
Olofsson, K., Lindberg, E., Holmgren, J., 2008. A method for linking field-surveyed and aerial-detected single trees using cross correlation of position images and the optimization of weighted tree list graphs. Hill RA, rosette J, Suárez J proc. SilviLaser 2008. In: 8th Int. Conf. LiDAR Appl. For. Assess. Invent. Heriot-Watt Univ. Edinburgh, UK, 17–19 Sept. 2008, pp. 95–104.
Olofsson, K., Holmgren, J., Olsson, H., 2014. Tree stem and height measurements using terrestrial laser scanning and the RANSAC algorithm. Remote Sens. 6, 4323–4344. https://doi.org/10.3390/rs6054323.
Persson, H.J., Olofsson, K., Holmgren, J., 2022. Two-phase forest inventory using very-high-resolution laser scanning. Remote Sens. Environ. 271, 112909 https://doi.org/10.1016/j.rse.2022.112909.
Pires, R. de P., Olofsson, K., Persson, H.J., Lindberg, E., Holmgren, J., 2022. Individual tree detection and estimation of stem attributes with mobile laser scanning along boreal forest roads. ISPRS J. Photogramm. Remote Sens. 187, 211–224. https://doi.org/10.1016/j.isprsjprs.2022.03.004.
Puliti, S., Breidenbach, J., Astrup, R., 2020. Estimation of forest growing stock volume with UAV laser scanning data: can it be done without field data? Remote Sens. 12, 1245. https://doi.org/10.3390/RS12081245.
R Core Team, 2020. R: A Language and Environment for Statistical Computing. R Foundation for Statistical Computing.
Raumonen, P., Casella, E., Calders, K., 2015. Massive-Scale Tree Modelling from TLS Data. https://doi.org/10.5194/isprsannals-II-3-W4-189-2015.
Roussel, J.R., Auty, D., Coops, N.C., Tompalski, P., Goodbody, T.R.H., Meador, A.S., Bourdon, J.F., de Boissieu, F., Achim, A., 2020. lidR: an R package for analysis of airborne laser scanning (ALS) data. Remote Sens. Environ. 251, 112061 https://doi.org/10.1016/j.rse.2020.112061.
Saĉkov, I., Scheer, A., Bucha, T., 2019. A comparison of two tree detection methods for estimation of Forest stand and ecological variables from airborne LiDAR data in central European forests. Cent. Eur. For. J. 11 https://doi.org/10.3390/rs11121431.
Snowdon, P., 1991. A ratio estimator for bias correction in logarithmic regressions. Can. J. For. Res. 21, 720–724.
Sparks, A.M., Corrao, M.V., Smith, A.M.S., 2022. Cross-comparison of individual tree detection methods using low and high pulse density airborne laser scanning data. Remote Sens. 14 https://doi.org/10.3390/rs14143480.
Stovall, A.E.L., Anderson-teixeira, K.J., Shugart, H.H., 2018. Assessing terrestrial laser scanning for developing non-destructive biomass allometry. For. Ecol. Manag. 427, 217–229. https://doi.org/10.1016/j.foreco.2018.06.004.
Sun, Y., Jin, X., Pukkala, T., Li, F., 2022. Predicting individual tree diameter of larch (Larix olgensis) from UAV-LiDAR data using six different algorithms. Remote Sens. 14 https://doi.org/10.3390/rs14051125.
Vastaranta, M., Kankare, V., Holopainen, M., Yu, X., Hyyppä, J., Hyyppä, H., 2012. Combination of individual tree detection and area-based approach in imputation of forest variables using airborne laser data. ISPRS J. Photogramm. Remote Sens. 67, 73–79. https://doi.org/10.1016/j.isprsjprs.2011.10.006.
Wang, Y., Hyyppa, J., Liang, X., Kaartinen, H., Yu, X., Lindberg, E., Holmgren, J., Qin, Y., Mallet, C., Ferraz, A., Torabzadeh, H., Morsdorf, F., Zhu, L., Liu, J., Alho, P., 2016. International benchmarking of the individual tree detection methods for modeling 3-D canopy structure for Silviculture and Forest ecology using airborne laser scanning. IEEE Trans. Geosci. Remote Sens. 54, 5011–5027. https://doi.org/10.1109/TGRS.2016.2543225.
Yu, X., Hyyppä, J., Holopainen, M., Vastaranta, M., 2010. Comparison of area-based and individual tree-based methods for predicting plot-level forest attributes. Remote Sens. 2, 1481–1495. https://doi.org/10.3390/rs2061481.
Zhang, W., Qi, J., Wan, P., Wang, H., Xie, D., Wang, X., Yan, G., 2016. An easy-to-use airborne LiDAR data filtering method based on cloth simulation. Remote Sens. 8, 1–22. https://doi.org/10.3390/rs8060501.

III

International Journal of Applied Earth Observation and Geoinformation 140 (2025) 104607

Contents lists available at ScienceDirect

International Journal of Applied Earth Observation and Geoinformation

journal homepage: www.elsevier.com/locate/jag

Boreal tree species classification using airborne laser scanning data annotated with harvester production reports, and convolutional neural networks

Raul de Paula Pires *, Christoffer Axelsson, Eva Lindberg, Henrik Jan Persson, Kenneth Olofsson, Johan Holmgren

Dept. of Forest Resource Management. Swedish University of Agricultural Sciences, Umeå, Sweden

ARTICLE INFO

Keywords:
Tree species classification
Convolutional neural networks
Aerial laser scanning
Dual-wavelength
Harvester data

ABSTRACT

This study explores the potential of spatially explicit Harvester Production Reports (HPRs) for automatic annotation of Aerial Laser Scanning (ALS) data at tree-level, enabling accurate tree species classification using Convolutional Neural Networks (CNNs). By integrating HPRs into the modelling process, this approach provides a practical solution for addressing challenges in remote sensing data annotation for forestry applications. The ALS data were acquired in managed Norway spruce-dominated forests in southern Sweden using a dual-wavelength system composed by two monochromatic sensors. Thus, three datasets were produced: the 905 nm miniVUX dataset (~100 points/m^2), the 1550 nm VUX dataset (~875 points/m^2), and the dual-wavelength dataset (~975 points/m^2), the last being a junction of the two first datasets. The automatic annotation was performed by matching tree records in the HPR and ALS data based on spatial proximity and height similarity, with a total of 45,516 HPR-recorded tree positions being linked to ALS-derived segments and assigned species labels based on HPR records. Then, the individual tree-level ALS point clouds were converted into 2D images from multiple viewing angles, with varying image dimensions and pixel sizes to accommodate trees of different sizes. These images served as input for CNN-based classification, enabling species identification across ALS datasets with varying spectral and spatial resolutions. The CNN models were trained and evaluated to classify trees into Norway spruce, Scots pine, Deciduous, and a "Noise" class for segmentation errors. The classification accuracy varied according to the dataset used, with the dual-wavelength dataset achieving the highest macro-F1 score (0.896), followed by the VUX dataset (0.894) and miniVUX dataset (0.835). These findings highlight spatially explicit HPRs as efficient, high-quality reference data for CNN-based tree species classification with minimal annotation effort.

1. Introduction

Precision forestry applications integrate remote sensing technologies and estimation techniques to enhance sustainable forest management. By providing detailed insights into tree-level attributes like tree health and timber quality, they allow informed decision-making and optimal resource allocation (Fardusi et al., 2017; Fassnacht et al., 2024). Commonly, precision forestry is supported by advanced remote sensing technologies, such as Light Detection and Ranging (LiDAR) sensors, and high resolution aerial imagery, which are used to collect detailed data on forests and enable the retrieval of information at individual tree-level. (Holopainen et al., 2014).

A key component of such forest assessments is the accurate estimation of tree species composition, which plays a critical role in management and conservation efforts (Fassnacht et al., 2016; Yu et al., 2017). Diverse tree species composition enhances ecosystem resilience, providing niches for different organisms, and mitigating the risks associated with pests and diseases (FAO and UNEP, 2020). In addition to its ecological value, tree species composition is of key interest to the forest industry as different species are suitable for different end uses due to species-specific wood properties, such as fiber length and resistance to traction.

* Corresponding author.
E-mail addresses: raul.de.paula.pires@slu.se (R.P. Pires), christoffer.axelsson@slu.se (C. Axelsson), eva.lindberg@slu.se (E. Lindberg), henrik.persson@slu.se (H.J. Persson), kenneth.olofsson@slu.se (K. Olofsson), johan.holmgren@slu.se (J. Holmgren).

https://doi.org/10.1016/j.jag.2025.104607
Received 2 January 2025; Received in revised form 11 April 2025; Accepted 15 May 2025
Available online 21 May 2025

When it comes to mapping forest characteristics, LiDAR is one of the most commonly used tools (Coops et al., 2021; Nilsson et al., 2017). These sensors can be used to distinguish tree species based on their unique structural features, such as branch patterns and shapes (Holmgren and Persson, 2004; Terryn et al., 2020; Xi et al., 2020). For instance, Terryn et al. (2020) classified five species using branch patterns in Terrestrial Laser Scanning (TLS) data, achieving 80 % accuracy. Analogously, Qian et al. (2023) achieved 90.9 % accuracy using Aerial Laser Scanning (ALS) data to differentiate six species, leveraging vertical slices of point clouds to geometric shapes. Beyond structural features, multispectral LiDAR sensors offer additional spectral reflectance data from forest canopies (Takhtkeshha et al., 2024). The use of such systems for tree species identification has been widely explored in the scientific literature (Budei et al., 2018; Mielczarek et al., 2023; Yu et al., 2017), with some studies pointing out improvements in the retrieval of species-specific forest parameters (Kukkonen et al., 2019a, 2019b) and tree detection (Huo and Lindberg, 2020) when using multispectral LiDAR compared to other remote sensing data sources.

As remote sensing technologies advance, they generate increasingly complex datasets that require sophisticated analytical methods. For this reason, deep learning – in particular Convolutional Neural Networks (CNNs) – has gained prominence in analyzing remote sensing data due to its ability to analyze complex spectral and spatial patterns (Mäyrä et al., 2021; Sothe et al., 2020), with tree species classification being one of the most common tasks performed by CNNs in the fields of forestry and forest conservation (Kattenborn et al., 2021). For example, Wu et al. (2024) used a CNN for band selection in hyperspectral images, reducing data dimensionality for faster processing. Their FAST 3D-CNN P-Net classified nine tree species with 97 %-99 % accuracy across different areas. In the recent years, deep learning has been used for tree species classification in different types of remote sensing data, including RGB images (Carvalho et al., 2022; Liu et al., 2019; Onishi and Ise, 2021; Schiefer et al., 2020), satellite optical data (Bolyn et al., 2022; Hızal et al., 2024), multi- and hyperspectral imagery (Fricker et al., 2019; Ma et al., 2024; Sothe et al., 2020; Wang and Jiang, 2024; Xu et al., 2024), and LiDAR point clouds (Murray et al., 2024; Seidel et al., 2021).

Despite the success, different challenges arise when using such deep neural networks for forestry-related applications. One major bottleneck is the need for large datasets during model training, as acquiring high-quality, georeferenced annotated data is often time-consuming and expensive (Kattenborn et al., 2021). To address this challenge, strategies such as data augmentation (He et al., 2023; Oubara et al., 2022) and synthetic data generation are employed (Bryson et al., 2023; Xiang et al., 2023), increasing the training data diversity. Finally, emerging technologies such as UAV-borne laser scanners (UAVLS) and MLSs can be used to efficiently measure forest attributes, such as diameter at breast height (DBH) and stem volume, over large areas in short times (Hyyppä et al., 2022, 2020; Pires et al., 2022; Puliti et al., 2020), generating training data in sufficient amounts.

While such methods improve the availability of training data, complementary sources can further enhance model performance and reduce reliance on field surveys. A promising alternative is the use of spatially explicit Harvester Production Reports (HPRs) as training data for estimating forest attributes. HPRs are a by-product of mechanized harvesting, generated in large quantities as a part of routine forestry operations. These reports contain detailed georeferenced information on each harvested tree, such as taper and species, making them particularly valuable for precision forestry applications. When equipped with accurate positioning systems, HPRs provide the exact type of annotations required by precision forestry – at tree-level, accurate and spatially explicit. Thus, they represent a cost-effective way of enhancing remote sensing-based inventories, significantly reducing the resources needed for field data collection (Lindroos et al., 2015; Söderberg et al., 2021).

Despite their potential, HPRs remain underutilized in the context of deep learning applications for tree species classification. Leveraging HPRs as large-scale training data could significantly reduce reliance on field surveys while improving the accuracy of species classification models. In addition, such data source could enhance the estimation of continuous forest variables such as DBH and stem volume (Hauglin et al., 2018; Karjalainen et al., 2022; Maltamo et al., 2019; Noordermeer et al., 2023), and qualitative variables such as different kinds of forest damage (Hansen et al., 2023; Jamali et al., 2023).

Given the possibilities introduced by remote sensing, deep learning, and new training data sources, our main objective is to propose a method for automatically classifying tree species at single-tree level. For that, we use HPRs to automatically annotate ALS data at tree-level, and use the annotated data to train a tree species classification CNN. In addition, we investigate the proposed technique's performance under ALS datasets with different properties, namely different spectral and spatial resolutions.

2. Material and methods

2.1. Study area

The study area is located in central Sweden (59°46́N, 14°31́E – Fig. 1). Altogether, 17 stands were used in the study, with areas varying from 3.7 ha to 16.8 ha. The stands were selected according to their planned harvesting dates, between 2021 and 2022. On the harvested stands (Table 1) the dominant tree species are Norway spruce (*Picea abies* (L.) H. Karst.) – 79 %, Scots pine (*Pinus sylvestris* L.) – 11 %, and

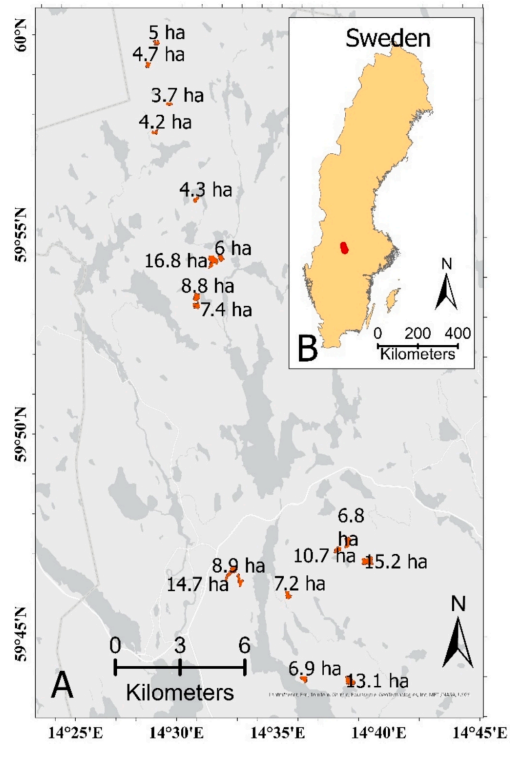

Fig. 1. (A) Map of the study area with the 17 harvested stands and their respective areas in hectares (ha). (B) Approximate location of the study area in Sweden, in red. (For interpretation of the references to color in this figure legend, the reader is referred to the web version of this article.)

Table 1
Forest areas' mean characteristics per tree species. DBH = Diameter at breast height in cm. SD = standard deviation.

Tree species	Mean DBH (± SD)	Basal area per hectare (m^2/ha)	Volume per hectare (m^3/ha)
Scots pine	25.5 (± 6.05)	6.02	59.7
Norway spruce	20.1 (± 7.99)	37.3	357
Deciduous	20.9 (± 7.96)	4.38	36.4
All species	**20.7 (± 7.99)**	**47.7**	**453**

Birch (*Betula* spp.) – 10 %.

2.2. Aerial laser scanning data

The stands were scanned in September 2021 using the Finnish Geospatial Institute's (FGI) dual-wavelength ALS system (Hakula et al., 2023). This system included two monochromatic LiDAR sensors: the Riegl miniVUX-1UAV (905 nm, NIR) and the Riegl VUX-1HA (1550 nm, SWIR), mounted on a helicopter flying 100 m above ground at 50 km/h. Due to technical issues, the system's third scanner (green wavelength) did not collect data, resulting in a dual-wavelength point cloud.

The point cloud was pre-processed and normalized using the LAStools software (Rapidlasso GmbH, Germany). Individual tree crowns were segmented using the Holmgren et al. (2022) algorithm, developed for boreal forests and achieving an F1 score of 0.86 for trees with DBH ≥ 10 cm (Pires et al., 2024). This method, previously used as the tree segmentation method for tree species classification studies (Axelsson et al., 2023; Persson et al., 2022), requires sample trees for crown density model creation. Accordingly, 122 trees were manually segmented to calibrate the model. The segmentation produced polygons representing individual tree crowns, with the highest point within each polygon identified as the treetop. To simulate different ALS systems, returns from the two sensors were separated post-segmentation, creating three datasets: mini-VUX (NIR), VUX (SWIR), and a dual-wavelength dataset combining both. Table 2 summarizes the characteristics of these datasets.

2.3. Harvester production reports

Altogether, 69,253 trees from 17 stands were harvested from November 2021 to October 2022 using cut-to-length (CTL) harvesters by John Deere (Moline, Illinois, United States) equipped with a positioning system. The positioning system consisted of two Global Navigation Satellite System (GNSS) receivers mounted on the harvester's cabin in order to establish its position and bearing. Built-in sensors enabled the recording of the boom angle and boom extension at the time of tree felling. However, the extension of the last part of the boom could not be recorded. Together, the integrated sensors for boom extension and angle and the GNSS on the harvester's cabin make it possible to calculate the position of each tree during felling. The positions of 34 stumps were taken with a RTK GNSS and used to assess the accuracy of the positions obtained with the harvester system. The distances between the stumps and harvester positions ranged from 0.1 to 2.1 m, with a mean of 0.38 m.

From the HPRs we extracted each tree's position, species, DBH, and the log lengths. Subsequently, the hprCM software (Skogforsk, 2022) was used to estimate each tree's volume and total height based on the information on the HPR. The HPR files stored four species classes, "Norway spruce", "Scots pine", "Birch", and "Other broadleaves". The "Birch" and "Other broadleaves" classes were combined into a single "Deciduous" class.

Table 2
Description of the aerial laser scanning (ALS) datasets used for tree species classification. PRR: Pulse Repetition Rate.

	ALS dataset		
	Mini-VUX (1)	**VUX (2)**	**Dual-wavelength (1 + 2)**
Sensor(s)	miniVUX-1UAV	VUX-1HA	miniVUX-1UAV (1) + VUX-1HA (2)
Footprint (cm) at 100 m from the target	16 x 5	5	16 x 5 (1) + 5 (2)
PRR (kHz)	100	1017	100 (1) + 1017 (2)
Scan speed (revolutions/s)	100	143	100 (1) + 143 (2)
Point density (points/m^2)	100	875	975 (1 + 2)
Wavelength (nm)	905	1550	905 (1) + 1550 (2)

2.4. Linking harvested trees to ALS data

Linking harvested trees to ALS segments was crucial for creating an annotated dataset with individual tree point clouds assigned to species classes. This was achieved by matching tree positions and heights between harvested trees and ALS-derived segments, using treetops from ALS segments as reference positions. For each harvested tree position, the product of horizontal distance (d) and height difference (dh) between the tree and neighboring treetops was calculated. If a treetop was within 1 m of the harvested tree, the closest treetop was linked to the harvested tree. If no treetops were within 1 m, the tree was linked to the treetop with the smallest $d \times dh$ value. Maximum allowed values were $d = 3.5$ m and $dh = 4$ m.

Segmented tree crowns, i.e. treetops, that were not linked to harvested trees were assumed to be trees that remained standing after the harvest or to be commission errors from individual tree segmentation. Harvested trees that were not linked to a tree crown were assumed omission errors from the individual tree segmentation.

Altogether, 45,516 tree positions were linked to an ALS-derived segment, representing 65.7 % of all harvested trees. Of those, 36,162 trees (79.4 %) were Norway spruces, 5,397 trees (11.9 %) Scots pine, and 3,957 (8.7 %) were deciduous trees. The proportion of trees linked to an ALS-derived segment increases with DBH (Fig. 2). In smaller DBH classes, e.g. from 5 – 10 cm, the majority of harvested trees were not linked to any ALS-derived segment. Conversely, this proportion decreases as the DBH increases, with the majority of trees with DBH ≥ 10 cm being linked to an ALS-derived segment.

2.5. Conversion of point clouds to 2D images

We used a CNN designed for 2D image classification – described further in section 2.6. Therefore, the individual tree point clouds were converted into images. The general workflow for this conversion involved transforming the individual tree point clouds into 2D images from four angles by rasterizing them in the X vs. Z plane at 45° intervals. At that stage, the pixel size was dynamically determined based on point density to ensure accurate representation of varying tree sizes and shapes, and the pixel values assigned according to the ALS dataset used, preserving relevant structural and spectral information. Finally, the pixel values were normalized and the images resized to a standard 160 × 320 pixels for CNN classification.

The rasterization was done in the X vs. Z plane, generating four 2D representations per tree by rotating the tree point cloud around the Z-axis at 45° intervals (0°, 45°, 90°, and 135°). It was performed independently for each ALS dataset and tree, producing variable image dimensions and pixel sizes tailored to tree size and dataset characteristics. Using fixed image dimension and pixel size for rasterizing the tree point clouds could lead to inaccuracies in their 2D representations. For instance, fixed image and pixel sizes could potentially cause trees to be cropped, if the number of pixels is not enough to cover their full extent, or blurred, if the pixel size is too large relative to the tree's size. By using variable pixel and image sizes, we were able to better represent the different tree sizes and shapes. This approach maintained the resolution of the original point cloud data, ensuring higher point density datasets were represented with higher-resolution images, while lower-density

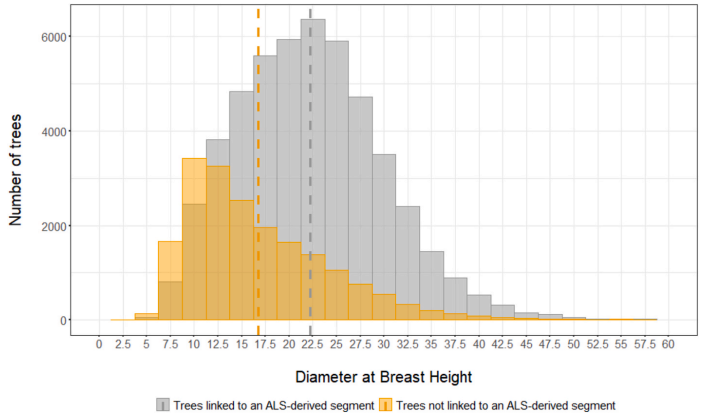

Fig. 2. Diameter at breast height (DBH) distribution of trees linked and not linked to an aerial laser scanning (ALS)-derived segment. The dashed lines represent the mean DBH of each category.

datasets retained appropriate detail levels.

Fig. 3 shows how point clouds of trees with different sizes were represented in two dimensions. Prior to rasterization, the extent of the point cloud for each rotation angle was used to define the area to be rasterized, ensuring accommodation of the entire point cloud within the raster frame. For each ALS dataset (*i*), tree (*j*) and rotation angle (*a*), the pixel size (*ps*) of the resulting 2D image was calculated according to formula 1. In this calculation, the pixel area was determined as the inverse of the point density in the X vs. Z direction post-rotation, representing the area a single point would occupy if all the returns in the point cloud were uniformly distributed within the raster frame.

$$ps_{ija} = \sqrt{(x_{ija} * z_{ija})/n_{ij}} \quad (1)$$

where, *n* is the number of returns in the tree segment.

Once the raster frame and pixel size were established for each *i, j* and *a*, pixel values were assigned based on the ALS dataset used. In order to assess the implication of adding spectral information in the images used for classification, the pixel values in mini-VUX- and VUX-derived images was set as the number of returns within each pixel considering the full depth of a tree's point cloud. In other words, no intensity values in the two monochromatic datasets were used. The pixel values were normalized image-wise within the range of 0 to 255, with 0 indicating no points in the pixel and 255 corresponding to the 95th percentile of the pixel values pre-normalization. Pixels with values greater than or equal to the 95th percentile of pixel values were set as 255, resulting in grayscale images with 256 shades, ranging from white (0) to black (255).

In contrast, the images derived from dual-wavelength ALS data were created using an RGB false color composite combining NIR and SWIR. In each pixel, the red channel was assigned the mean intensity of the NIR points, green as the mean intensity of the SWIR points, and blue as the Normalized Near Infrared Index (NDII), calculated using NIR and SWIR according to formula 2. For these images, pixels lacking returns from either channel were assigned an NDII value of zero. Afterwards, the RGB values of each image were normalized to a range between 0 and 255, where 0 represented the absence of returns, and 255 indicated the highest mean intensity value before normalization.

$$NDII_k = \frac{nir_k - swir_i}{nir_i + swir_i} \quad (2)$$

where *nir* is the mean intensity of returns from the miniVUX-1UAV sensor, and *swir* is the mean intensity of returns from the VUX-1HA sensor in pixel *k*.

Finally, all images were resized to the standard dimensions of 160 (width) by 320 (height) pixels.

2.6. Tree species classification

To ensure an even representation of each tree species class and mitigate potential bias towards over-represented classes, the dataset was balanced by reducing the number of instances in each class to match the smallest class. Thus, the number of trees in the Norway spruce and Scots pine classes was reduced to 3,957 trees to match the Deciduous class.

The dataset was visually inspected to create a "Noise" class for commission errors from tree segmentation. In this context, an image was classified as noise if we could not identify an obvious tree shape on the image within the dual-wavelength dataset. This step aimed to classify potential commission errors from the tree segmentation process as such, increasing the prediction accuracy for the tree species classes. If the images of a given segment were considered noise while inspecting the dual-wavelength dataset, they were sorted to the "Noise" class in all three ALS datasets. During this process, 228 trees were removed from the analysis due to being assigned the wrong species class, representing 0.5 % of all matched trees. These removals could be a result of faulty annotations by the harvester operator or errors in the matching procedure. Since species assignment is manually performed by the operator, human error is possible. Additionally, mismatches between harvester-derived and ALS-derived positions may have contributed to these removals. Altogether, 853 trees were sorted out from the other classes and allocated in the "Noise" class, resulting in 3772, 3559 and 3459 trees in the Pine, Spruce and Deciduous classes, respectively.

We used YOLOv8s-cls, a CNN from the YOLO family, for species classification due to its strong performance and user-friendly implementation in PyTorch (Jocher et al., 2023). The *YOLOv8s-cls* model, suitable for small-class problems, was trained for 15 epochs using default settings (Appendix A). Each tree was represented by four images from different views, resulting in nearly 14,000 images per class. Thirty percent of these were reserved for validation at each epoch's end. YOLO networks have demonstrated success in object detection tasks, including tree detection and segmentation (Straker et al., 2023) and wood surface knot detection (Fang et al., 2021), making YOLOv8 an ideal choice for this study.

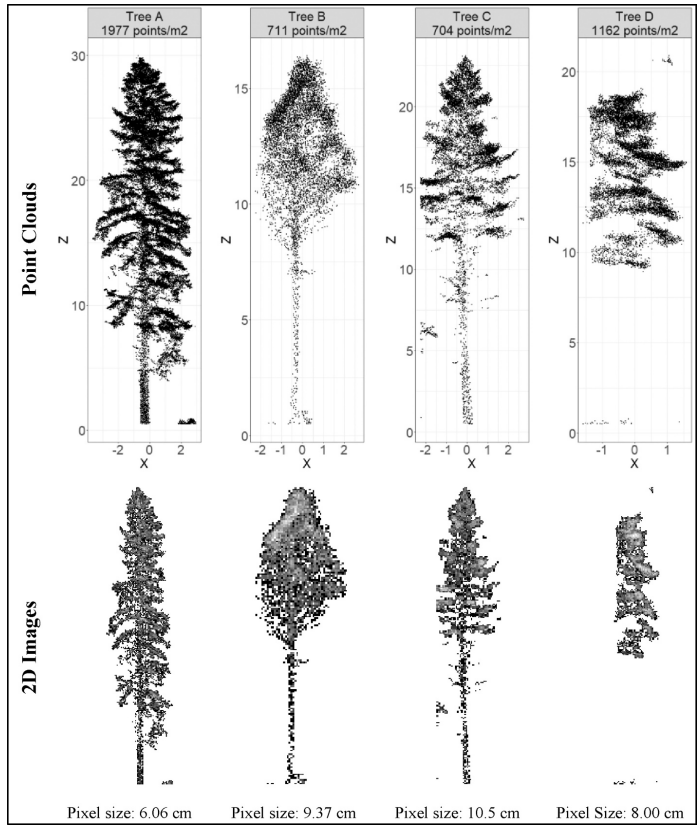

Fig. 3. Schematic representation of the rasterization of two trees with different point densities and sizes. Tree A: Norway spruce. Tree B: Deciduous tree. Tree C: Scots pine. Tree D: Pine tree under wrong segmentation, i.e. noise. The different shades of gray in the 2D image represent the number of points in each pixel. X and Z are in meters.

2.7. Accuracy Assessment

The tree species classification model's accuracy was assessed by comparing observed and predicted species for each tree. Due to the limited number of stands ($S = 17$), we opted for a leave-one-stand-out validation approach. For each stand s, the model was trained using data from all other stands ($S - s$) and applied to s. By doing so, we ensure that no trees from s are seen during the training process. This process was repeated S times, generating predictions for all stands while evaluating how the model is able to generalize when applied to different stands. During validation, the model predicted species independently for each tree projection, producing four probability vectors per ALS-derived segment. These vectors were averaged to create a single probability vector per segment, assigning the class with the highest probability to the segment. The leave-one-stand-out results are shown in a confusion matrix together with evaluation metrics such as user's and producer's accuracy (UA and PA as in formulas 3 and 4, respectively), the F1 score (formula 5), and overall accuracy (formula 6). Complementarily, the macroF1 represents the mean of the F1 score across all classes.

$$UA_C = TP_c/(TP_c + FP_C) \quad (3)$$

$$PA_C = TP_c/(TP_c + FN_C) \quad (4)$$

$$F1_C = 2 \bullet UA_C \bullet PA_C/(UA_C + PA_C) \quad (5)$$

$$OA = \frac{1}{N} \bullet \sum_i^C TP_i \quad (6)$$

where TP is the number of true positives, FP are the false positives, and FN are the false negatives of class C. N represents the number of trees analyzed in this study.

3. Results

3.1. Conversion of point clouds to 2D images

Fig. 4 shows examples of 2D images generated from different ALS datasets for each classification category. Mini-VUX-based images had the lowest average resolution (27.6 cm pixel size, Table 3), often lacking finer details such as branch structures or visible trunks, which appeared blurred or absent. In contrast, images generated with VUX and dual-wavelength datasets had higher resolutions, averaging 10.1 cm and 9.52 cm pixel sizes, respectively, revealing finer details (Fig. 4, Table 3).

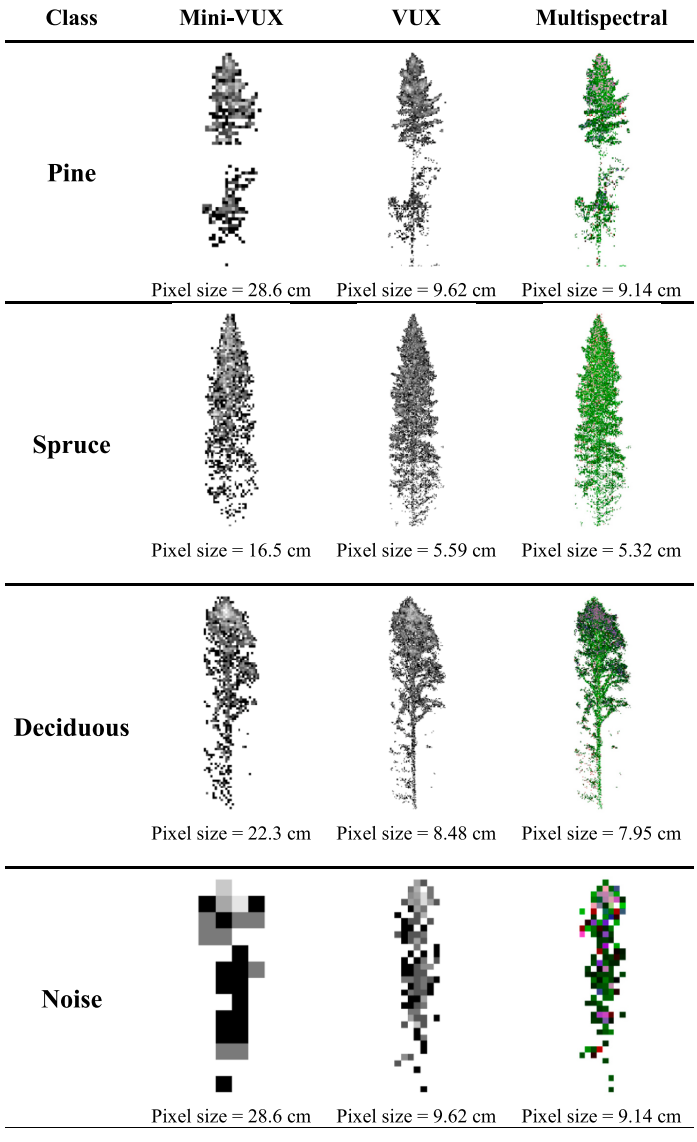

Fig. 4. Two dimensional representations of individual tree point clouds produced with different aerial laser scanning datasets.

In average, the Deciduous class had the largest pixel sizes of the tree species classes regardless of the dataset being used to generate the images (Table 3). This can be at least partially explained by the fact that the ALS data was collected in the beginning of the Autumn season, when the deciduous trees start shedding leaves, thus, intercepting less laser pulses then the other tree classes.

3.2. Tree species classification

Tables 4, 5 and 6 show the confusion matrixes and accuracy metrics for the classifications performed on the mini-VUX, VUX and dual-wavelength datasets, respectively. Fig. 5 shows an example of a a stand point cloud with all detected trees classified. The highest overall accuracies and macro-F1 obtained while using the dual-wavelength data for classification (Table 6), followed by the classification performed on the VUX data (Table 5). The classification done using the mini-VUX data showed the lowest F1 score for the three species classes and noise class, resulting in a macro F1 of 0.835 (Table 4).

The tree species classes showed the highest F1 score when using dual-wavelength images for classification, ranging from 0.923 to 0.942

Table 3
Average pixel size (cm) for the tree species classes and noise class (± standard deviation). Different letters in the last row denote statistically significant differences according to Student's *t*-test at a 95 % confidence level.

Class	Mini-VUX	VUX	Dual-wavelength
Pine	26.7 (± 5.88)	9.23 (± 2.1)	8.76 (± 1.98)
Spruce	27 (± 6.04)	9.61 (± 2.3)	9.11 (± 2.17)
Deciduous	27.5 (± 6.43)	10.5 (± 2.83)	9.88 (± 2.62)
Noise	38.9 (± 11.8)	16.4 (± 5.57)	15.4 (± 5.14)
All classes	**27.6 a (± 7.04)**	**10.1b (± 3.07)**	**9.52c (± 2.86)**

from Spruce to Decidous, resulting in a macro-F1 of 0.934 when not considering the Noise class. Analogously, when using VUX-based images, the F1 scores ranged from 0.914 (Spruce) to 0.937 (Pine), resulting in a macro-F1 of 0.926 when disregarding the Noise class. Finally, the lowest classification accuracy for the tree species classes was obtained while using mini-VUX-based images (Table 4). With this dataset, the F1 scores ranged from 0.84 for the Deciduous class to 0.876 for the Spruce class, with a macro F1 of 0.861 when considering only the tree species classes. The F1 scores were the lowest for the Noise class regardless of the ALS dataset used for modelling and inference. For this class, the F1 scores were 0.756, 0.798 and 0.783 when using the mini-VUX, VUX and dual-wavelength datasets, respectively.

Even though improvements in the classification accuracy were observed across all classes when using ALS datasets with higher spatial and spectral resolutions, some classes benefited more from the higher resolution datasets than others. For example, when using the mini-VUX dataset for classification, the Deciduous class exhibited the lowest accuracy among the tree species classes (F1 = 0.840). However, this class showed intermediate classification accuracy when using VUX (F1 = 0.928) and the highest accuracy of all species groups when using the dual-wavelength dataset (F1 = 0.942), representing more an improvement of 12.1 % on the F1 score. In contrast, the Pine class' F1 score improved 8.07 % and Spruce class' 5.37 % when comparing the classification done using mini-VUX and dual-wavelength data.

We also examined the relationship between classification accuracy and stand conditions such as tree density, basal area and species mixture measures. However, no meaningful correlation was observed ($R^2 < 0.1$), suggesting that classification performance was not strongly influenced by these factors.

4. Discussion

4.1. Using HPRs for tree species classification

In this study, we used harvester production reports to automatically annotate three ALS datasets, with different spatial and spectral resolutions. With this approach, 45,516 ALS-derived individual tree segments were labeled with tree species information by matching spatially explicit information from HPRs to the ALS-derived single tree positions, representing 65.7 % of the trees harvested in the study area. This proportions align with other studies reporting rates form from 42.8 % (Mäyrä et al., 2021) to 69.3 % (Hamraz et al., 2019).

Despite links being established across all DBH classes, many harvested trees remained unlinked (Fig. 2). In this study, we could not determine the exact reasons for this, as not all trees in the study area were harvested. Common forestry practices, such as leaving shelter wood or partially harvesting stands, may explain some missing links. Additionally, the tree segmentation method used has shown reduced detection rates for smaller trees (Holmgren et al., 2022; Pires et al., 2024), suggesting that improved detection of small trees in ALS data could enhance linking rates.

This is a known limitation of ALS-based tree detection and segmentation, as smaller individuals in the understory that are often occluded. In this study, many of the harvested trees that were not linked to ALS-derived segments fell within lower DBH classes (Fig. 2), suggesting

Table 4
Confusion matrix of predictions made using the mini-VUX-based images. OA = Overall accuracy.

		Observed Species				User's accuracy	F1 score
		Pine	Spruce	Deciduous	Noise		
Predicted Species	Pine	3190	137	292	17	87.7 %	0.867
	Spruce	245	3233	206	97	89.8 %	0.876
	Deciduous	257	158	2886	114	84.5 %	0.840
	Noise	30	71	75	625	78 %	0.756
Producer's accuracy		85.7 %	87.6 %	83.4 %	73.3 %	**OA = 85.4 %**	**macroF1 = 0.835**

Table 5
Confusion matrix of predictions made using the VUX-based images. OA = Overall accuracy.

		Observed Species				User's accuracy	F1 score
		Pine	Spruce	Deciduous	Noise		
Predicted Species	Pine	3409	85	57	5	95.9 %	0.937
	Spruce	203	3362	109	80	89.6 %	0.914
	Deciduous	94	76	3207	85	92.6 %	0.928
	Noise	16	76	86	686	79.4 %	0.798
Producer's accuracy		91.6 %	93.4 %	92.7 %	80.1 %	**OA = 91.6 %**	**macroF1 = 0.894**

Table 6
Confusion matrix of predictions made using the dual-wavelength images. OA = Overall accuracy.

		Observed Species				User's accuracy	F1 score
		Pine	Spruce	Deciduous	Noise		
Predicted Species	Pine	3455	103	87	9	94.6 %	0.937
	Spruce	198	3392	60	100	90.4 %	0.923
	Deciduous	45	43	3242	97	94.6 %	0.942
	Noise	24	61	70	650	80.8 %	0.783
Producer's accuracy		92.8 %	94.2 %	93.7 %	75.9 %	**OA = 92.3 %**	**macroF1 = 0.896**

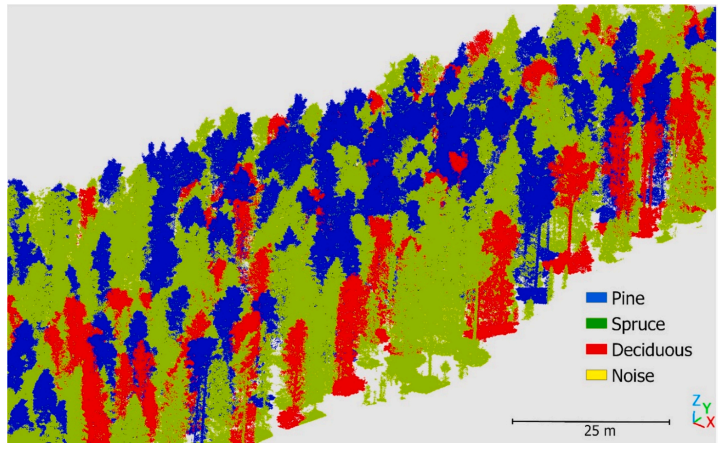

Fig. 5. Example of a stand's point cloud after tree species classification under the proposed methodology.

that suppressed trees were underrepresented in the annotated dataset. The omission of these trees introduces a potential source of bias, as the classification model is predominantly trained on dominant and co-dominant individuals. Similar issues have been reported in previous studies, which found that small or suppressed trees are frequently missing from ALS-derived individual tree-level inventories (Xu et al., 2014a, 2014b).

To mitigate this limitation, future research could explore strategies such as targeted data augmentation for suppressed trees to increase their representation during model training. Alternatively, the integration of complementary datasets, such as benchmark datasets (Puliti et al., 2023b) from structurally heterogeneous stands or synthetic point clouds that simulate occluded understory trees, may help models learn features of suppressed individuals more effectively. These approaches can provide a partial workaround to underrepresentation by enriching the training data, even when direct segmentation of suppressed trees is not feasible.

Nevertheless, the annotation effort required in this study was significantly lower compared to manual interpretation of LiDAR point clouds or traditional field data collection. Annotation remains a major challenge for training deep learning models, which often require a large number of annotated instances (Hamedianfar et al., 2022). Hence, HPRs can simplify this process and provide additional tree size attributes such as DBH, height, and volume, which are important for various modeling tasks (Hauglin et al., 2018; Karjalainen et al., 2022; Maltamo et al., 2019; Noordermeer et al., 2023).

4.2. Conversion of point clouds to 2D images

Conversion of three-dimensional point clouds to two-dimensional representations is a common approach to detection, segmentation and classification problems when using deep learning on point clouds (Kattenborn et al., 2021), either by using a single- or multi-view 2D-CNNs (Zhang et al., 2023). With such approach, users are able to apply well-established deep learning architectures and frameworks used for 2D data processing also on data originally acquired in three dimensions. For instance, Persson et al. (2022) converted individual tree ALS point clouds to 2D images from different views in order to use a CNN for tree species classification. Puliti et al. (2023a) used UAVLS data to create 2D vertical projections of Norway spruce trees' and train a whorl detector using the YOLOv5 framework (Jocher, 2020). In addition, Hamraz et al. (2019) estimated the conifer and deciduous proportions at area-level using either a LiDAR-based Digital Surface Model (DSM) or projections of the LiDAR point cloud from different viewpoints. Moreover, Straker et al. (2023) performed instance segmentation of individual trees using YOLOv5 and UAVLS-based Canopy Height Models (CHM).

When it comes to tree species classification at tree-level, Briechle et al. (2021) converted UAVLS point clouds with approximately 53 points/m^2 to 2D side view projections. In their study, the pixel size was set to 10 cm and the image size was set to accommodate the largest tree in the dataset without cropping it, which resulted in a considerable loss of detail when projecting smaller trees. In a simpler conversion approach, Hell et al. (2022) generated side-view images of tree-level ALS point clouds (with approximately 80 points/m^2) by producing scatterplots with the point locations in the vertical direction. These scatterplots were written as 150 x 150 pixel images and used as input for a CNN. However, in order to avoid smaller trees being represented with more details than bigger trees, only adult forest trees were included in the analysis.

We were able to avoid shortcomings related to projecting point clouds with different dimensions by using variable pixel sizes and image dimensions while projecting the ALS-derived segments into 2D images and, later, resizing all the images to the standard 320x160 pixel resolution to be used by the CNN. This allowed us to use the state-of-the-art YOLOv8 framework for classification (Jocher et al., 2023), which is known for its user friendliness, speed and accuracy. In addition, the memory required to store 2D images of 320x160 pixels was considerably smaller than the one that would be required if storing point clouds, especially when considering that the average point density was nearly 1000 points/m^2.

4.3. Tree species classification using ALS data

Tree species classification accuracies varied with the ALS dataset used. Using the dual-wavelength dataset (NIR and SWIR returns), the macro-F1 score was 0.896, and overall accuracy (OA) reached 92.3 %. Similar performance was achieved with VUX dataset images (macro-F1 = 0.894, OA = 91.6 %), while mini-VUX dataset predictions yielded lower accuracy (macro-F1 = 0.835, OA = 85.4 %). The VUX dataset's higher spatial resolution resulted in a 6.2 % OA increase over mini-VUX, with the macro-F1 rising from 0.835 to 0.894. Conversely, using dual-wavelength data only slightly improved OA (from 91.6 % to 92.3 %) and macro-F1 (from 0.892 to 0.893). This discrepancy may be attributed

to differences in point density and laser beam footprint: the VUX dataset had footprints of nearly 20 cm2 at 100 m, while mini-VUX footprints were approximately 63 cm2, reducing visibility of smaller features like fine branches in mini-VUX-derived images. In other words, similar tree species classification accuracies were obtained when using the monochromatic VUX dataset and the dual-wavelength dataset under the proposed methodology. This result can be at least partially explained by the fact that CNNs such as the one used in this study are designed to learn from local patterns in images (Hamedianfar et al., 2022; Kattenborn et al., 2021), such as the different tree shapes and branches. Consequently, when classifying Pine, Spruce, Deciduous, and Noise, which differ substantially in shape (Figs. 3 and 4), point density and small footprint scanning might have been more determinant than spectral information.

The observed differences in classification accuracy across tree species highlight the role of the tree crowns' structural complexity and spectral information in species differentiation (Nauber et al., 2024; Qian et al., 2023; Terryn et al., 2020). The Deciduous class, which exhibit more variable and heterogeneous crown structures, benefited the most from the VUX and dual-wavelength datasets likely due to the increased spatial resolution capturing finer details necessary for accurate classification. The further improvement observed with dual-wavelength data suggests that spectral information enhances species differentiation by capturing variations in foliage properties (Shi et al., 2018a, 2018b). In contrast, Pine and Spruce classes showed smaller accuracy gains, indicating that their more uniform crowns are more easily distinguishable even with lower-resolution datasets. However, this study is limited to a single geographical region and a few species groups. Hence, it was not possible to access how the spectral information from dual-wavelength LiDAR point cloud would influence tree species classification accuracy when classifying more species groups or trees from different biomes.

Yet, the classification accuracies obtained are in-line with other studies that have attempted tree species classification using either single- or multi-wavelength LiDAR data in similar forest types. For example, Axelsson et al. (2023) used a dual-wavelength ALS system (532 nm and 1064 nm) and k-nn imputation to classify Pine, Spruce, and Deciduous trees, obtaining OA of 91.1 % and macro-F1 of 0.861. Hakula et al. (2023) used multispectral ALS (532 nm, 905 nm and 1550 nm) and random forest for classifying similar species, obtaining OA of 90.8 % and macro-F1 of 0.901.

Regarding deep learning approaches, our CNN-based method using 2D projections aligns with similar methodologies that have shown high classification accuracy. Mäyrä et al. (2021) used 3D-CNNs with ALS and hyperspectral images, obtaining OA of 87 % and macro F1 equal to 0.86 for four species groups. Briechle et al. (2021) achieved high accuracy (OA = 96.1 % and macro–F1 = 0.96) when combining LiDAR-derived side views and multispectral images in a 2D-CNN but noted reduced accuracy using LiDAR alone (OA = 80.4 %, macro-F1 = 0.8). Finally, Hell et al. (2022), used side-view 2D projections of individual trees from LiDAR data to classify seven tree species in temperate forests, reaching an overall accuracy of 87 %.

In addition to using 2D images or point cloud projections, authors have used deep learning models for classification directly in 3D point clouds. For example, Liu et al. (2022) benchmarked six point cloud-based deep learning models to classify eight species classes in dense MLS point clouds, achieving F1 scores ranging from 0.718 to 0.996. Murray et al. (2024) obtained weighted F1 scores of 0.63 when classifying the leading tree species and 0.85 when differentiating between coniferous- and broadleaf-dominated forest plots by using point-based deep learning in ALS data with approximately 40 points/m^2. These studies highlight that deep learning approaches are highly effective for tree species classification, particularly when incorporating high-resolution data. While point cloud-based methods provide a more direct way of processing LiDAR data, they typically require higher computational power. Our approach, using 2D projections with CNNs provides a simpler alternative while maintaining competitive accuracy.

Regardless of the architecture or type of model chosen, the automatic annotation used in our analysis can significantly affect how deep learning models are trained by eliminating the bottleneck of training data collection and manual annotation, enabling more scalable and efficient model development. By leveraging HPRs for species labeling, this approach enhances the feasibility of large-scale tree species classification efforts and opens new possibilities for integrating operational forestry data into remote sensing applications.

The classification method's performance could be improved by refining tree segmentation techniques, particularly for smaller trees. This could lead to an increase in the proportion of linked trees and improve dataset completeness. Apart from tree species classification, harvester data could be valuable for estimating other forest attributes, such as tree health, wood quality, or growth rates, by leveraging the recorded DBH, height, and volume measurements and expanding the usage of harvester data in remote sensing-based analyses.

5. Conclusion

This study proposes a method for automatically classifying tree species at the single-tree level using ALS data, deep learning, and harvester production reports. By using the HPRs to annotate ALS data, we effectively trained a tree species classification CNN, achieving macroF1 scores ranging from 0.835 to 0.896. The results indicate that spatially explicit HPRs are a promising data source for tree species identification at the single-tree level. Moreover, the best classification performance was achieved when using the dual-wavelength ALS dataset under the proposed methodology, closely followed by VUX dataset. The worst classification performance was obtained when using the mini-VUX data for classification. Future research should focus on implementing similar methodologies for diverse species groups, such as different deciduous trees.

CRediT authorship contribution statement

Raul de Paula Pires: Writing – original draft, Visualization, Validation, Methodology, Formal analysis, Conceptualization. **Christoffer Axelsson:** Writing – review & editing, Software, Methodology. **Eva Lindberg:** Writing – review & editing, Supervision, Resources, Methodology, Conceptualization. **Henrik Jan Persson:** Writing – review & editing, Supervision, Conceptualization. **Kenneth Olofsson:** Writing – review & editing, Methodology, Conceptualization. **Johan Holmgren:** Writing – review & editing, Supervision, Software, Resources, Methodology, Funding acquisition, Conceptualization.

Declaration of competing interest

The authors declare that they have no known competing financial interests or personal relationships that could have appeared to influence the work reported in this paper.

Acknowledgements

This study was financed by Stora Enso, and the Kempe foundations through the project "Estimating Forest Resources and Quality-related Attributes Using Automated Methods and Technologies" which was part of the Tandem Forest values research program (Grant Number TF 2019-0064). In addition, funding was provided by the Hildur and Sven Wingquist foundation for forest science research though the project "Multi sensor remote sensing for improved information in forest management planning" (Grant number 17/18-2 / 107-5 SOJOH) and the Bo Rydin Foundation for Scientific Research thought the project "F 06/21 Multi-phase inventory of forest using high-resolution laser scanning". Finally, co-financing was provided by the Swedish Foundation for Strategic Environmental Research with the research program Mistra Digital Forest (DIA 2017/14 #6). The authors wish to thank Skogforsk

and Stora Enso for performing the harvester data collection and providing the harvester data logs. Finally, the authors would also like to thank the Finnish Geospatial Institute for the collection of aerial laser scanning data.

Author contributions

Raul de P. Pires: Conceptualization, Methodology, Validation, Formal analysis, Writing – Original Draft, and Visualization. **Christoffer Axelsson**: Methodology, Software, Writing - Review & Editing. **Eva Lindberg**: Conceptualization, Methodology, Resources, Writing - Review & Editing, and Supervision. **Henrik J. Person**: Conceptualization, Methodology, Writing - Review & Editing, and Supervision. **Kenneth Olofsson**: Conceptualization, Methodology, Writing - Review & Editing, and Supervision. **Johan Holmgren**: Conceptualization, Methodology, Software, Resources, Writing - Review & Editing, Supervision, and Funding acquisition.

Appendix A. Yolov8s-cls hyperparameters

task: classify; **mode**: train; **model**: yolov8s-cls.yaml; **epochs**: 15; **patience**: 3; **batch**: 16; **imgsz**: 320; **save**: true; save_**period**: −1; **cache**: true; **device**: 0; **workers**: 8; **exist_ok**: false; **pretrained**: false; **optimizer**: auto; **verbose**: true; **seed**: 27; **deterministic**: true; **single_cls**: false; **rect**: true; **cos_lr**: false; **close_mosaic**: 10; **resume**: false; **amp**: true; **fraction**: 1.0; **profile**: false; **freeze**: null; **overlap_mask**: truemask_ratio: 4; **dropout**: 0.25; **val**: true; **split**: val; **save_json**: false; **save_hybrid**: false; **conf**: null; **iou**: 0.7; **max_det**: 300; **half**: false; **dnn**: false; **plots**: true; **source**: null; **show**: false; **save_txt**: false; **save_conf**: false; **save_crop**: false; **show_labels**: true; **show_conf**: true; **vid_stride**: 1; **stream_buffer**: false; **line_width**: null; **visualize**: false; **augment**: false; **agnostic_nms**: false; **classes**: null; **retina_masks**: false; **boxes**: true; **format**: torchscript; **keras**: false; **optimize**: false; **int8**: false; **dynamic**: false; **simplify**: false; **opset**: null; **workspace**: 4; **nms**: false; **lr0**: 0.01; **lrf**: 0.01; **momentum**: 0.937; **weight_decay**: 0.0005; **warmup_epochs**: 3.0; **warmup_momentum**: 0.8; **warmup_bias_lr**: 0.1; **box**: 7.5; **cls**: 0.5; **dfl**: 1.5; **pose**: 12.0; **kobj**: 1.0; **label_smoothing**: 0.0; **nbs**: 64; **hsv_h**: 0.015; **hsv_s**: 0.7; **hsv_v**: 0.4; **degrees**: 0.0; **translate**: 0.1; **scale**: 0.5; **shear**: 0.0; **perspective**: 0.0; **flipud**: 0.0; **fliplr**: 0.5; **mosaic**: 1.0; **mixup**: 0.0; **copy_paste**: 0.0; **cfg**: null; **tracker**: botsort.yaml.

Data availability

The authors do not have permission to share data.

References

Axelsson, C.R., Lindberg, E., Persson, H.J., Holmgren, J., 2023. The use of dual-wavelength airborne laser scanning for estimating tree species composition and species-specific stem volumes in a boreal forest. Int. J. Appl. Earth Obs. Geoinf. 118, 103251. https://doi.org/10.1016/j.jag.2023.103251.

Bolyn, C., Lejeune, P., Michez, A., Latte, N., 2022. Mapping tree species proportions from satellite imagery using spectral–spatial deep learning. Remote Sens. Environ. 280, 113205. https://doi.org/10.1016/j.rse.2022.113205.

Briechle, S., Krzystek, P., Vosselman, G., 2021. Silvi-Net – A dual-CNN approach for combined classification of tree species and standing dead trees from remote sensing data. Int. J. Appl. Earth Obs. Geoinf. 98, 102292. https://doi.org/10.1016/j.jag.2020.102292.

Bryson, M., Wang, F., Allworth, J., 2023. Using Synthetic Tree Data in Deep Learning-Based Tree Segmentation Using LiDAR Point Clouds. Remote Sens. 15. https://doi.org/10.3390/rs15092380.

Budei, B.C., St-Onge, B., Hopkinson, C., Audet, F.A., 2018. Identifying the genus or species of individual trees using a three-wavelength airborne lidar system. Remote Sens. Environ. 204, 632–647. https://doi.org/10.1016/j.rse.2017.09.037.

Carvalho, M. de A., Marcato, J., Martins, J.A.C., Zamboni, P., Costa, C.S., Siqueira, H.L., Araújo, M.S., Gonçalves, D.N., Furuya, D.E.G., Osco, L.P., Ramos, A.P.M., Li, J., de Castro, A.A., Gonçalves, W.N., 2022. A deep learning-based mobile application for tree species mapping in RGB images. Int. J. Appl. Earth Obs. Geoinf. 114, 103045. DOI: 10.1016/j.jag.2022.103045.

Coops, N.C., Tompalski, P., Goodbody, T.R.H., Queinnec, M., Luther, J.E., Bolton, D.K., White, J.C., Wulder, M.A., van Lier, O.R., Hermosilla, T., 2021. Modelling lidar-derived estimates of forest attributes over space and time: A review of approaches and future trends. Remote Sens. Environ. 260, 112477. https://doi.org/10.1016/j.rse.2021.112477.

FAO, UNEP, 2020. The State of the World's Forests 2020. Forests, biodiversity and people. Rome. DOI: 10.4060/ca8642en.

Fardusi, M.J., Chianucci, F., Barbati, A., 2017. Concept to practices of geospatial information tools to assist forest management & planning under precision forestry framework: A review. Ann. Silvic. Res. 41, 3–14. https://doi.org/10.12899/asr-1354.

Fassnacht, F.E., Latifi, H., Stereńczak, K., Modzelewska, A., Lefsky, M., Waser, L.T., Straub, C., Ghosh, A., 2016. Review of studies on tree species classification from remotely sensed data. Remote Sens. Environ. 186, 64–87. https://doi.org/10.1016/j.rse.2016.08.013.

Fassnacht, F.E., White, J.C., Wulder, M.A., Næsset, E., 2024. Remote sensing in forestry: current challenges, considerations and directions. Forestry 97, 11–37. https://doi.org/10.1093/forestry/cpad024.

Fricker, G.A., Ventura, J.D., Wolf, J.A., North, M.P., Davis, F.W., Franklin, J., 2019. A convolutional neural network classifier identifies tree species in mixed-conifer forest from hyperspectral imagery. Remote Sens. 11. https://doi.org/10.3390/rs11192326.

Hakula, A., Ruoppa, L., Lehtomäki, M., Yu, X., Kukko, A., Kaartinen, H., Taher, J., Matikainen, L., Hyyppä, E., Luoma, V., Holopainen, M., Kankare, V., Hyyppä, J., 2023. Individual tree segmentation and species classification using high-density close-range multispectral laser scanning data. ISPRS Open J. Photogramm. Remote Sens. 9. https://doi.org/10.1016/j.ophoto.2023.100039.

Hamedianfar, A., Mohamedou, C., Kangas, A., Vauhkonen, J., 2022. Deep learning for forest inventory and planning: a critical review on the remote sensing approaches so far and prospects for further applications. For. an Int. J. for. Res. 1–15. https://doi.org/10.1093/forestry/cpac002.

Hamraz, H., Jacobs, N.B., Contreras, M.A., Clark, C.H., 2019. Deep learning for conifer/deciduous classification of airborne LiDAR 3D point clouds representing individual trees. ISPRS J. Photogramm. Remote Sens. 158, 219–230. https://doi.org/10.1016/j.isprsjprs.2019.10.011.

Hansen, E., Wold, J., Dalponte, M., Gobakken, T., Noordermeer, L., Ørka, H.O., 2023. Estimation of the occurrence, severity, and volume of heartwood rot using airborne laser scanning and optical satellite data. Eur. J. Remote Sens. 56. https://doi.org/10.1080/22797254.2023.2229501.

Hauglin, M., Hansen, E., Sørngård, E., Næsset, E., Gobakken, T., 2018. Utilizing accurately positioned harvester data: Modelling forest volume with airborne laser scanning. Can. J. for. Res. 48, 913–922. https://doi.org/10.1139/cjfr-2017-0467.

He, Y., Jia, K., Wei, Z., 2023. Improvements in Forest Segmentation Accuracy Using a New Deep Learning Architecture and Data Augmentation Technique. Remote Sens. 15. https://doi.org/10.3390/rs15092412.

Hell, M., Brandmeier, M., Briechle, S., Krzystek, P., 2022. Classification of Tree Species and Standing Dead Trees with Lidar Point Clouds Using Two Deep Neural Networks: PointCNN and 3DmFV-Net. PFG -. J. Photogramm. Remote Sens. Geoinf. Sci. 90, 103–121. https://doi.org/10.1007/s41064-022-00200-4.

Hızal, C., Gülsu, G., Akgün, H.Y., Kulavuz, B., Bakırman, T., Aydın, A., Bayram, B., 2024. Forest Semantic Segmentation Based on Deep Learning Using Sentinel-2 Images. Int. Arch. Photogramm. Remote Sens. Spat. Inf. Sci. - ISPRS Arch. 48, 229–236. https://doi.org/10.5194/isprs-archives-XLVIII-4-W9-2024-229-2024.

Holmgren, J., Lindberg, E., Olofsson, K., Persson, H.J., 2022. Tree crown segmentation in three dimensions using density models derived from airborne laser scanning. Int. J. Remote Sens. 43, 299–329. https://doi.org/10.1080/01431161.2021.2018149.

Holmgren, J., Persson, Å., 2004. Identifying species of individual trees using airborne laser scanner. Remote Sens. Environ. 90, 415–423. https://doi.org/10.1016/S0034-4257(03)00140-8.

Holopainen, M., Vastaranta, M., Hyyppä, J., 2014. Outlook for the next generation's precision forestry in Finland. Forests 5, 1682–1694. https://doi.org/10.3390/f5071682.

Huo, L., Lindberg, E., 2020. Individual tree detection using template matching of multiple rasters derived from multispectral airborne laser scanning data. Int. J. Remote Sens. 41, 9525–9544. https://doi.org/10.1080/01431161.2020.1800127.

Hyyppä, E., Hyyppä, J., Hakala, T., Kukko, A., Wulder, M.A., White, J.C., Pyörälä, J., Yu, X., Wang, Y., Virtanen, J.P., Pohjavirta, O., Liang, X., Holopainen, M., Kaartinen, H., 2020. Under-canopy UAV laser scanning for accurate forest field measurements. ISPRS J. Photogramm. Remote Sens. 164, 41–60. https://doi.org/10.1016/j.isprsjprs.2020.03.021.

Hyyppä, E., Kukko, A., Kaartinen, H., Yu, X., Muhojoki, J., Hakala, T., Hyyppä, J., 2022. Direct and automatic measurements of stem curve and volume using a high-resolution airborne laser scanning system. Sci. Remote Sens. 5, 100050. https://doi.org/10.1016/j.srs.2022.100050.

Jamali, S., Olsson, P.O., Ghorbanian, A., Müller, M., 2023. Examining the potential for early detection of spruce bark beetle attacks using multi-temporal Sentinel-2 and harvester data. ISPRS J. Photogramm. Remote Sens. 205, 352–366. https://doi.org/10.1016/j.isprsjprs.2023.10.013.

Jocher, G., 2020. YOLOv5 by Ultralytics (Version 7.0). DOI: 10.5281/zenodo.3908559.

Jocher, G., Chaurasia, A., Qiu, J., 2023. Ultralytics YOLO (Version 8.0.0).

Karjalainen, T., Mehtätalo, L., Packalén, P., Malinen, J., Næsset, E., Gobakken, T., Maltamo, M., 2022. In-situ calibration of stand level merchantable and sawlog volumes using cut-to-length harvester measurements and airborne laser scanning data. For. an Int. J. for. Res. 95, 105–117. https://doi.org/10.1093/forestry/cpab031.

Kattenborn, T., Leitloff, J., Schiefer, F., Hinz, S., 2021. Review on Convolutional Neural Networks (CNN) in vegetation remote sensing. ISPRS J. Photogramm. Remote Sens. 173, 24–49. https://doi.org/10.1016/j.isprsjprs.2020.12.010.

Kukkonen, M., Maltamo, M., Korhonen, L., Packalen, P., 2019a. Comparison of multispectral airborne laser scanning and stereo matching of aerial images as a single sensor solution to forest inventories by tree species. Remote Sens. Environ. 231, 111208. https://doi.org/10.1016/j.rse.2019.05.027.

Kukkonen, M., Maltamo, M., Korhonen, L., Packalen, P., 2019b. Multispectral Airborne LiDAR Data in the Prediction of Boreal Tree Species Composition. IEEE Trans. Geosci. Remote Sens. 57, 3462–3471. https://doi.org/10.1109/TGRS.2018.2885057.

Lindroos, O., Ringdahl, O., Hera, P.L., Hohnloser, P., Hellström, T., 2015. Estimating the position of the harvester head – A key step towards the precision forestry of the future? Croat. J. for. Eng. 36, 147–164.

Liu, B., Huang, H., Su, Y., Chen, S., Li, Z., Chen, E., Tian, X., 2022. Tree Species Classification Using Ground-Based LiDAR Data by Various Point Cloud Deep Learning Methods. Remote Sens. 14. https://doi.org/10.3390/rs14225733.

Liu, J., Wang, X., Wang, T., 2019. Classification of tree species and stock volume estimation in ground forest images using Deep Learning. Comput. Electron. Agric. 166, 105012. https://doi.org/10.1016/j.compag.2019.105012.

Ma, Y., Zhao, Y., Im, J., Zhao, Y., Zhen, Z., 2024. A deep-learning-based tree species classification for natural secondary forests using unmanned aerial vehicle hyperspectral images and LiDAR. Ecol. Indic. 159. https://doi.org/10.1016/j.ecolind.2024.111608.

Maltamo, M., Hauglin, M., Næsset, E., Gobakken, T., 2019. Estimating stand level stem diameter distribution utilizing harvester data and airborne laser scanning. Silva Fenn. 53, 1–19. https://doi.org/10.14214/sf.10075.

Mäyrä, J., Keski-Saari, S., Kivinen, S., Tanhuanpää, T., Hurskainen, P., Kullberg, P., Poikolainen, L., Viinikka, A., Tuominen, S., Kumpula, T., Vihervaara, P., 2021. Tree species classification from airborne hyperspectral and LiDAR data using 3D convolutional neural networks. Remote Sens. Environ. 256. https://doi.org/10.1016/j.rse.2021.112322.

Mielczarek, D., Sikorski, P., Archiciński, P., Ciężkowski, W., Zaniewska, E., Chormański, J., 2023. The Use of an Airborne Laser Scanner for Rapid Identification of Invasive Tree Species Acer negundo in Riparian Forests. Remote Sens. 15. https://doi.org/10.3390/rs15010212.

Murray, B.A., Coops, N.C., Winiwarter, L., White, J.C., Dick, A., Barbeito, I., Ragab, A., 2024. Estimating tree species composition from airborne laser scanning data using point-based deep learning models. ISPRS J. Photogramm. Remote Sens. 207, 282–297. https://doi.org/10.1016/j.isprsjprs.2023.12.008.

Nauber, T., Hodač, L., Wäldchen, J., Mäder, P., 2024. Parametrization of biological assumptions to simulate growth of tree branching architectures. Tree Physiol. 44. https://doi.org/10.1093/treephys/tpae045.

Nilsson, M., Nordkvist, K., Jonzén, J., Lindgren, N., Axensten, P., Wallerman, J., Egberth, M., Larsson, S., Nilsson, L., Eriksson, J., Olsson, H., 2017. A nationwide forest attribute map of Sweden predicted using airborne laser scanning data and field data from the National Forest Inventory. Remote Sens. Environ. 194, 447–454. https://doi.org/10.1016/j.rse.2016.10.022.

Noordermeer, L., Ørka, H.O., Gobakken, T., 2023. Imputing stem frequency distributions using harvester and airborne laser scanner data: a comparison of inventory approaches. Silva Fenn. 57, 1–20.

Onishi, M., Ise, T., 2021. Explainable identification and mapping of trees using UAV RGB image and deep learning. Sci. Rep. 11, 1–15. https://doi.org/10.1038/s41598-020-79653-9.

Oubara, A., Wu, F., Amamra, A., Yang, G., 2022. Survey on Remote Sensing Data Augmentation: Advances, Challenges, and Future Perspectives, in: Senouci, M.R., Boulahia, S.Y., Benatia, M.A. (Eds) Advances in Computing Systems and Applications. CSA 2022. Lecture Notes in Networks and Systems, Vol 513. Springer, Cham., pp. 95–104. DOI: 10.1007/978-3-031-12097-8_9.

Persson, H.J., Olofsson, K., Holmgren, J., 2022. Two-phase forest inventory using very-high-resolution laser scanning. Remote Sens. Environ. 271, 112909. https://doi.org/10.1016/j.rse.2022.112909.

Pires, R. de P., Lindberg, E., Persson, H.J., Olofsson, K., Holmgren, J., 2024. Mobile laser scanning as reference for estimation of stem attributes from airborne laser scanning. Remote Sens. Environ. 315, 114414. DOI: 10.1016/j.rse.2024.114414.

Pires, R. de P., Olofsson, K., Persson, H.J., Lindberg, E., Holmgren, J., 2022. Individual tree detection and estimation of stem attributes with mobile laser scanning along boreal forest roads. ISPRS J. Photogramm. Remote Sens. 187, 211–224. DOI: 10.1016/j.isprsjprs.2022.03.004.

Puliti, S., Breidenbach, J., Astrup, R., 2020. Estimation of forest growing stock volume with UAV laser scanning data: Can it be done without field data? Remote Sens. 12, 1245. https://doi.org/10.3390/RS12081245.

Puliti, S., Mclean, J.P., Cattaneo, N., Fischer, C., Astrup, R., 2023a. Tree height-growth trajectory estimation using uni-temporal UAV laser scanning data and deep learning. For. an Int. J. for. Res. 96, 37–48. https://doi.org/10.1093/forestry/cpac026.

Puliti, S., Pearse, G., Surový, P., Wallace, L., Hollaus, M., Wielgosz, M., Astrup, R., 2023b. FOR-instance: a UAV laser scanning benchmark dataset for semantic and instance segmentation of individual trees. arXiv Prepr. arXiv2309.01279.

Qian, C., Yao, C., Ma, H., Xu, J., Wang, J., 2023. Tree Species Classification Using Airborne LiDAR Data Based on Individual Tree Segmentation and Shape Fitting. Remote Sens. 15. https://doi.org/10.3390/rs15020406.

Schiefer, F., Kattenborn, T., Frick, A., Frey, J., Schall, P., Koch, B., Schmidtlein, S., 2020. Mapping forest tree species in high resolution UAV-based RGB-imagery by means of convolutional neural networks. ISPRS J. Photogramm. Remote Sens. 170, 205–215. https://doi.org/10.1016/j.isprsjprs.2020.10.015.

Seidel, D., Annighöfer, P., Thielman, A., Seifert, Q.E., Thauer, J.H., Glatthorn, J., Ehbrecht, M., Kneib, T., Ammer, C., 2021. Predicting Tree Species From 3D Laser Scanning Point Clouds Using Deep Learning. Front. Plant Sci. 12, 1–12. https://doi.org/10.3389/fpls.2021.635440.

Shi, Y., Skidmore, A.K., Wang, T., Holzwarth, S., Heiden, U., Pinnel, N., Zhu, X., Heurich, M., 2018a. Tree species classification using plant functional traits from LiDAR and hyperspectral data. Int. J. Appl. Earth Obs. Geoinf. 73, 207–219. https://doi.org/10.1016/j.jag.2018.06.018.

Shi, Y., Wang, T., Skidmore, A.K., Heurich, M., 2018b. Important LiDAR metrics for discriminating forest tree species in Central Europe. ISPRS J. Photogramm. Remote Sens. 137, 163–174. https://doi.org/10.1016/j.isprsjprs.2018.02.002.

Söderberg, J., Wallerman, J., Almäng, A., Möller, J.J., Willén, E., 2021. Operational prediction of forest attributes using standardised harvester data and airborne laser scanning data in Sweden. Scand. J. for. Res. 36, 306–314. https://doi.org/10.1080/02827581.2021.1919751.

Sothe, C., De Almeida, C.M., Schimalski, M.B., La Rosa, L.E.C., Castro, J.D.B., Feitosa, R. Q., Dalponte, M., Lima, C.L., Liesenberg, V., Miyoshi, G.T., Tommaselli, A.M.G., 2020. Comparative performance of convolutional neural network, weighted and conventional support vector machine and random forest for classifying tree species using hyperspectral and photogrammetric data. Giscience Remote Sens. 57, 369–394. https://doi.org/10.1080/15481603.2020.1712102.

Straker, A., Puliti, S., Breidenbach, J., Kleinn, C., Pearse, G., Astrup, R., Magdon, P., 2023. Instance segmentation of individual tree crowns with YOLOv5: A comparison of approaches using the ForInstance benchmark LiDAR dataset. ISPRS Open J. Photogramm. Remote Sens. 9, 100045. https://doi.org/10.1016/j.ophoto.2023.100045.

Takhtkeshha, N., Mandlburger, G., Remondino, F., Hyyppä, J., 2024. Multispectral Light Detection and Ranging Technology and Applications: A Review. Sensors 24. https://doi.org/10.3390/s24051669.

Terryn, L., Calders, K., Disney, M., Origo, N., Malhi, Y., Newnham, G., Raumonen, P., Åkerblom, M., Verbeeck, H., 2020. Tree species classification using structural features derived from terrestrial laser scanning. ISPRS J. Photogramm. Remote Sens. 168, 170–181. DOI: 10.1016/j.isprsjprs.2020.08.009.

Wang, J., Jiang, Y., 2024. A Hybrid convolution neural network for the classification of tree species using hyperspectral imagery. PLoS One 19, e0304469. https://doi.org/10.1371/journal.pone.0304469.

Wu, J., Chen, L., Wang, J., Li, Y., Chen, E., Zhang, X., 2024. A novel framework combining band selection algorithm and improved 3D prototypical network for tree species classification using airborne hyperspectral images. Comput. Electron. Agric. 219, 108813. https://doi.org/10.1016/j.compag.2024.108813.

Xi, Z., Hopkinson, C., Rood, S.B., Peddle, D.R., 2020. See the forest and the trees: Effective machine and deep learning algorithms for wood filtering and tree species classification from terrestrial laser scanning. ISPRS J. Photogramm. Remote Sens. 168, 1–16. https://doi.org/10.1016/j.isprsjprs.2020.08.001.

Xiang, B., Wielgosz, M., Kontogianni, T., Peters, T., Puliti, S., Astrup, R., Schindler, K., 2023. Automated forest inventory: analysis of high-density airborne LiDAR point clouds with 3D deep learning. DOI: 10.1016/j.rse.2024.114078.

Xu, Q., Hou, Z., Maltamo, M., Tokola, T., 2014a. Retrieving suppressed trees from model-based height distribution by combining high-and low-density airborne laser scanning data. Can. J. Remote Sens. 40, 233–242. https://doi.org/10.1080/07038992.2014.935933.

Xu, Q., Hou, Z., Maltamo, M., Tokola, T., 2014b. Calibration of area based diameter distribution with individual tree based diameter estimates using airborne laser scanning. ISPRS J. Photogramm. Remote Sens. 93, 65–75. https://doi.org/10.1016/j.isprsjprs.2014.03.005.

Xu, S., Wang, R., Shi, W., Wang, X., 2024. Classification of Tree Species in Transmission Line Corridors Based on YOLO v7. Forests 15, 1–17. https://doi.org/10.3390/f15010061.

Yu, X., Hyyppä, J., Litkey, P., Kaartinen, H., Vastaranta, M., Holopainen, M., 2017. Single-sensor solution to tree species classification using multispectral airborne laser scanning. Remote Sens. 9, 1–16. https://doi.org/10.3390/rs9020108.

Zhang, H., Wang, C., Tian, S., Lu, B., Zhang, L., Ning, X., Bai, X., 2023. Deep learning-based 3D point cloud classification: A systematic survey and outlook. Displays 79, 102456. https://doi.org/10.1016/j.displa.2023.102456.

Acta Universitatis Agriculturae Sueciae

Doctoral Thesis No. 2025:77

This thesis investigates how complementary data sources can expand the availability of tree-level information for forest inventories based on remote sensing. These include close-range laser scanning, harvester production reports, and synthetic point clouds. The four studies demonstrate methods for deriving stem attributes, training airborne laser scanning-based models, automating annotation, and simulating stem defects. Results show that such data can provide ground-truth information of sufficient quality and scale to support modelling.

Raul de Paula Pires received his doctoral education at the Department of Forest Resource Management at the Swedish University of Agricultural Sciences (SLU), in Umeå. He holds a double MSc degree, Agriculture and Forestry from the University of Eastern Finland, and Spatial and Ecological Modelling in European Forestry, from the University of Lleida, in Spain.

Acta Universitatis Agriculturae Sueciae presents doctoral theses from the Swedish University of Agricultural Sciences (SLU).
SLU generates knowledge for the sustainable use of biological natural resources. Research, education, extension, as well as environmental monitoring and assessment are used to achieve this goal.

ISSN 1652-6880
ISBN (print version) 978-91-8124-061-0
ISBN (electronic version) 978-91-8124-107-5